Title

Modeling Genetic Control of Vector-borne Infectious Diseases: Mechanistic and Machine Learning Approaches

Author

Mondal, Agastya

Publication Date

2024

Peer reviewed|Thesis/dissertation

Modeling Genetic Control of Vector-borne Infectious Diseases: Mechanistic and Machine Learning Approaches

by

Agastya Mondal

A dissertation submitted in partial satisfaction of the

requirements for the degree of

Doctor of Philosophy

in

Epidemiology

in the

Graduate Division

of the

University of California, Berkeley

Committee in charge:

Professor John M. Marshall, Chair
Professor Michael Boots
Professor Lexin Li

Summer 2024

Modeling Genetic Control of Vector-borne Infectious Diseases:
Mechanistic and Machine Learning Approaches

Abstract

Modeling Genetic Control of Vector-borne Infectious Diseases:
Mechanistic and Machine Learning Approaches

by

Agastya Mondal

Doctor of Philosophy in Epidemiology

University of California, Berkeley

Professor John M. Marshall, Chair

This dissertation presents computational approaches to understand the entomological and epidemiological dynamics associated with malaria transmission and genetic vector control. From both mechanistic and deep learning perspectives, this work provides a computational toolkit to i) estimate the entomological and epidemiological impacts of novel genetic vector control tools, ii) understand the relationship between genetic parameters and outcomes of interest, and iii) emulate and calibrate complex mechanistic models of malaria transmission to external data.

Chapter 1 surveys the current landscape of vector control interventions and provides historical context to this work. Chapter 2 proposes a "decoupled" vector-human mechanistic model to estimate the impacts on prevalence and clinical incidence of malaria associated with the deployment of genetic vector control tools in *Anopheles* mosquitoes. Combining an entomological model of gene inheritance with an epidemiological model of malaria transmission via a novel sampling algorithm, this framework provides a modular way to simulate the impacts of genetic vector control interventions. Chapter 3 uses this framework to quantify the relative importance of various genetic parameters in a CRISPR-Cas9-based homing gene drive on epidemiological outcomes of interest, parameterized to two African locations of interest across varying transmission intensities. Finally, Chapter 4 provides a deep learning framework to emulate a complex model of malaria transmission and use this approach in conjunction with approaches from numerical optimization to calibrate the model to external data. Taken together, this work contributes to the advancement of computational modeling in epidemiology and holds potential for the design and implementation of urgently-needed novel interventions for vector control. Chapter 5 concludes this work by considering its implications and potential future directions.

Contents

List of Figures

List of Tables

Acknowledgments

This work is the product of many years of rich collaborations with both peers and mentors. I would like to first thank my advisor, John Marshall, for taking a chance on me, someone with a less-than-traditional pathway to academia. His guidance and intuition deeply shaped this work and my skills as a computational scientist. I would like to thank my mentors – Prashanth Selvaraj, Rushil Anirudh, Ana Bento, Robel Kassa, Sam Scarpino, Larry Brilliant, Amy Lockwood, Karen Pak Oppenheimer, Lisa Danzig, Art Reingold – for their wisdom and belief in me. Because of them, I was continually reminded to keep pushing and recognizing the value of my work. To my peers at Berkeley and beyond – Nerissa Nance, Kevin Chen, Váleri Vásquez, Rodrigo Corder, Eileen Gutiérrez, Yun Tao, Laura Alexander, Sean Wu, Moon Choi-McInturff, Héctor Sánchez C. – I have learned so much from all of you, and I am grateful for our continued friendship. To the businesses in San Francisco, Seattle, and Berkeley that fueled the writing of this dissertation (there are too many to name, but particularly the oat milk cortados at Grand Coffee and the sandwiches at Rhea's Deli kept me going), thank you for nourishing my body and mind. Thank you to the folks at ICL (Penny Hancock, Thomas Churcher, Azra Ghani) for hosting my fantastic summer in London. Finally, a sincere thank you to my committee members (Mike Boots and Lexin Li), my Hopkins friends, San Francisco roommates, mom, Kamal, and my partner Anjali for their steadfast and unwavering support in me throughout this challenging process. I could not have done it without them.

Chapter 1

Introduction

1.1 A brief history of vector control

Parasites and vectors

> ... With tears and toiling
> breath,
> I find thy cunning seeds,
> O million-murdering Death.

Epidemiologist Ronald Ross wrote these words in 1897 [1], following his groundbreaking discovery that mosquitoes transmit the parasite that cause the deadly disease malaria. Malaria is one of humanity's oldest diseases. *Mala aria*, Italian for "bad air", was initially thought to be spread through tainted marshland air (a consequence of the now-debunked miasma theory of disease transmission). Traces of the malaria parasite were found in mosquitoes preserved in amber dating over 30 million years ago. Texts from Ancient Greece, China, and Rome refer to the deadly malarial fevers that plagued their societies. Though malaria has been around since the earliest humans, advances in clinical science in the 19th century allowed for a more detailed study of the disease. Building on the work of Louis Pasteur and Alphonse Laveran, who respectively identified microbes as the cause of infectious diseases and discovered malaria parasites in patients' blood, Ross developed a comprehensive theory of malaria transmission. During his time in the Indian Medical Service in Secunderabad, Ross discovered the malaria parasite in the stomach tissue of a mosquito which had previously fed on a patient with malaria. He continued this research in birds, showing that the mosquito served as an intermediary host for malaria, which then transmitted the parasite through its salivary glands. For this work, Ross would be awarded the Nobel Prize for Physiology or Medicine in 1902. Ross's work ushered in a new era of malaria research. Notably in 1899, Giovanni Battista Grassi, Amico Bignani, and Giuseppe Bastianelli were the first to show the reciprocal transmission of *Plasmod-*

ium parasites between *Anopheles* [1] mosquitoes and humans.

Diseases such as yellow fever, dengue, and Zika, spread by the *Aedes* genus of mosquito, similarly affect large swathes of the human population. U.S. Army Corps physician Walter Reed showed in 1901 that yellow fever was indeed spread by a specific type of mosquito, later confirmed to be the *Aedes* genus. Reed's work most notably allowed for proper vector control measures to be implemented during the construction of the Panama Canal, whose progress had been severely hampered by widespread vector-borne disease in the area. Though research into these diseases has been ongoing for decades, their resilience and severity underscores the urgent need for novel vector control interventions. Though *Aedes*-borne diseases are not the focus of this work, it is important to recognize that often these diseases affect one another [2, 3], and the vector control interventions described here can be applied to different vectors more broadly.

Vector control and disease management

Though vector control technology has advanced significantly in the last century, the majority of efforts worldwide center on managing vectors through bed net and pesticide use alongside managing disease via drugs and vaccines. In his review of mosquito nets, Okumu [4] states that bed nets are some of the oldest insect control interventions, with uses dating back to the 5th century BC (though these uses were likely ceremonial or gnat-related). 1912 saw the introduction of the powerful insecticide *dichlorodiphenyltrichloroethane* (DDT), whose widespread use became the foundation for anti-malaria campaigns during and after World War II. Due to concerns about its effects on human health and the environment, DDT was phased out, but bed nets treated with synthetic insecticide compounds became widespread in the 1980s and 1990s. Beginning in the 2000s, however, challenges of distribution and reported resistance to insecticides led to the stagnation of bed net use worldwide. Nonetheless, insecticide-treated bed nets remain a foundational vector control intervention.

Alongside long-lasting insecticide-treated bed nets (LLINs), indoor residual spraying (IRS) of pesticides has become a widespread vector control intervention. As most malaria vectors are endophilic (i.e., they rest indoors after taking a blood meal), indoor residual spraying can target mosquitoes at a different point in the feeding cycle as compared to bed nets and therefore can maximize disease prevention when deployed in conjunction. The World Health Organization (WHO) operational manual on IRS [5] states that

> IRS can contribute to the elimination of malaria if rigorously applied. Historically, malaria was controlled by draining areas of standing water near habitations and using screens to prevent mosquitoes from entering living areas. But the tremendous accomplishments of malaria programmes in Europe, Asia

[1] The word *Anopheles* comes from the Greek for "good-for-nothing."

> and the Americas, which resulted in hundreds of millions of lives being saved between the 1940s and the 1980s, was largely due to the addition of IRS as a vector-control intervention. More recently, the scale-up of IRS in Africa has contributed, together with LLINs and improved diagnostic testing and treatment, to remarkable declines in malaria burden and all-cause childhood mortality. IRS is highly effective when properly applied, but it requires adequate national programme capacity, structures and systems.

As with insecticide-treated nets, resistance to IRS is a major driver in its stagnation in the campaigns to eliminate malaria [6, 7]. Though IRS may be more cost-effective than bed net distribution [8] in terms of cases prevented, bed nets' relative ease of use make them the most widely-used vector control intervention. Between 2008 and 2010, over 290 million bed nets were distributed in sub-Saharan Africa, for example.

Management of malaria is multifaceted. While vector control interventions focus primarily on prevention of disease transmission, products targeting the severe morbidity and mortality associated with malaria infection have been widely deployed. Historically, quinine and its derivatives were used in the management of acute malaria infection. However, widespread drug resistance has made these types of drugs less desirable in the modern day. Artemisinin-based combination therapies generally are recommended in resistant infections, as widespread resistance to artemisinin has not yet been observed. Antimalarial drugs target various stages of infection development, and some are prophylactic while others are therapeutic. As with insecticides, resistance to antimalarial drugs is a major cause for concern and the persistence of malaria infection worldwide. White [9] details the genetic and epidemiological bases of antimalarial drug resistance. Interestingly, even resistance to detection via rapid diagnostic test has been observed and poses challenges in the design and development of malaria tests [10]. In 2021, the WHO endorsed the RTS,S vaccine for "broad use" in children, making it the first malaria vaccine candidate to be rolled out globally. The vaccine had been in development since the 1980s by scientists from GlaxoSmithKline. It targets towards pediatric cases of malaria in high endemic regions. As of 2023, over 4.5 million doses of the vaccine had been administered. While the vaccine is effective in reducing the severity of pediatric malaria, it does not reduce overall transmission and therefore should be administered alongside other vector control interventions.

Here, we have briefly described some traditional vector control and disease management interventions that are widely used in malaria-endemic regions. The WHO identifies four major threats to the progress of malaria eradication: vector insecticide resistance, invasive vector species, antimalarial drug efficacy and resistance, and parasite *Pfhrp2/3* gene deletions. These threats require novel approaches to combat the stagnating efficacy of the interventions described here.

Epidemiology of vector-borne disease in the modern day

Vector-borne diseases continue to account for significant morbidity and mortality worldwide, particularly in sub-Saharan Africa and tropical nations. According to the CDC, malaria accounted for over 600,000 deaths in 2020, despite the widespread rollout of interventions between 2010-2020 (which are estimated to have reduced global malaria mortality by 36%) [11]. Because malaria can be a lifelong disease, it presents significant strains on local health and economic systems. One study [12] estimated that the global cost of government, out-of-pocket, prepaid private, healthcare seeking, patient care, and medication expenditures exceeded $4 billion USD in 2016 alone. Pediatric cases of malaria are particularly deadly, as children rapidly lose maternal immunity to the disease but have not yet accumulated enough immunity via exposure. Other neglected tropical diseases such as dengue, yellow fever, and Zika continue to pose urgent health challenges. The control of dengue is particularly interesting, as its four serotypes and varying levels of cross-immunity in human populations have led to its recurrent cycling and hyper-endemicity in some regions [13]. Despite global commitments and increased funding, vector-borne diseases continue to levy a significant burden and acutely shape the priorities of health agencies and NGOs worldwide.

Of particular interest is the role that climate change is expected to play in the epidemiology of vector-borne disease. Thomson and Stanberry [14] outline various climate drivers of disease. For malaria, they say that land-use changes, extreme heat effects on infrastructure, and migration has increased the risk of malaria. Work from Mordecai's group [15] additionally indicates that the optimal temperature for malaria transmission is much lower than expected. Arboviruses such as dengue are increasingly appearing in temperate regions [16] due to increased temperatures creating more habitable environments for the *Aedes* mosquito. Additionally, Thomson and Stanberry state that extreme flooding and temperature may change how water is stored, which could in turn create more optimal breeding environments for disease-capable mosquitoes. Climate-related drivers of vector-borne disease will require novel approaches in managing these complex diseases.

1.2 Mathematical models of vector-borne disease transmission

The Ross-Macdonald model of malaria transmission

Mathematical models have been deployed in various fields, including energy planning, financial analysis, and genomics [17–23]. Mathematical models of vector-borne disease transmission have been in use for over a hundred years. Ronald Ross formulated the first mechanistic model of malaria transmission in 1911, and George Macdonald expanded on it in 1956 by quantifying the impact of vector control and considering superinfection [24].

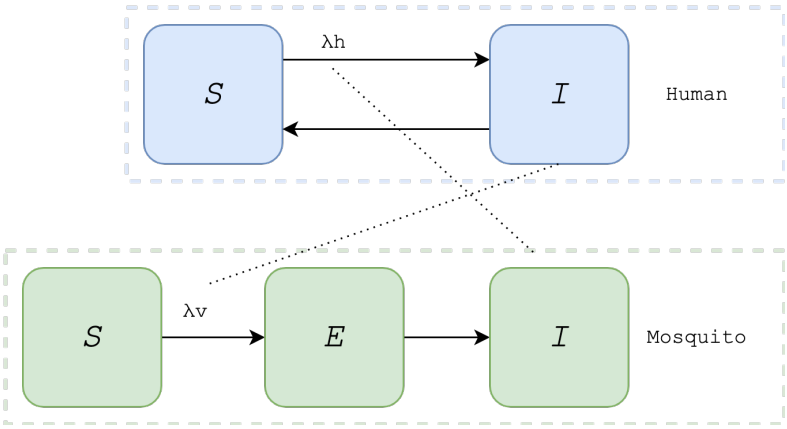

Figure 1.1: **Schematic showing a simple Ross-Macdonald-style model of malaria transmission.** Humans move between susceptible (S) and infectious (I) states per the level of infectiousness in the mosquito population (λ_H), and similarly mosquitoes move between susceptible (S), incubating (E), and infectious (I) states depending on the level of infectiousness in the human population (λ_V).

This class of models forms the basis of most vector-borne disease transmission models today, and therefore its study is warranted here before considering more complex scenarios. At its simplest, the Ross-Macdonald model of malaria transmission considers two human states $\{S_H, I_H\}$ representing susceptible and infectious humans, respectively. Reciprocal transmission of the malaria pathogen occurs when a mosquito feeds on an infected human, and passes through susceptible, incubating, and infectious states $\{S_V, E_V, I_V\}$. A schematic for this model is shown in Figure 1.1.

The deterministic version of this model is governed by the set of differential equations:

$$\begin{aligned}
\frac{dS_H}{dt} &= -(\frac{V}{H})a(\frac{I_V}{V})b_H S_H + rI_H \\
\frac{dI_H}{dt} &= (\frac{V}{H})a(\frac{I_V}{V})b_H S_H - rI_H \\
\frac{dS_V}{dt} &= \mu_V V - a(\frac{I_H}{H})b_V S_V - \mu_V S_V \\
\frac{dE_V}{dt} &= a(\frac{I_H}{H})b_V S_V - \gamma E_V - \mu_V E_V \\
\frac{dI_V}{dt} &= \gamma E_V - \mu_V I_V
\end{aligned}$$

The set of parameters governing this model is shown in Table 1.1.

Symbol	Description
V	Size of mosquito population
H	Size of human population
a	Mosquito biting rate
b_H	Human infection probability
r	Human recovery rate
γ	Mosquito rate of progression to infectiousness
b_V	Mosquito infection probability
μ_V	Mosquito birth and death rate

Table 1.1: **Parameters of the Ross-Macdonald model of malaria transmission.**

The *force of infection* on humans represents the rate of infection in humans per unit time and is expressed as:

$$\lambda_H(t) = (\frac{V}{H})a(\frac{I_V}{V})b_H$$

Similarly, the rate of infection on mosquitoes per unit time is given by:

$$\lambda_V(t) = a(\frac{I_H}{H})b_V$$

While the model described here represents a simplified version of malaria transmission, it forms the basis for the models subsequently discussed.

Complex models of malaria transmission

Here, we briefly review three complex models of malaria transmission, each of which provides a more comprehensive understanding of the relationship between vector, host, and environment. These models have been used extensively in policy planning and quantifying the impact of vector control interventions. First, we discuss the Imperial College London (ICL) model of malaria transmission, noting that this model will be discussed in more depth in Chapter 2. Originally published in 2010 [25], the ICL model is an individual-based, stochastic model of malaria transmission. The model includes age structure, immunity, biting heterogeneity, and three aggregated vector species (*An. gambiae s.s.*, *An. funestus*, *and An. arabiensis*). The initial model was used to fit parameters to prevalence data from 34 African settings, and project the impact of various intervention packages. Subsequent analyses using the model included estimating the impact of attractive toxic sugar-baited mosquito traps [26], RTS,S anti-malaria vaccines [27], mosquito feeding behavior [28], among many others. While maintaining relative parsimony, the ICL malaria transmission model has served as the foundation of a wide range of modeling efforts,

and captures the key biological processes underpinning malaria transmission. Another comprehensive transmission model, OpenMalaria [29], was first published in 2007 by researchers from The Swiss Tropical and Public Health Institute. OpenMalaria is an individual, microsimulation-based model of malaria transmission incorporating the dynamics of parasitemia, infection, and transmission in geospatial contexts. The model has been extended to include the impact of anti-malaria interventions such as vaccines, bednets, and chemoprevention. Bayesian emulators have also been built on top of OpenMalaria simulation data [30] in order to calibrate the model to external data in a computationally efficient manner. We take inspiration from this work in designing machine learning-based emulators of malaria transmission models in later chapters. Finally, we mention the EMOD model developed by the Institute for Disease Modeling and the Bill and Melinda Gates Foundation [31–33]. Similar to OpenMalaria, EMOD is an individual-based mechanistic model of malaria transmission. EMOD specifies vector biology and within-host dynamics in great detail, with asexual parasite and gametocyte development tracked in each host as the infectious process progresses. Various types of immunity to sexual parasites are also tracked via genetic parameters. EMOD has been extended to incorporate spatial dynamics and novel interventions such as gene drive systems [34]. The EMOD model will be the focus of Chapter 4. While the details of each model have been omitted here, we have briefly outlined the main malaria transmission models that are used by researchers to estimate intervention outcomes. More specialized models exist [35, 36] to address specific interventions or aspects of the transmission cycle.

1.3 Overview of genetic vector control interventions

Given the stagnation in efficacy of traditional vector control tools such as LLINs and IRS against the mortality and morbidity associated with malaria infection, researchers are increasingly interested in genetic tools to control disease. Broadly, genetic vector control refers to a class of interventions that target the vector (i.e., the disease-transmitting mosquito) at the genetic level to interrupt its ability to transmit a pathogen. In the context of malaria, this generally refers to modifying *Anopheline* mosquitoes in a way to prevent their ability to transmit the *Plasmodium* pathogen. Genetic interventions have been developed for other disease vectors, such as *Aedes* mosquitoes and ticks [37, 38]. These interventions are attractive because they do not require continuous distribution of materials or high adherence to be effective. Additionally, interventions based on advances in CRISPR-Cas9 gene editing allow these interventions to be highly efficacious in their spread and impact. Here, we briefly describe three classes of genetic vector control techniques: the sterile insect technique (SIT), *Wolbachia*-based interventions, and gene drive.

Sterile insect technique (SIT) interventions

SIT interventions have been explored since the 1970s [39]. Broadly, SIT methods involve the release of large numbers of sterile male insects. When these sterile male insects mate with wild females, their reproductive potential decreases. The ultimate goal is then the local elimination or suppression of the pest population. Historically, SIT programs have succeeded against pests such as the screwworm fly, Mediterranean fruit fly (Medfly), and the pink bollworm [40]. Due to advances in gene-editing technologies, a better understanding of mosquito lifecycle, and a scale-up of agricultural pest management programs, interest in the deployment of SIT technologies has increased. For example, in recent years Akbari and colleagues [41–43] have coupled CRISPR-based gene editing with SIT to develop an efficacious population suppression tool in *Drosophila*, *Aedes*, and *Anopheles* termed precision-guided sterile insect technique (pgSIT). pgSIT exploits CRISPR-gene editing to disrupt genes associated with male viability and female fertility to deliver eggs which give rise to sterile male insects. Other SIT-like genetic interventions such as release of insects carrying a dominant lethal (RIDL) target other aspects of the mosquito lifecycle in order to suppress populations. In this intervention, a genetic modification renders female mosquitoes flightless. This is effectively lethal as flightless mosquitoes cannot mate, seek hosts, avoid predators, or transmit disease. While these techniques have shown promise in the lab, there is inadequate understanding of the ecological implications of eliminating entire mosquito populations, and thus population suppression techniques such as SIT may be less appealing than other types of genetic vector control interventions [44].

Wolbachia interventions

Wolbachia is a common bacterium found in over 60% of all insects [45], but interestingly not found in the *Aedes aegypti* mosquito, the primary vector for dengue, yellow fever, Zika, and other diseases. Researchers have found that the dengue virus is unable to replicate in *Aedes* mosquitoes in which *Wolbachia* has been introduced externally. This finding led to the development of *Wolbachia*-based interventions against dengue in countries like Singapore and Indonesia, resulting in a significant decrease in dengue incidence [46, 47]. *Wolbachia*-based interventions for malaria control are under active research, but malaria poses unique challenges. Unlike dengue, malaria can be transmitted by at least 40 different strains of *Anopheles* mosquitoes [48], so interventions must be more broadly applicable to different mosquito strains. Additionally, unlike *Aedes*, some strains of *Wolbachia* are naturally occurring in *Anopheles* mosquitoes. Therefore, new strains must be discovered that can provide the same viral replication blocking properties as *Wolbachia* in *Aedes* mosquitoes. Nonetheless, *Wolbachia*-based interventions for vector control are promising and continue to be developed and deployed worldwide.

Gene drive interventions

Finally, we turn our attention to gene drive interventions, which are the primary focus of this dissertation. Broadly, gene drives refer to selfish genetic elements which are transmitted to progeny in a super-Mendelian (i.e., > 50%) manner [49]. While these types of genetic elements occur naturally [50–54], their properties can be exploited due to advances in CRISPR-Cas9 gene editing technologies. These synthetic gene drives have proven to be highly efficacious in laboratory settings. In the context of vector control, the goal is to rapidly spread a disease-refractory gene through a mosquito population. These genes can be related to fitness, transmission potential, lifespan, and host-seeking behavior, among others. Here, we briefly review two paradigms of gene drive technology and illustrate some examples of each. Generally, gene drive interventions fall into one of two categories: population suppression and population modification/replacement.

Population suppression refers to a gene drive technique in which harmful genes are forced into a vector population in order to diminish or crash them, thus leading to fewer disease-transmitting vectors. Homing gene drives (gene drives in which CRISPR-Cas9 induce a targeted double-stranded break in order to convert a wild allele to a drive allele) have shown suppression efficacy in *Anopheles* [55]. Products have targeted female fertility through the *doublesex* gene to bias sex ratios and reduce the number of viable females [56]. The main challenges of widespread deployment of suppression drives includes the accumulation of resistant, nonfunctional alleles and the potential unintended ecological consequences of eliminating an entire species [57]. In contrast, population modification (or replacement) strategies do not intend to crash wild mosquito populations. Instead, they aim to drive transmission-blocking effector genes into mosquito populations and therefore "replace" wild mosquitoes with those that cannot transmit disease. While these approaches may be more robust to unintended ecological consequences and neighboring species invasion, their deployment has their own set of challenges. Primarily, the relative fitness of transgenic mosquitoes and the accumulation of resistant alleles pose barriers to achieving complete replacement. Nonetheless, advanced genetic techniques alongside robust modeling is an active area of research, with new constructs and models illuminating the necessary characteristics required of a population replacement program to achieve a desired epidemiological impact [58].

Gene drives hold great promise in reducing the burden of vector-borne disease. Alongside the challenges of developing a genetic construct in the lab, the deployment of gene drive organisms will require buy-in from a wide variety of stakeholders including national vector control programs, community implementation groups, funders, modelers, and genetic scientists. In 2020, a group of scientists published a set of commitments required to successfully deploy a gene drive program [57]. These commitments include fair partnership, transparency, product safety, efficacy, regulatory evaluation, risk/benefit assessments, monitoring, and mitigation. While these categories are purposefully broad,

they represent important policy implications of developing a gene drive program beyond the genetics alone. As these products leave the lab and enter field trials, these overarching commitments are paramount in ensuring that these interventions are deployed in an equitable and safe way.

1.4 Model-informed target product profiles

Here, we will discuss the application of a policy tool known as a target product profile (TPP) to the development of gene drive products. TPPs are planning tools that provide a list of preferred characteristics and minimum criteria products must satisfy as they progress through the development pipeline. TPPs for gene drive mosquitoes are becoming increasingly relevant as the technology matures and moves closer to release. A draft TPP for a population modification gene drive product has been proposed [59], and a workshop hosted by the Foundation for the National Institutes of Health (FNIH) discussed TPPs for gene drive products at length [57]. A common theme from these publications is that, while TPPs should be based as much as possible on empirical studies, rigorous modeling will be needed where empirical data is not available. Key outcomes for vector control tools are entomological (i.e., effects on mosquito populations) and epidemiological (i.e., effects on human health outcomes) and can only be observed following a release, meaning that the initial decision to release will be based on model predictions.

Fortunately, there has been a growth in malaria modeling over the last 10–15 years, with several detailed models being published that concisely describe malaria transmission dynamics in the mosquito vector and human host. These include OpenMalaria [60] and the Imperial College London malaria model [25, 61]. Over this same period, other novel malaria control tools have also been developed and advanced through stages of laboratory and field-testing - most recently and visibly, attractive targeted sugar baits (ATSBs) [62] and malaria vaccines [63]. These provide case studies for the application of mathematical models to TPPs, and we draw from these previous analyses to explore the role that mathematical models should play in informing TPPs for mosquito gene drive products.

Model-informed target product profiles for other malaria control tools

As the goals of TPPs are product-focused, much of the modeling work in this area does not feature in academic journals. We therefore focus on a handful of published modeling analyses, each conducted by a different research group, that have supported TPP specification for ATSBs [26], odor-baited traps [64], and long-acting injectable drugs (LAIs) for seasonal malaria prevention [65]. We summarize these analyses, and additional TPP modeling analyses for malaria vaccines [63] and vector control pesticides [66, 67], in Figure 1.2.

Product	Attractive targeted sugar baits	Odor-baited traps	Vector control pesticides	Long-acting injectable drugs	Malaria vaccines
Product parameters	Excess mosquito mortality rate due to ATSBs (ATSB feeding rate, mortality rate upon feeding)	Attractiveness of traps to mosquitoes, cost per trap	Excess probability of mosquito diversion &/or death before feeding	Initial LAI protective efficacy, shape & half-life of decay in protective efficacy	Initial vaccine efficacy, duration of protection, dose regime (timing & titre/efficacy of 4th dose)
Intervention parameters	N/A (although ATSB coverage determines feeding date)	Trap coverage (number of traps per 1000 people)	Pesticide coverage (treated LLINs & outdoor products)	LAI coverage	Vaccine coverage (first 3 doses, 4th dose)
Target outcomes	>30% reduction in all-ages clinical malaria incidence or prevalence	Reduction in EIR equivalent to that achieved by 50% coverage with LLINs	Highest reduction in EIR for user/household & community	Clinical malaria cases averted (children 0-5 years) equivalent to that achieved by SMC	Most clinical malaria cases averted (children 0-5 years) for 10 years following introduction
Models used	Imperial College London malaria model	Deterministic model of mosquito host-seeking & ovipositing	Deterministic model of mosquito host-seeking & ovipositing	*OpenMalaria*	Imperial College London malaria model
Settings considered	Baseline malaria prevalence of 10-50%, varying degrees of seasonal transmission	Baseline EIR of 200 infective bites per person per year (high transmission settings)	Baseline EIR of 200 infective bites per person per year, equal numbers of humans & cattle	Settings that resemble Mali & Senegal (seasonality, mosquito species, interventions)	4 distinct transmission settings (initial malaria prevalence of 5%, 15%, 30%, 45%)
Minimally acceptable criteria	Excess mosquito mortality rate >0.05 or >0.1 per mosquito per day	Traps more attractive than humans, >20-130 traps per 1000 people, cost per trap < $4-$27	High coverage with mosquito-toxic profiles is optimal, deterrence provides personal protection	Sigmoidal protective efficacy profile, half-life > duration of transmission season	High initial vaccine efficacy, high titre of 4th dose, long interval between 3rd & 4th doses
References	Fraser et al.	Okumu et al.	Killeen et al. Killeen and Moore	Burgert et al.	Hogan et al.

ATSB, attractive targeted sugar bait; EIR, entomological inoculation rate; LAI, long-acting injectable drug; SMC, seasonal malaria chemoprevention.

Figure 1.2: **Model-informed target product profiles for malaria and vector control tools.**

Lessons from attractive targeted sugar baits

ATSBs were proposed as an outdoor vector control strategy to complement existing indoor tools such as LLINs and indoor residual spraying with insecticides (IRS), and work by attracting mosquitoes to the fruity or flowery scent of a bait laced with a combination of sugar and an oral toxin [68]. In 2008, a field study demonstrated that ATSBs were capable of reducing Anopheles gambiae mosquito populations by 90% in Bandiagara, a semi-arid area of Mali [69]. Then in 2017, a randomized controlled trial (RCT) involving 14 villages in Mali demonstrated that ATSBs were capable of significantly reducing An. gambiae populations, including sporozoite-infected females, when LLINs were already present [62]. Both studies had focused on entomological outcomes (i.e., mosquito density and sporozoite infection), and a mathematical model was used to estimate the expected epidemiological impact based on the RCT results [26] prior to planning epidemiological RCTs.

Predicting outcomes, especially epidemiological ones, based on product parameters embodies the primary role that mathematical models play in informing TPPs. For ATSBs, the key product parameter is the excess daily mosquito mortality rate caused by the intervention, which was estimated to be 0.09 per mosquito per day from the Mali RCT [26]. In this study, the Imperial College London malaria model [25, 61] was used to predict all-ages malaria prevalence and clinical incidence following intervention with ATSBs in

a range of transmission settings (baseline malaria prevalence ranging from 10-50% with varying degrees of seasonal transmission). This malaria model includes acquired and maternal human immunity, symptomatic and asymptomatic infection, human age structure, mosquito biting heterogeneity, and antimalarial drug therapy and prophylaxis [25]. A detailed mosquito life history model is also included, incorporating vector control tools such as LLINs and IRS [28, 70]. Predictions from this model suggest that the RCT-inferred excess mosquito mortality rate due to ATSBs should result in reductions in malaria prevalence exceeding 30% and reductions in clinical incidence exceeding 50% for the range of transmission settings considered [26].

This analysis addressed questions directly informative of a TPP for ATSBs. An excess mortality rate due to ATSBs of ~ 0.05 per mosquito per day or higher was predicted to result in a $> 30\%$ reduction in clinical incidence in a range of settings, and an excess mortality rate of ~ 0.1 per mosquito per day or higher was found to result in a $> 30\%$ reduction in malaria prevalence [26]. Depending on the target outcome, either of these excess mortality rates could be considered a minimum criterion that would enable approval of an epidemiological field trial. An important caveat to note is that the excess mortality rate is expected to vary by environmental setting. For instance, in lush settings with an abundance of alternative sugar sources, the excess mortality rate due to ATSBs is expected to be lower. The key product parameter is therefore location-specific, and an environmental assay, such as the feeding rate on attractive sugar baits marked with dyes, would be needed to assess TPP alignment in a new location. That said; the analysis clearly demonstrates the strength of mathematical models in predicting target epidemiological outcomes for a given product parameter in a range of transmission settings.

Lessons from odor-baited traps

Odor-baited traps have long been discussed as a form of vector control [71], although their use to date has been limited to mosquito monitoring [72]. In 2010, a series of papers were published detailing odor-baited traps that are more attractive to mosquitoes than humans [64, 73], and a deterministic model describing mosquito host-seeking and ovipositing behavior [74] was adapted to model vector control with odor-baited traps in addition to LLINs [75]. One of the motivations for this mathematical analysis was to inform a TPP for odor-baited traps, as a prototype version, while potentially effective, was considered too expensive for a community-scale trial. The modeling analysis considered the entomological inoculation rate (EIR) - the rate at which people are exposed to infectious mosquito bites - as the outcome of interest, and calibrated the model to a baseline EIR greater than 200 infective bites per person per year, representing locations in Africa where transmission is consistently high.

To produce a TPP for odor-baited traps, key intervention parameters were explored - the attractiveness of traps to mosquitoes, and the number of traps per 1000 people that would

produce a reduction in EIR equivalent to that achieved by 50% coverage with LLINs (a level of coverage considered generally attainable throughout Africa). Given the number of traps required, a corresponding maximum cost per trap was calculated in order for the traps to be at least as cost-effective as LLINs. The analysis concluded that the traps should be more attractive than humans, and that 20–130 traps per 1000 people would be needed to produce the target EIR reduction. This equated to a maximum cost per trap of $4 to $27, which includes costs of production, transport, installation, operation and maintenance [75]. An interesting point raised by this and many TPP analyses is that target product characteristics can be traded off against each other - i.e., a more attractive trap can afford to be more expensive as fewer traps are required. The analysis also emphasized the importance of a comparative cost analysis, and this was influential in preventing these odor-baited traps from being adopted at scale.

Lessons from long-acting injectable drugs for seasonal malaria prevention

LAIs have been proposed as an alternative to monthly seasonal malaria chemoprevention (SMC) with oral anti-malarials in the hope that longer-lasting injectable drugs can remedy the spread of drug-resistance and the low adherence rates and high deployment costs of SMC [76]. In order for LAIs to be implemented, they must be shown to be non-inferior to existing interventions, and in lieu of clinical studies, a preliminary modeling analysis was conducted [65]. In this study, the OpenMalaria model [60] was used to predict clinical malaria cases averted by LAIs compared to SMC in the intervention age group (children 0–5 years of age). Simulations were conducted for settings that resemble Mali and Senegal in terms of seasonality, mosquito species and interventions, with these two countries being chosen because they are locations where SMC is implemented and clinical trials are frequently conducted [65]. The OpenMalaria model is an individual-based simulation of malaria in humans, including heterogeneity in mosquito biting, human immunity and disease susceptibility, and is linked to a deterministic model of mosquito life history [60, 77].

Key product parameters that were varied in this analysis describe initial LAI protective efficacy (i.e., the chance that a malaria case is prevented upon treatment with a LAI) and the shape and half-life of decay in protective efficacy. LAI coverage (i.e., the proportion of the intervention age group receiving the LAI at the beginning of a transmission season) was also varied. Results suggest that the shape of decay in protective efficacy is key, with protective efficacy profiles that remain high for an extended period (e.g. sigmoidal efficacy profiles) being essential to establish non-inferiority of LAIs. The required half-life of protective efficacy mirrored the duration of seasonal transmission in each setting, and a trade-off was observed between protective efficacy and coverage. Given the importance of decay in LAI protective efficacy, it was recommended that studying this phenomenon be prioritized in potential clinical studies [65]. Another interesting aspect of this analysis was the use of machine learning to infer non-inferior tool profiles and parameter

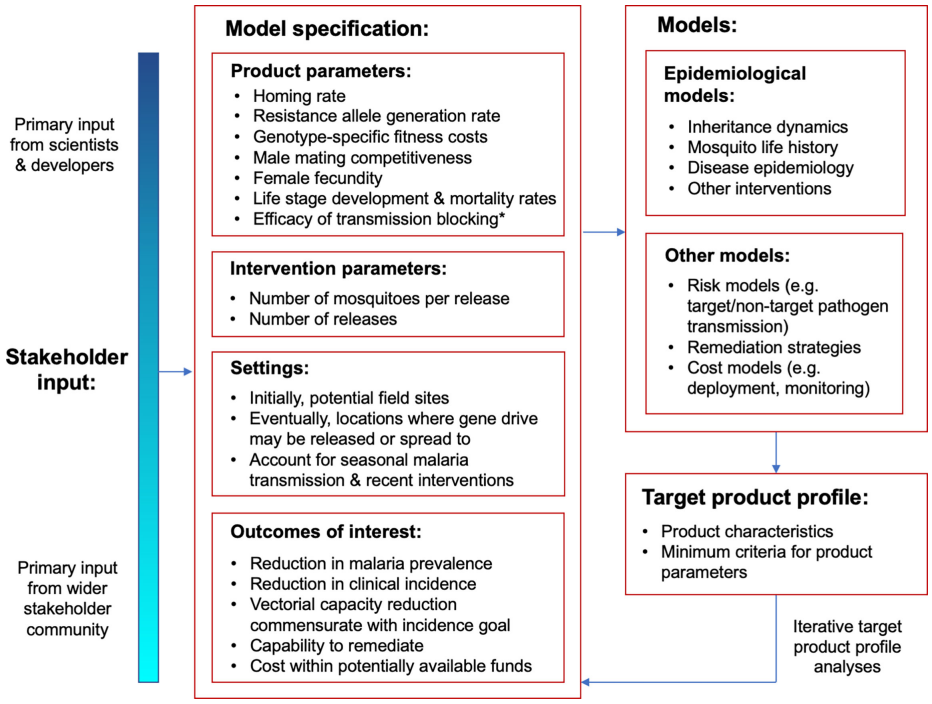

Figure 1.3: **Schematic representation of the role of mathematical models in informing target product profiles (TPPs) for gene drive mosquitoes.** Stakeholder input follows a gradient with scientists and developers providing primary input on product parameters and the wider stakeholder community providing primary input on outcomes of interest. The flowchart applies to both population modification and population suppression gene drive systems, although the product parameter for efficacy of transmission blocking only applies to population modification systems.

sensitivities based on a database of TPP malaria model simulations [78].

Special considerations for mosquito gene drive products

For mosquito gene drive products, reliable predictions from mathematical models will be required to inform TPPs prior to the first field release, as any release could potentially be irreversible. This elevates the need for rigorous modeling analyses, as accurate predictions of safety and efficacy will be required in the absence of field-testing. Here, we describe some of the special considerations that apply to mosquito gene drive products when developing model-informed TPPs, in particular concerning product parameters, target outcomes, biosafety and cost (Figure 1.3).

Product parameters

Gene drive mosquito products can be described by many parameters. The FNIH workshop on TPPs, for instance, listed homing rate, rate of functional resistance allele generation, male mating competitiveness, female fecundity, and the development and mortality rates of each life stage all as important product parameters [57]. Additionally, intervention parameters such as the number and size of releases require specification. In order to provide meaningful criteria for each parameter, consultation with molecular biologists and field ecologists will be essential to narrow the space of parameter exploration, and a machine learning approach will likely assist in exploring the refined parameter space, as it did for LAIs [78]. Previous modeling studies can also help to refine parameter space [79]. For example, the EMOD individual-based model of mosquito population dynamics [31] was used to determine the homing rate, resistance allele generation rate and female fecundity parameters required for persistent reduction of disease-competent mosquitoes in sub-Saharan African settings [80]. Fitness parameters consistently emerge as highly influential on gene drive model outcomes, and given the inaccuracy of estimating these prior to a field release, a conservative approach would be to focus on their lower bounds when generating criteria for other parameters.

Target outcomes

Ongoing discussions will likely be needed to define target outcomes for gene drive mosquito products. Epidemiological outcomes, such as reductions in clinical incidence and prevalence, are likely to be required by stakeholders such as the World Health Organization, with questions remaining over exactly what the target reduction should be. TPPs are blunt instruments, and any target reduction decided upon will likely represent a compromise between demonstrating significant public health benefit, and having an achievable goal that will enable the technology to progress along the product development pipeline. The precedent from the ATSB analysis is a 30% reduction in clinical malaria incidence or prevalence [26], while at the FNIH workshop on TPPs, a 20-50% reduction in clinical malaria incidence was discussed [57]. Such target decisions should involve a wider range of stakeholders as the technology gets closer to field release, and should include consideration of national malaria control targets, and recent and current interventions used.

Key decisions also need to be made regarding the modeled transmission settings, as these will have a significant influence on TPP specification. The LAI analysis presents an interesting case study by selecting two locations where comparable interventions and field studies have been conducted [65]. For gene drive mosquito projects, similar reasoning would support modeling population suppression products in Mali, Burkina Faso, Kenya or Uganda (field sites of the Target Malaria project), and population modification products in São Tomé and Príncipe or the Union of the Comoros (field sites of the UC Irvine Malaria Initiative). Models in these settings should take into account seasonal malaria

transmission profiles alongside current interventions being implemented. If the scale of gene drive interventions grows, then TPPs should consider a representative range of settings, spanning a diversity of local vector ecologies, and malaria transmission and intervention profiles.

For settings with more than one malaria vector present, entomological outcomes may be more suitable than epidemiological ones. To illustrate this, an alternative malaria vector could hypothetically prevent elimination of a target vector species from resulting in a 20-50% reduction in clinical malaria incidence due to the nonlinear relationship between the EIR and malaria incidence [81]. To remedy this, the target outcome could be specified as an inferred 20-50% reduction in malaria incidence due to the target species, calculated in terms of a reduction in species-specific vectorial capacity commensurate with the epidemiological goal. Other target outcomes are also important, and may include a rate of spread expected to produce the desired epidemiological impact within the time frame of a field trial (perhaps two years), and a minimum duration of effect of perhaps three years [26].

Biosafety and cost considerations

Finally, modeling may play a role in assessing some of the biosafety and cost dimensions of gene drive mosquito TPPs. One aspect of biosafety is the availability of products and strategies to remediate gene drive-modified organisms from the environment in the event of unwanted consequences or a shift in public opinion. The need and capability to remediate gene drive organisms is still being discussed [82, 83]; however, in the absence of extensive field data, modeling can provide insights to determine minimum criteria and capabilities for insecticide-based campaigns or genetic systems such as ERACR (element reversing the autocatalytic chain reaction) [84, 85] in order to achieve a defined level of transgene confinement or removal.

Some aspects of a model-informed TPP may overlap with risk assessment. For instance, whether there is a tolerable mosquito biting rate that would not be expected to enhance transmission of target and non-target pathogens [44]. Lastly, as demonstrated by case studies of odor-baited traps and LAIs, costing is another important dimension of TPPs that modeling may help to inform. Analyses focusing on deployment costs suggest that, due to their self-propagating nature, highly effective gene drives are expected to be more cost-effective than currently-available tools [86]; however, similarly detailed analyses have yet to be conducted for monitoring requirements, which are expected to be a cost driver for the technology [87]. That said; gene drives occupy a distinct niche in the malaria control toolkit due to their ability to spread and be effective despite compliance rates; therefore, costs may be best assessed against potentially available funds rather than the costs of other interventions.

1.5 Organization of this dissertation

Thus far, we have presented the preliminaries that form the basis of this dissertation; namely, the history of vector control, the epidemiology of vector-borne disease in the modern day, genetic interventions, and the role of mathematical modeling in the design of vector control products. Drawing from each of these facets, this dissertation presents three novel computational applications of gene drive modeling. Chapter 2 proposes a modeling framework to link the release of gene drive interventions in *Anopheles gambiae* to fine-scale epidemiological outcomes such as clinical incidence and prevalence. This modeling framework utilizes a sampling algorithm to link two disparate mathematical formulations (in this case, vector and human models), allowing them to communicate. This sampling algorithm can be generalized to other vector-host disease systems. Chapter 3 uses this model to develop a target product profile (TPP) for a population replacement gene drive system. By sampling thousands of biologically feasible parameter sets for product characteristics relevant to population replacement gene drive systems, we are able to statistically interrogate the relationship between genetic parameters and their expected epidemiological impact in two sub-Saharan African settings. With this analysis, we can develop "operational ranges" of each genetic parameter and evaluate them against TPP criteria for epidemiological impact. Finally, Chapter 4 presents a deep learning methodology to emulate and calibrate a complex model of malaria transmission to external data. As mathematical models become more complex and computationally demanding, model emulators can serve as important tools to reduce their computational footprint. In addition, models will need to be continually updated with estimates from field trials, and emulators can be used to align model parameters with external data. We show that, by drawing from the deep machine learning literature, we can design computationally efficient emulators of malaria transmission models and use them to calibrate the original model to field data. We hope that, taken together, this work can provide the designers of urgently-needed vector control interventions with a set of computational tools to evaluate their products and push them closer to deployment.

Chapter 2

MGDrivE 3: A decoupled vector-human framework for epidemiological simulation of mosquito genetic control tools and their surveillance

2.1 Introduction

Since the advent of CRISPR-based gene-editing, mosquito genetic control technology has been advancing at a rapid pace, with a plethora of novel genetic constructs being developed in the lab and the prospect of field releases being discussed in earnest. For malaria vectors, recent constructs include a suppression gene drive targeting the *doublesex* gene in *Anopheles gambiae* [56], a replacement gene drive linked to dual antimalarial effector genes in both *An. gambiae* and *Anopheles coluzzii* [88], and a genetic version of the sterile insect technique engineered in *An. gambiae* [41]. As the prospect of environmental releases of constructs like these nears, there is a need for increasingly detailed mathematical models to predict the spread of genes through populations, as well as their epidemiological and biosafety implications [58].

Disease transmission is a key area requiring further development in mosquito genetic control models. Models thus far have tended to emphasize entomological properties and outcomes, such as changes in allele frequencies over time and geographical spread [79, 80, 89, 90]., and while epidemiological dynamics have sometimes been incorporated, models have tended to utilize simple representations of vector-borne disease transmission, such as the Ross-Macdonald model of malaria transmission, with some exceptions [34]. Meanwhile, detailed models of malaria transmission have been developed by several groups [25, 60, 91] incorporating symptomatic and asymptomatic infection, variable parasite density in humans, age structure, mosquito biting heterogeneity, and interventions

such as vector control utilizing long-lasting insecticide-treated nets (LLINs) and indoor residual spraying with insecticides (IRS), and antimalarial drug therapy. Incorporating this level of epidemiological detail into mosquito genetic control models would be of great utility considering that genetic control tools will likely be implemented alongside other interventions, expected epidemiological impacts should be a focus in developing these products [58], and initial field trials are expected to have a measured entomological outcome alongside a modeled epidemiological one [57].

Surveillance is another key area requiring inclusion in mosquito genetic control models. Models thus far have tended to record allele frequencies and population densities directly from model output, while incorporating traps explicitly within models would allow questions related to the optimal density and placement of traps to be explored. This would be useful to assess monitoring requirements to both: i) accurately measure effectiveness of genetic control (e.g., establishment and persistence of alleles at future field sites), and ii) detect unintended spread of transgenes beyond the testing or trial site [87]. This latter concern is of particular importance for non-localized gene drive mosquito projects, which have potential to spread on a wide, potentially regional, scale. Efficient, model-informed surveillance programs are therefore essential, as surveillance is expected to be a major cost driver for this technology.

Previously, our group developed MGDrivE (Mosquito Gene Drive Explorer) [89] to model the spatial population dynamics of a variety of mosquito genetic control systems, and MGDrivE 2 [92], incorporating simple models of malaria and arbovirus transmission, seasonality in mosquito populations, and a novel formulation of mosquito and human state space utilizing stochastic Petri nets (SPNs). Here, we present MGDrivE 3, a new version of MGDrivE 2 that incorporates three major developments: i) a decoupled sampling algorithm allowing the vector and human portions of the model to be readily modularized, and hence for the mosquito portion of MGDrivE to be paired with a more-detailed epidemiological framework, ii) a version of the Imperial College London (ICL) malaria transmission model [25, 91], which incorporates age structure, various forms of immunity, human and vector interventions, and more meaningful disease outcomes, and iii) surveillance functionality that tracks mosquitoes captured by traps throughout the simulation. As such, parasite transmission can now be modeled according to mosquito genotype, genetic control interventions can now be modeled alongside other interventions (such as LLINs, IRS and antimalarial drugs), and the dynamical and surveillance implications of mosquito traps can now be modeled.

In this chapter, we describe the new features implemented in MGDrivE 3. Additionally, we present an example applying the framework to a hypothetical release of a CRISPR-based homing gene drive system linked to dual disease-refractory genes and their implications for malaria transmission in a low-transmission island setting. Simulations are also presented demonstrating surveillance of a similar drive system by a network of mosquito

traps. We conclude with a discussion of future directions and applications of MGDrivE 3 to the development and application of mosquito genetic control tools towards the goal of vector-borne disease control.

2.2 Design and implementation

As with the MGDrivE 2 framework [92], MGDrivE 3 incorporates modules for inheritance (the distribution of offspring genotypes for given maternal and paternal genotypes), mosquito life history (development from egg to larva to pupa to adult), landscape (the distribution and movement of mosquitoes through a metapopulation), and epidemiology (reciprocal pathogen transmission between mosquitoes and humans). MGDrivE 3 offers three substantial improvements beyond the functionality included in MGDrivE 2 - a sampling algorithm that allows decoupling of the mosquito and human model components, incorporation of a more detailed malaria transmission model, and inclusion of mosquito traps - each described in depth below. The software was developed using the R programming language, and retains the SPN formulation of the MGDrivE 2 package.

Decoupled vector-host sampling framework

Decoupling the vector and host portions of the modeling framework is a major contribution of MGDrivE 3. Vector-borne disease models describe the reciprocal transmission of pathogens between vectors and hosts. Prior models have represented the vector and host state space as compartmental models represented by ordinary [24] or partial differential equations (PDEs) [25, 91], or as individual-based models [93, 94]. In each of these models, vectors and hosts have the same state space and mathematical representation. In MGDrivE 3, the vector model is formulated as a SPN with a discrete state space, so we developed a sampling framework to allow the vector and host models to communicate, even if they have different representations.

Decoupling of vector-borne disease models is facilitated by the fact that all the vector model needs to know about the host model is the density and level of infectiousness in hosts, and vice versa. Communicating between the two model portions can therefore be accomplished by exchanging two composite parameters: i) the force of infection on hosts (λ_H), i.e., the probability that a host is infected per unit time, and ii) the force of infection on vectors (λ_V), i.e., the probability that a vector is infected per unit time. For malaria, λ_H is equal to the entomological inoculation rate (EIR, the number of infectious mosquitoes per human multiplied by their human biting rate) multiplied by the probability of the human becoming infected given an infectious bite. Similarly, λ_V is proportional to the human biting rate multiplied by the proportion of humans that are infectious multiplied by the probability of the mosquito becoming infected [24].

A schematic of an inter-model sampling algorithm for malaria, which we implement in this paper, is depicted in Figure 2.1. At each model iteration: i) the host model samples λ_H from the vector model, ii) the host model increments its infectious states for a time equal to one time step, iii) the vector model samples λ_V from the host model, and iv) the vector model increments its infectious states for one time step. While the MGDrivE 3 vector model is represented as an SPN with discrete state space, it is agnostic to how the host model is represented, which in this case is a system of PDEs with continuous state space [25, 91]. Additional considerations in implementing this algorithm include: i) choosing a time step appropriate to both models, ii) ensuring the MGDrivE 3 vector model produces output consistent with the vector model within the host model that it replaces, and iii) validating the EIR produced by the combined model framework. While a specific use case is presented in Figure 2.1, this inter-model sampling framework applies generally - it could equally be applied to models of arboviruses transmitted by *Aedes aegypti* [95], or to models of citrus greening disease transmitted by *Diaphorina citri* [96], provided the appropriate model adjustments are made.

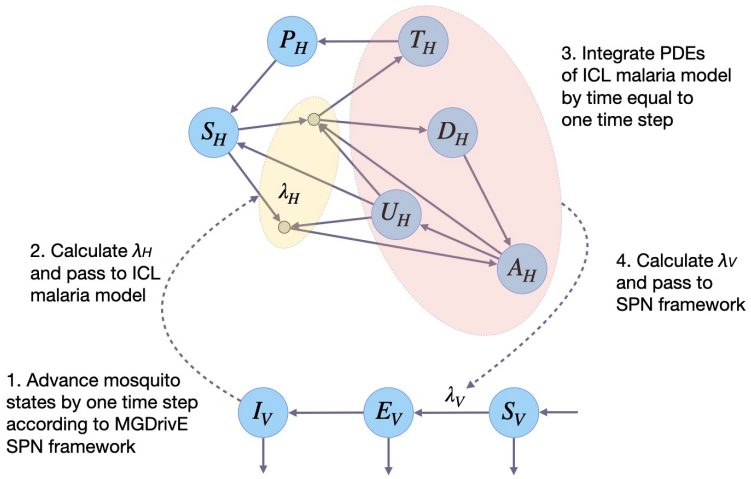

Figure 2.1: **Schematic of decoupled vector-host sampling algorithm for malaria.** MGDrivE 3 uses a stochastic Petri net framework to model progression of adult female mosquitoes from susceptible (S_V) to exposed/latently infected (E_V) to infectious for malaria (I_V). This framework is linked to an adapted version of the Imperial College London (ICL) malaria model, which is represented as a set of partial differential equations. In the ICL model, humans progress from susceptible (S_H) to either symptomatic or asymptomatic infection. Humans who develop a symptomatic infection and are either treated (T_H) or diseased and untreated (D_H). Treated humans advance to a prophylactic protection state (P_H) and eventually become susceptible again. Untreated symptomatic humans develop successively lower-density infections, from symptomatic to asymptomatic but detectable by rapid diagnostic test (RDT) (A_H) to asymptomatic and undetectable by RDT (U_H). Asymptomatic humans can also be super-infected. To allow the two frameworks to communicate, at each time step: i) the ICL human model samples the force of infection in humans (λ_H) from the MGDrivE 3 vector model, ii) the ICL human model increments its infectious states for a time equal to one time step, iii) the MGDrivE 3 vector model samples the force of infection in vectors (λ_V) from the ICL human model, and iv) the MGDrivE 3 vector model increments its infectious states for one time step.

Malaria transmission model

Given the decoupled sampling algorithm, we incorporated an adapted version of the malaria model developed by the ICL malaria modeling group [25, 91] into MGDrivE 3. The MGDrivE 3 vector framework may be linked to several published malaria models; however, the ICL model represents a suitable level of parsimony for the current stage of development, as it can be described by a succinct set of PDEs while incorporating several important features of malaria epidemiology, and has been fitted to extensive malaria data sets throughout sub-Saharan Africa [25, 91]. Important epidemiological details captured

in this model include symptomatic and asymptomatic infection, variable parasite density and superinfection in humans, human age structure, mosquito biting heterogeneity, and antimalarial drug therapy and prophylaxis. The model also includes several forms of immunity: i) pre-erythrocytic immunity reduces the probability of infection if bitten by an infectious mosquito; ii) acquired and maternal clinical immunity represent the effects of blood stage immunity on reducing the probability of developing clinical symptoms and severe illness; and iii) detection immunity represents the effects of blood stage immunity on reducing the detectability of an infection and onward transmission to mosquitoes.

The state space is modeled as a set of partial differential equations (PDEs). The infection states are: susceptible (S), treated symptomatic disease (T), untreated symptomatic disease (D), asymptomatic infection that is detectable by rapid diagnostic test (RDT) (A), sub-patent infection that is undetectable by RDT (U), and post-treatment prophylaxis (P). The force of infection on humans (which depends on the EIR) is denoted Λ, the probability that symptoms develop after an infectious challenge is denoted Φ, and the fraction of clinical cases that receive effective treatment is denoted f_T. The set of human state PDEs is shown below, with a representing age and t representing time.

$$\frac{\partial S}{\partial t} + \frac{\partial S}{\partial a} = -\Lambda S + \frac{P}{d_P} + \frac{U}{d_U}$$

$$\frac{\partial T}{\partial t} + \frac{\partial T}{\partial a} = \Phi f_T \Lambda (S + A + U) - \frac{T}{d_T}$$

$$\frac{\partial D}{\partial t} + \frac{\partial D}{\partial a} = \Phi (1 - f_T) \Lambda (S + A + U) - \frac{D}{d_D}$$

$$\frac{\partial A}{\partial t} + \frac{\partial A}{\partial a} = (1 - \Phi) \Lambda (S + U) + \frac{D}{d_D} - \Phi \Lambda A - \frac{A}{d_A}$$

$$\frac{\partial U}{\partial t} + \frac{\partial U}{\partial a} = \frac{A}{d_A} - \frac{U}{d_U} - \Lambda U$$

$$\frac{\partial P}{\partial t} + \frac{\partial P}{\partial a} = \frac{T}{d_T} - \frac{P}{d_P}$$

Here, d_i indicates the mean duration of state i. Additionally, the model includes four forms of population-level immunity:

- Pre-erythrocytic immunity, I_B, reduces the probability of infection if bitten by an infectious mosquito;
- Acquired and maternal clinical immunity, I_{CA} and I_{CM}, represent the effects of blood stage immunity in reducing the probability of developing clinical symptoms; and

- Detection immunity, I_D, represents the effect of blood stage immunity in reducing the detectability of an infection and onward transmission to mosquitoes.

The PDEs describing immunity are below. Note that ε represents the EIR, u_i limits the rate at which immunity can be boosted at high exposure for immunity state i, and d_i determines the duration of immunity for immunity state i.

$$\frac{\partial I_B}{\partial t} + \frac{\partial I_B}{\partial a} = \frac{\varepsilon}{\varepsilon u_B + 1} - \frac{I_B}{d_B}$$
$$\frac{\partial I_{CA}}{\partial t} + \frac{\partial I_{CA}}{\partial a} = \frac{\Lambda}{\Lambda u_c + 1} - \frac{I_{CA}}{d_{CA}}$$
$$\frac{\partial I_{CM}}{\partial t} + \frac{\partial I_{CM}}{\partial a} = \frac{-I_{CM}}{d_{CM}}$$
$$\frac{\partial I_D}{\partial t} + \frac{\partial I_D}{\partial a} = \frac{\Lambda}{\Lambda u_d + 1} - \frac{I_D}{d_D}$$

Each immunity function is transformed to a reduction in the appropriate infection probability via a Hill function.

Instead of numerically solving the PDEs directly, we first discretize the model by age category and biting heterogeneity. To discretize by age, we augment each infection state by an age category. For example, if we had two age categories 0-10 years and 10-100 years, then we would have susceptible compartments S_1 and S_2, where S_1 contains the people in the 0-10 year category and S_2 contains the people in the 10-100 year category. This would apply for all infection states. In addition, each compartment contains a rate at which people age and therefore move between age compartments.

Then, each PDE becomes a discrete ODE representing an age compartment. For example,

$$\frac{dS_i}{dt} = -\Lambda S_i + \frac{P_i}{d_P} + \frac{U_i}{d_U} - \eta_i S_i + \eta_{i-1} S_{i-1}$$

gives the rate equation for the susceptible (S) state for age category i where η_i gives the aging rate from $S_i \longrightarrow S_{i+1}$ and similarly η_{i-1} gives the aging rate from $S_{i-1} \longrightarrow S_i$. For the youngest age group, the $\eta_{i-1} S_{i-1}$ term would be left out, and for the oldest age group, the $\eta_i S_i$ term would be left out.

One implementation note is that the model assumes a fixed latent period of 12 days after an infectious challenge from a mosquito, after which either symptoms develop or an asymptomatic infection proceeds. Because of this fixed delay, the equations are technically formulated as "delay differential equations," where the current state depends on the

previous state.

To initialize the distribution of disease and immunity states, the model takes as input the baseline EIR, the age structure of the population, the proportion of treated cases, and baseline entomological parameters. Some of the mosquito life cycle parameters will vary in the presence of interventions, which will be described in the next section.

In incorporating certain genetic vector control tools - e.g., gene drive systems intended to spread disease-refractory genes into mosquito populations [88, 97] - an important addition to the epidemiological framework is transmission parameters that are mosquito genotype-specific. In the ICL malaria model, the force of infection on humans, $\lambda_H(a,t)$, is dependent on both age, a, and time, t, and is a product of the EIR, $\varepsilon(a,t)$, and the transmission probability, b, i.e.:

$$\lambda_H(a,t) = \varepsilon(a,t)b$$

A given human could be bitten by a mosquito having any genotype, g, from the set of all genotypes, $\mathcal{G}$, proportional to its time-varying frequency in the population, $p_g(t)$. For an effector gene that blocks mosquito-to-human transmission, the transmission probability, b_g, will be genotype-specific, and so the expected transmission probability is equal to the time-varying weighted average:

$$b(t) = \sum_{g \in \mathcal{G}} p_g(t) b_g$$

Incorporating more epidemiological detail into the model of transmission dynamics also allows more nuanced epidemiological outcomes to be calculated. As the ICL malaria model is age-stratified, both malaria prevalence and incidence can be calculated according to age group. Prevalence is calculated across all infectious human compartments - treated and untreated symptomatic disease, asymptomatic but detectable by rapid diagnostic test (RDT), and asymptomatic but undetectable by RDT - since each of these compartments contributes to onwards transmission of malaria to mosquitoes. Clinical incidence refers to new clinical malaria cases within a defined time interval, and is of particular relevance to the healthcare system. One commonly reported metric is malaria prevalence among children aged 2-10 years [98], as pediatric cases of malaria tend to be the most severe. Mathematically, we define *PfPr* as the sum of all individuals in infectious disease states: symptomatic and treated (T), symptomatic and untreated (D), asymptomatic patent infection (A), and asymptomatic subpatent infection (U). Therefore, the all-ages (often denoted by the subscript 0-99 to denote the entire lifespan in years) pathogen prevalence at a given time point, t, is given by:

$$PfPr_{[0-99]}(t) = \sum_{a \in \mathcal{A}} (A_a(t) + U_a(t) + D_a(t) + T_a(t))$$

where $\mathcal{A}$ is the set of all age compartments. Similarly, the 0-2 years *PfPr* is given by:

$$PfPr_{[0-2]}(t) = A_{[0-2]}(t) + U_{[0-2]}(t) + D_{[0-2]}(t) + T_{[0-2]}(t)$$

As for clinical incidence, we first define some parameters:

- ϕ: the probability of acquiring clinical disease upon infection (proportional to immunity levels via a Hill function);
- λ_H: the force of infection on humans (linearly proportional to the EIR, ε); and
- Y: the sum of non-clinical disease states, susceptible (S), asymptomatic patent infection (A), and subpatent infection (U).

Then we can define the all-ages clinical incidence as:

$$CI_{[0-99]}(t) = \sum_{a \in \mathcal{A}} \phi_a(t) \lambda_{H,a}(t) Y_a(t)$$

and the 0-2 years clinical incidence as:

$$CI_{[0-2]}(t) = \phi_{[0-2]}(t) \lambda_{H,[0-2]}(t) Y_{[0-2]}(t)$$

Generally, we are interested in these outcomes with respect to their baseline or pre-intervention values. In our analyses, we will calculate the reduction in prevalence and clinical incidence as our outcomes of interest. As we will be running many stochastic repetitions of the simulation for a given parameter set, the mean reduction over the repetition set and simulation timespan will be used.

Additional interventions and seasonality

Additional functionality has been included in both the vector and host portions of the MGDrivE 3 framework to incorporate currently-available interventions that genetic control tools would likely be implemented in conjunction with. While a range of novel vector control tools are currently under development [99]; the mainstay of malaria interventions for the last two decades has been a combination of LLINs, IRS and antimalarial drugs - largely artemisinin-combination therapy (ACT). Some combination of these interventions will invariably be present when a genetic control intervention is implemented, and it is important to characterize their implications for both vector population dynamics and vector-borne disease transmission. We model the impact of LLINs and IRS on mosquito life history parameters according to the elaborated feeding cycle model developed by Le Menach *et al.* [70] and adapted by Griffin *et al.* [25, 91]. Within this framework, LLINs and IRS increase the mortality rate and decrease the biting rate of adult mosquitoes, and also decrease the egg-laying rate by virtue of extending the gonotrophic cycle. The proportion of symptomatic malaria cases that receive antimalarial drug therapy is included

within the ICL malaria model [25, 91].

First, we assume that, at baseline, we have three proportions of active vector control interventions, $\{\chi_{IRS}, \chi_{LLIN}, \chi_{ACT}\}$, which represent the proportion of humans in the model covered by the given intervention. Then, χ_{ACT} corresponds to the proportion of symptomatically infected humans that are treated upon infection, f_T.

Then, $\{\chi_{IRS}, \chi_{LLIN}\}$ jointly modify various mosquito life cycle parameters. First, we model the impact of LLINs and IRS on the length of the mosquito gonotrophic cycle (i.e., the time taken for a mosquito to take a blood meal and lay eggs before seeking its next blood meal). This time can be divided into τ_1 (the time spent foraging) and τ_2 (the time spent ovipositing and resting). Then, the length of the gonotrophic cycle in the presence of vector control is given by:

$$\frac{1}{\delta_c} = \frac{\tau_1(0,0)}{1-z} + \tau_2$$

where $\tau_1(0,0)$ represents the time spent foraging with LLIN and IRS coverages of zero, and:

$$\begin{aligned} z = Q_0 c_{LLIN} \theta_B r_{LLIN} + Q_0 c_{IRS} \theta_I r_{IRS} + \\ Q_0 c_{LLIN,IRS} (\theta_I - \theta_B) r_{IRS} + \\ Q_0 c_{LLIN,IRS} \theta_B r_{IRS,LLIN} \end{aligned}$$

Here, Q_0 represents the human blood index, θ_B represents the proportion of bites taken on a person in bed, θ_I represents the proportion of bites taken on a person outdoors, r_{IRS} represents the probability of repeating a feeding attempt in the presence of IRS, $r_{IRS,LLIN}$ represents the probability of repeating a feeding attempt in the presence of IRS and LLINs, and:

$$\begin{aligned} c_{LLIN} &= \chi_{LLIN} - \chi_{LLIN}\chi_{IRS} \\ c_{IRS} &= \chi_{IRS} - \chi_{LLIN}\chi_{IRS} \\ c_{LLIN,IRS} &= \chi_{LLIN}\chi_{IRS} \\ c_0 &= 1 - \chi_{LLIN} - \chi_{IRS} + \chi_{LLIN}\chi_{IRS} \end{aligned}$$

Then, with the modified gonotrophic cycle calculated (δ_C), we can model the impact of LLINs and IRS on the adult mosquito death rate. We express the mortality rate in the presence of vector control as:

$$\mu_{V,C} = -\log p(\chi_{IRS}, \chi_{LLIN})$$

where p represents the probability of an adult mosquito surviving one day. Then we can break down p into two components p_1 (the probability of surviving the mosquito stage) and p_2 (the probability of surviving the blood meal stage):

$$p(\chi_{IRS}, \chi_{LLIN}) = (p_1(\chi_{IRS}, \chi_{LLIN}) p_2)^{\delta_c}$$

where:

$$p_1(\chi_{IRS}, \chi_{LLIN}) = \frac{p_1(0,0)w}{1 - zp_1(0,0)}$$

z is the same as above and w gives the probability that a mosquito successfully feeds and survives a single feeding attempt:

$$\begin{aligned} w = 1 - Q_0 + Q_0 c_0 + Q_0 c_{LLIN}(1 - \theta_B + \theta_B s_{LLIN}) + \\ Q_0 c_{IRS}(1 - \theta_I + \theta_I s_{IRS}) + \\ Q_0 c_{IRS,LLIN}((\theta_B - \theta_I) s_{IRS} + 1 - \theta_I + \theta_B s_{LLIN,IRS}) \end{aligned}$$

Here, s_{LLIN} and s_{IRS} represent the probability of feeding and surviving in the presence of LLINs and IRS, respectively. The non-intervention survival probabilities are given by:

$$\begin{aligned} p_1(0,0) &= e^{-\mu_V \tau_1(0,0)} \\ p_2 &= e^{-\mu_V \tau_2} \end{aligned}$$

Now, we have mathematical expressions for the gonotrophic cycle length and adult mortality rate (δ_c and $\mu_{V,c}$ respectively). We can finally model the impact of LLINs and IRS on the egg laying rate of the adult female mosquito. In the absence of vector control, the egg laying rate is given by:

$$\beta = \frac{\varepsilon \mu_V}{e^{\frac{\mu_V}{\delta}} - 1}$$

where ε is the number of viable eggs laid per oviposition cycle. Then, with the previously defined parameters, the egg laying rate in the presence of vector control interventions is simply:

$$\beta_c = \frac{\varepsilon \mu_{V,c}}{e^{\frac{\mu_{V,c}}{\delta_c}} - 1}$$

Finally, we can modify the human biting rate per mosquito in the presence of LLINs and IRS. In the absence of interventions, the biting rate is given by:

$$a_V = \delta Q_0$$

The biting index under intervention is given by:

$$Q_c = 1 - \frac{1 - Q_0}{w}$$

where w is the calculated probability from above. Then, using the modified gonotrophic cycle length previously derived (δ_c), the modified biting rate is thus:

$$a_{V,c} = \delta_c Q_c$$

With these definitions in place, we have fully specified the impact of vector control interventions on mosquito life cycle parameters.

MGDrivE 3 also includes updated functionality for incorporating seasonal weather patterns. While MGDrivE 2 allows mosquito life history parameters, such as adult and larval development and mortality rates, to vary with time in response to environmental variables such as temperature and rainfall [92], the new framework utilizes environmental data to generate seasonal profiles to modulate these parameters. Rather than using raw daily rainfall data, which varies from year to year, the Umbrella R package [100] is used to fit a mixture of sinusoids to the rainfall data. This provides a more general characterization of the seasonal trends at a given location, and facilitates comparison across other locations with similar seasonal patterns. As with MGDrivE 2, development times are Erlang-distributed, and the model of White *et al.* [92] is used to modulate larval carrying capacity and hence density-dependent mortality in response to recent rainfall - a key driver for *Anopheles* population dynamics.

Traps and spatial surveillance

In MGDrivE 3, the landscape module of MGDrivE 2 has been extended to accommodate traps as part of the mosquito metapopulation. In MGDrivE and MGDrivE 2, the landscape module describes the distribution of mosquitoes across discrete, randomly-mixing population nodes, with movement between them quantified by a dispersal kernel [89, 92]. MGDrivE 3 additionally accommodates "trap nodes" in one of two ways: i) traps are placed within a subset of population nodes, and are associated with a probability of trapping for mosquitoes within the corresponding population node per unit time, and ii) traps are assigned their own nodes, and are associated with coordinates and an attractiveness kernel, which includes an amplitude, mean distance of attractiveness, and other parameters as required by the kernel function. The former case is appropriate for applications on a larger spatial scale (e.g., where population nodes represent villages that traps may be placed in), while the latter is appropriate for applications on a finer spatial scale (e.g., where nodes represent blood, sugar or water sources that traps are placed relative to). In both cases, the landscape including traps may be generated using MGSurvE (Mosquito Gene Surveillance) [101]. Here, the number and locations of traps may be user-specified, along with their trapping probabilities (for the former case) or attractiveness kernel parameters (for the latter case), which should be chosen according to the types of traps being modeled. Data analysis functions are provided to visualize the distribution of mosquitoes having certain genotypes that are captured by each trap over time.

2.3 Results

To demonstrate how MGDrivE 3 can be used to simulate releases of gene drive-modified mosquitoes, including implications for epidemiological outcomes and surveillance, we have provided examples and information on GitHub. In the first example, we model the release of a full gene drive system designed to drive malaria-refractory genes into

an *An. coluzzii* mosquito population with seasonal population dynamics, pre-existing interventions and transmission intensity calibrated to a setting resembling the island of São Tomé, São Tomé and Príncipe. The full gene drive system resembles one engineered in *An. coluzzii* [88], which includes dual linked effector genes targeting the malaria pathogen, and is one of the most promising population replacement systems in a mosquito vector to date. While we model this system in a setting chosen largely for its isolation [102], we note that regulatory and biosafety issues must be considered seriously for self-propagating systems with the potential to spread beyond their release site [103].

Four alleles are considered at the gene drive locus: an intact drive allele containing disease-refractory genes (denoted by "H"), a wild-type allele (denoted by "W"), a functional, cost-free resistant allele (denoted by "R"), and a non-functional or otherwise costly resistant allele (denoted by "B"). The inheritance dynamics of this system were fitted to laboratory cage data and are provided in Carballar-Lejarazú *et al.* [88] with model parameters summarized in Table. Notably, we considered a 10% fitness cost associated with mosquitoes carrying either one or two copies of the intact drive allele, as there were no major fitness loads inferred in the *An. coluzzii* cage experiments [88]; however, fitness costs due to integration and expression of the gene drive system could become apparent in the field. Additionally, we assume that mosquitoes carrying either one or two copies of the H allele confer complete mosquito-to-human transmission blocking, consistent with data from Carballar-Lejarazú *et al.* [88] for sporozoite thresholds $\geq 7,500$.

The life history module is parameterized with typical bionomic parameters for *An. coluzzii* [28, 104], with incorporation of a generalized seasonal profile that modulates certain life history parameters. In MGDrivE 3, as in MGDrivE 2, the carrying capacity of the environment for larvae is a function of recent rainfall, and a mathematical relationship from White *et al.* [28] is used to translate local rainfall data to larval carrying capacity; however, in this example, we capture broad variations in the rainfall profile of São Tomé and Príncipe using the umbrella [100] package in R, using a shapefile of the national administrative boundary and a three-year timeframe for rainfall data (Figure 2.2). Otherwise, the life history module mirrors that of MGDrivE 2, including mean-variance relationships describing development times of the juvenile life stages [105]. For the purpose of this demonstration, and to emphasize the novel epidemiological component of MGDrivE 3, the island of São Tomé was treated as a single randomly mixing population.

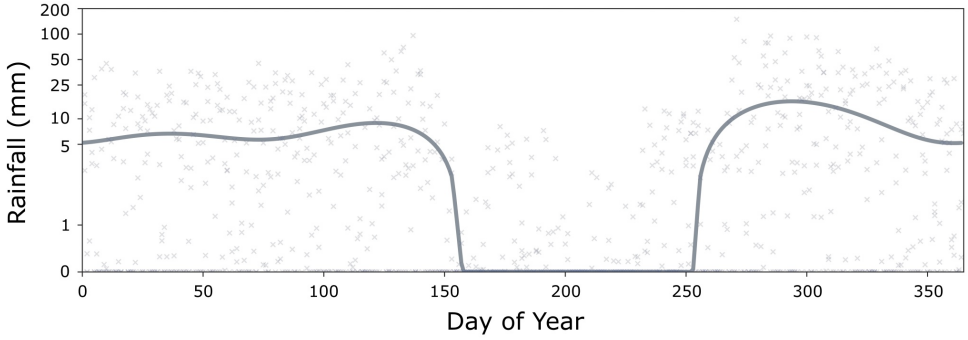

Figure 2.2: **Seasonal rainfall profile for São Tomé and Príncipe.** Points represent mean daily rainfall measurements (in mm) for the three years between January 1st, 2017 and December 31st, 2019. The solid line represents the seasonal rainfall profile, fitted using the umbrella [100] package in R, used to calculate the time-varying environmental carrying capacity for larvae in the life history module of MGDrivE 3.

The ICL malaria model is parameterized according to published intervention coverage and transmission levels for São Tomé and Príncipe - an LLIN coverage of 62%, IRS coverage of 66.5%, 2% of symptomatic malaria cases being treated with antimalarial drugs, and an all-ages *P. falciparum* prevalence of 2%, according to the World Health Organization Global Health Observatory (https://www.who.int/data/gho). The LLIN and IRS coverage parameters modify vector parameters in the life history module, while the antimalarial treatment parameter is input directly into the ICL model. Output from the ICL malaria model is then calibrated to all-ages malaria prevalence in the context of interventions and the seasonal rainfall profile by multiplying the carrying capacity for larvae by a constant. Other parameters of the ICL malaria model describe heterogeneity, human infectious periods, various types of immunity and treatment, and are as described in the original model [25, 91]. Finally, we note that these simulations are intended to demonstrate the software's capabilities and that, while the simulations are calibrated to data from São Tomé, they are not intended to provide an accurate forecast of gene drive dynamics on the island, or to imply approval of the intervention by the local population and regulatory agencies.

Simulation workflow

The code for running this simulation is available here. We begin by loading the MGDrivE and MGDrivE 2 packages in R to gain access to the inheritance cubes, mosquito life history and malaria modeling functionality required for the simulation. Next, we load the inheritance cube for the TP13 population replacement gene drive system in *An. coluzzii* [88]. This specifies the inheritance-biasing properties of the system, as well as its malaria transmission-blocking effect. Note that there are a variety of other inheritance

cubes available in the MGDrivE software - e.g., *Wolbachia* [106], release of insects carrying a dominant-lethal gene (RIDL) [107], precision-guided sterile insect technique (pgSIT) [41], population suppression gene drive [56], and remediation systems such as ERACR (element for reversal of the autocatalytic chain reaction) [85] - and users are also able to design their own inheritance cubes. Next, we specify general simulation parameters, such as the simulation length, the timestep of the stochastic model, and the timestep at which data is output (daily). Fitted reproductive fitness parameters for the TP13 construct in *An. coluzzii* [88] are loaded, and a 10% fitness load on male mating competitiveness and female fecundity is implemented, as described earlier.

Next, we specify details of the epidemiology module - baseline malaria prevalence, human population size, human age stratification, and coverage levels of LLINs, IRS and antimalarial drugs. Following this, as with MGDrivE 2, the "places" and "transitions" of the SPN formulation are set up using the "spn_P_epi_decoupled_node()" and "spn_T_epi_decoupled_node()" functions. Equilibrium values of states in the mosquito and human models are calculated using the "equilibrium_Imperial_decoupled()" function, and as the ICL malaria model requires the annual EIR to calculate the state distribution at equilibrium, a function is provided to convert malaria prevalence to EIR. Next, the seasonal rainfall profile used to calculate the larval carrying capacity time-series (described above) is used to calculate time-varying hazard rates for density-independent larval mortality. Custom time-varying hazard functions for larval mortality are provided, and hazard functions are provided for the mosquito life history and ICL malaria transmission models. The MGDrivE 2 vignette, "Simulation of Time-inhomogeneous Stochastic Processes," provides instructions for writing user-specified time-varying hazard functions. Finally, we specify the release scheme - genotypes, size and timing of releases - using an "events" dataframe.

With all model components specified, we call the "sim_trajectory_R_decoupled()" function to simulate model trajectories. This implements a tau-leaping algorithm to sample stochastic trajectories, and records daily output to an R dataframe. For further analysis external to R, we provide functionality to write simulation output to CSV files.

Entomological dynamics

In Figure 2.3, we display a potential visualization scheme for the entomological and epidemiological outcomes of the simulated gene drive mosquito release described above. This figure was generated in Python and is available here. We note that MGDrivE 3 is not dependent on Python, and the MGDrivE 3 R package provides basic plotting and analysis functions for model output visualization. In this case, we generated data for 15 stochastic model repetitions, and the dynamics displayed in Figure 2.3 depict the mean output of these repetitions. Figure 2.3(A) depicts allele frequencies for adult female mosquitoes over the simulation period. After eight consecutive releases of 20,000 male mosquitoes

homozygous for the TP13 construct (H), the H allele rapidly spreads through the population, reaching near-fixation within a few months. This is a result of the high accurate homing rate, as determined by laboratory experiments [88], relatively low fitness costs (estimated), and low rate of resistance allele generation. Homing-susceptible wild-type alleles (W) are quickly eliminated, although a few in-frame and out-of-frame resistance alleles (R and B, respectively) accumulate since, although they are generated infrequently, they slightly outcompete the H alleles in terms of fitness. Note that while these dynamics represent a potential outcome of TP13 gene drive mosquito releases, the dynamics are highly dependent on the relative fitness of H and R/B allele-carrying mosquitoes, while are difficult to accurately quantify outside the field.

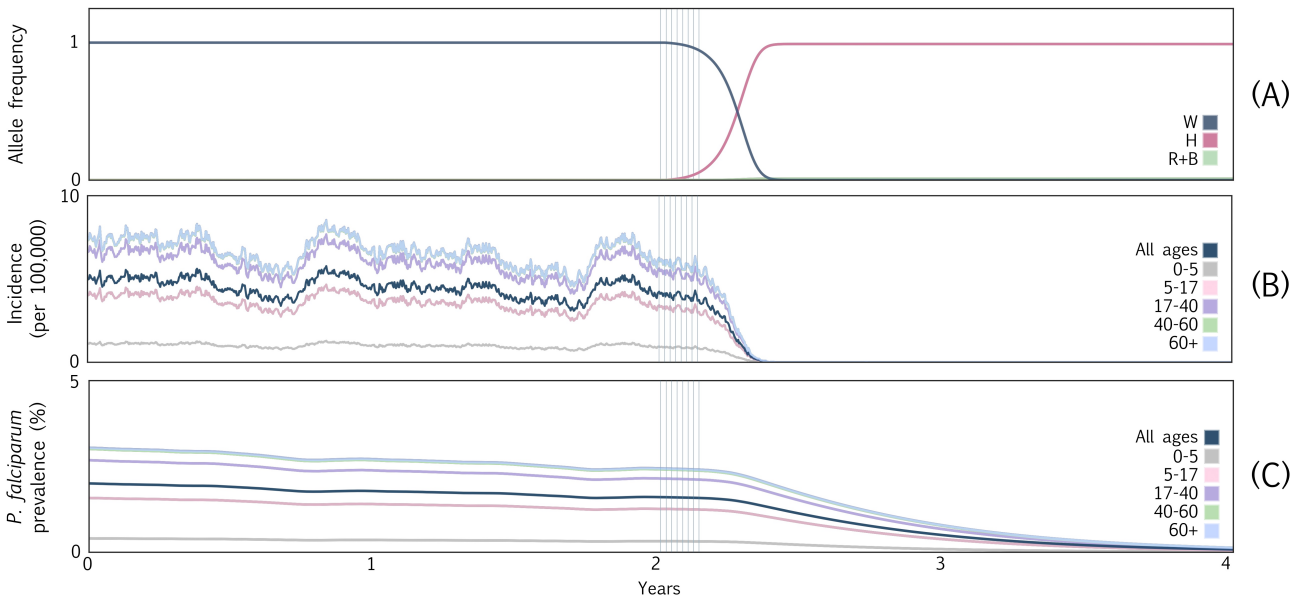

Figure 2.3: **Example MGDrivE 3 simulations for a full gene drive system designed to drive dual malaria-refractory genes into an *An. coluzzii* mosquito population with seasonal population dynamics, transmission intensity and interventions calibrated to a setting resembling the island of São Tomé, São Tomé and Príncipe.** The gene drive system resembles one recently engineered in *An. coluzzii* [88] in which all drive components - the Cas9, guide RNA and effector genes - are all present at the same locus. Four alleles are considered: an intact drive allele (denoted by "H"), a wild-type allele (denoted by "W"), a functional, cost-free resistant allele (denoted by "R"), and a non-functional or otherwise costly resistant allele (denoted by "B"). **(A)** Allele frequencies for adult female mosquitoes over the simulation period. Grey vertical bars beginning at year two denote eight consecutive weekly releases of 20,000 male mosquitoes homozygous for both the gene drive construct. The high efficiency of the drive system and low rate of resistance allele generation mean that almost no disease-competent *An. coluzzii* mosquitoes remain five months after the release. **(B)** Daily clinical malaria incidence per 100,000 people partitioned according to age group. Reductions in human incidence within five months of the release parallel spread of the drive construct in the mosquito population. **(C)** *P. falciparum* malaria prevalence partitioned according to age group. As humans recover from infection and few develop new infections, the *P. falciparum* parasite rate declines until it reaches near undetectable levels by year five.

Epidemiological dynamics

Here, we demonstrate the refined epidemiological outcomes obtained by linking the human portion of the ICL malaria transmission model to the vector portion of MGDrivE 3. We depict age-stratified clinical incidence in Figure 2.3(B) and age-stratified prevalence

in Figure 2.3(C). The rapid spread of the gene drive allele through the *An. coluzzii* population, and its strong modeled transmission-blocking effect, mean that humans are no longer exposed to new infectious mosquito bites five months after the beginning of the release schedule, and hence clinical incidence also falls to zero on this timescale. Notably, clinical incidence includes symptomatic cases that are either treated or untreated (i.e., the T_H and D_H compartments in the ICL malaria model depicted in Figure 2.1), and does not include asymptomatic cases that are either detectable or undetectable by RDTs (i.e., the A_H and U_H compartments depicted in Figure 2.1). Stochastic variation in clinical incidence is pronounced due to the small number of incident cases relative to the total population.

São Tomé is a low-transmission setting with little acquired immunity, so incidence and prevalence are lower in younger age groups (0-5 and 5-17 years old) due to maternal immunity and the lesser skin surface area available for mosquito bites. *P. falciparum* prevalence includes all diseased states - i.e., symptomatic disease, whether treated or untreated (T_H and D_H, respectively), and asymptomatic disease, whether detectable or undetectable by RDTs (A_H and U_H, respectively). Prevalence in the human population takes much longer to decline than incidence, as an individual can harbor *P. falciparum* parasites for 1-2 years if left untreated [108], which is common for asymptomatic infections. These predictions highlight the transformative promise of gene drive interventions for malaria control; however, we caution that there are several limitations - notably, treatment of São Tomé as a panmictic population of humans and mosquitoes, calibration to malaria prevalence data that is likely underreported [109], and lack of knowledge of the fitness and transmission parameters of gene drive mosquitoes in the field, including their evolution over several years - which preclude the confidence with which such predictions can be made.

Spatial surveillance

Finally, we demonstrate the capability of MGDrivE 3 to simulate surveillance of mosquitoes via traps placed throughout a landscape. The code for this example is available here. We used the MGSurvE framework [101] to optimize the placement of five traps across a spatial network resembling the southern portion of São Tomé, São Tomé and Príncipe. This landscape is described by Sánchez C. *et al.* [101] - namely, nodes were sourced from the São Tomé and Príncipe census and aligned with coordinates from Google Maps. Daily mosquito movement probabilities were derived using an ecology-motivated algorithm [110], with model output calibrated to mark-release-recapture experiments on *An. gambiae sensu lato* [111, 112]. Traps were placed within population nodes to represent placement within selected villages, and trapping probabilities were specified, along with the rest of the landscape, in MGSurvE.

We consider a release in the southernmost population node of the island and monitor the progression of gene drive phenotypes for trapped mosquitoes over time. As for the epidemiological simulation, we consider eight weekly releases of male *An. coluzzii* homozygous for the gene drive system. We consider a simplified version of the TP13 gene drive construct [88] with only a single resistance (R) allele. The cutting frequency at the target site for this construct is 1.0, and the rate of accurate homology-directed repair is 0.99. The inheritance cube is flexible to specify genotype-specific mating fitness, multipliers on adult mortality, male and female pupatory success, and reductions in fertility, but we do not modify them in this example. We model mosquitoes as accumulating in traps over the course of a week, after which they are counted and the traps are "reset." We also tally gene drive phenotypes when trapped mosquitoes are counted, considering a marker allele associated with both the intact drive allele (H) and the wild-type target allele (W) [88]. This allows us to distinguish the following genotypes: HH/HR, WW/WR, HW, and RR. Figure 2.4 depicts the time-series of gene drive marker phenotypes in each trap by week, with the time of first detection of a transgenic mosquito indicated by a vertical line for each trap. Output like this will be useful to model surveillance strategies for the progression of field trials and interventions, and the emergence of alternative alleles that could interfere with intervention effectiveness [87].

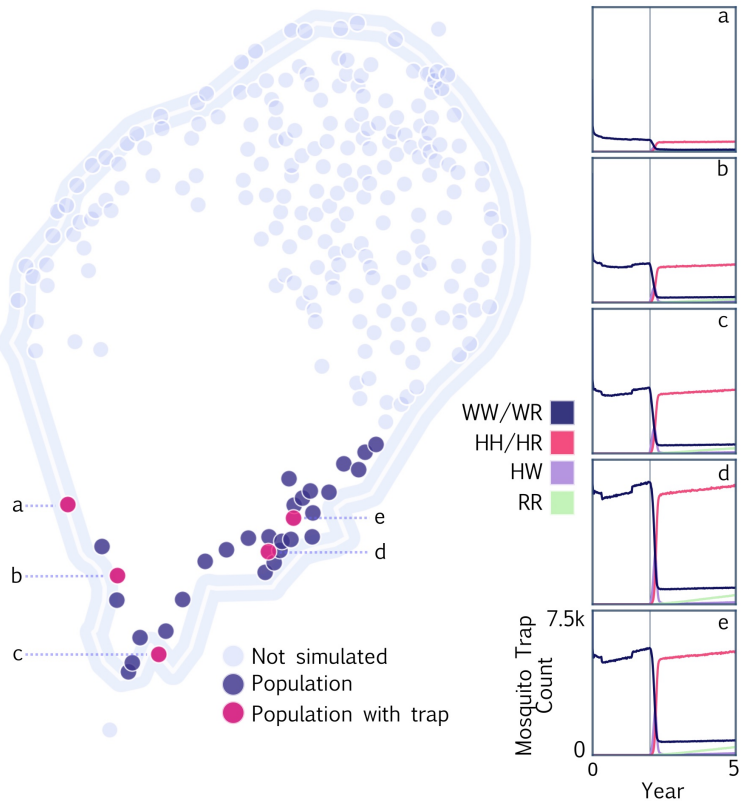

Figure 2.4: **Example MGDrivE 3 simulations for spatial surveillance of a full gene drive system on the island of São Tomé, São Tomé and Príncipe.** Mosquito population nodes represent villages and suburbs of comparable size with mosquito movement probabilities between localities derived from an ecology-motivated algorithm [110] and calibrated to mark-release-recapture data [111, 112]. Simulation was restricted to the southern portion of the island, with population nodes including traps depicted in pink and other population nodes depicted in blue. Traps were placed using the MGSurvE framework [101]. Eight weekly releases of a full gene drive system (cutting rate of 1.0 and homology-directed repair rate of 0.99) were simulated in the southernmost population node of the island, and the phenotype distribution of trapped mosquitoes is depicted for the five trap nodes in panels a-e. Vertical lines denote the time of first transgene detection for each trap.

2.4 Availability and future directions

MGDrivE 3 is available on CRAN as version 2.1.0 of the MGDrivE 2 package, due to naming conventions. The source code is under the GPL3 License and is free for other groups to modify and extend as needed. Mathematical details of the model formulation are available in the S1 Text. Examples for running MGDrivE 3 simulations are available

on GitHub, and documentation for MGDrivE 3 functions are available at the MGDrivE 2 project website. To run the software, we recommend using R version 3.1.0 or higher.

We are continuing development of the MGDrivE 3 software package and welcome suggestions and requests from the research community regarding future directions. As gene drive mosquito projects advance from the lab to the field, we intend our software to address the evolving modeling needs of the technology [83] - from contributing to TPPs [58] and environmental risk assessments [47], to planning field trials, interventions [79, 80] and surveillance programs [87]. The epidemiological extensions offered in MGDrivE 3 will enable more accurate predictions of implications of mosquito genetic control for disease transmission, which are relevant as an outcome for TPPs, and field trial and intervention planning. This will also enable prediction of the impact of genetic control interventions alongside other currently-implemented interventions such as LLINs, IRS and ACTs. The surveillance extensions included in MGDrivE 3 will enable assessment of mosquito trapping schemes to both: i) measure the effectiveness of genetic control strategies in the field, and ii) detect unintended spread of gene drive alleles beyond field sites, and the emergence of alternative alleles broadly [87].

Logistical modeling questions are invariably associated with larger state spaces - more genotypes to keep track of, more human and mosquito disease states, and larger metapopulation networks - which quickly approach the computational limits of the modeling framework. To address this, we are exploring numerical sampling algorithms to increase computational efficiency and speed, and the use of lower-level programming languages such as C++. We are also interested in linking the vector portion of MGDrivE 3 to other epidemiological models that capture human transmission dynamics more comprehensively - e.g., dengue models that incorporate multiple serotypes with temporary cross-protective immunity and complications related to antibody-dependent enhancement [95], and individual-based malaria transmission models that allow sources of heterogeneity to be incorporated more comprehensively and for infection history to be directly associated with immune status [25, 91]. There are also opportunities to adapt the framework to species of relevance to agriculture and conservation - e.g., enhanced epidemiological capabilities could be applied to citrus greening disease transmitted by *D. citri* [96], and surveillance functionality could be suitable for models of invasive rodents on islands [113].

Chapter 3

Model-informed target product profiles of population modification gene drive for malaria control

3.1 Introduction

Malaria continues to pose a major public health burden throughout much of the world, especially in sub-Saharan Africa, where over 90% of the cases and deaths occur [5]. Despite the wide-scale distribution of insecticide-based interventions and antimalarial drugs beginning in 2000, malaria persists at an unacceptably high level [114], and it is clear that new tools will be needed for continued reductions in disease incidence and mortality. Two of the most promising novel tools at present are malaria vaccines and gene drive-modified mosquitoes. Gene drive approaches bias inheritance in favor of an introduced allele intended to spread through the mosquito population, and fall into two main categories: i) "population suppression," whereby the introduced allele induces a fitness load or sex bias, reducing mosquito numbers, and ii) "population modification," whereby the introduced allele disrupts pathogen transmission, reducing mosquito vector competence [37]. Candidate constructs for both approaches have been developed in the laboratory - most notably: i) a CRISPR-based system that targets the *doublesex* gene in Anopheles gambiae, the main African malaria vector, causing sterility in female homozygotes and inducing collapse of cage populations [56], and ii) CRISPR-based systems carrying dual antimalarial effector genes in *An. gambiae* and *Anopheles coluzzii*, demonstrating rapid spread through cage populations [88]. Discussions regarding field trials of these systems are currently underway [115].

In order for gene drive mosquitoes to advance from the laboratory to environmental release, their characteristics will be assessed against target product profiles (TPPs) - planning tools that provide a list of preferred characteristics and minimum criteria products

must satisfy as they progress through the development pipeline. TPPs have recently been developed for a range of new malaria and vector control tools - including attractive targeted sugar baits (ATSBs) [26], long-acting injectable drugs [65], and malaria vaccines [63]. For mosquitoes engineered with low-threshold gene drive systems, developing and satisfying TPP criteria is particularly important given the potential for transgenes to become established in local mosquito populations following a release, and the expected difficulty of remediation efforts in the event of undesired outcomes or a shift in public opinion [103]. A draft TPP has been proposed for population modification gene drive products [59], and a workshop hosted by the Foundation for the National Institutes of Health (FNIH) discussed TPPs for gene drive products at length [57]. These preliminary discussions suggest a 20-50% reduction in clinical malaria incidence as a target outcome for a gene drive release, alongside a rate of spread that would produce this impact within the time frame of a field trial (less than a year), and a duration of impact of at least three years. These target outcomes are subject to change pending wider stakeholder input.

Mathematical models will necessarily inform TPP criteria for gene drive mosquitoes, as key target outcomes are primarily epidemiological (e.g., reductions in clinical incidence of malaria) and can only be observed following a release [58]. Models are therefore needed to infer target parameter values for gene drive mosquito products, such as rates of homing and resistance allele generation, based on target epidemiological outcomes in the context of a given release scheme and setting of interest. Fortunately, over the last 15 years, there has been a growth in the field of malaria modeling, with several detailed models being developed that concisely describe malaria transmission dynamics in the mosquito vector and human host [25, 31, 77]. Concurrently, and particularly since the advent of CRISPR-based gene editing, several modeling frameworks have been developed to describe the population dynamics of mosquito genetic biocontrol tools [79, 89, 116]. Most relevant to TPPs, Leung *et al.* [34] used the EMOD malaria model to infer parameter values for population modification gene drive systems expected to eliminate malaria in low-to-moderate transmission settings in the Sahel, West Africa. The Imperial College London (ICL) malaria model has also been used to model epidemiological outcomes of population suppression and modification gene drives [117, 118].

Here, we investigate parameter values for population modification gene drives that satisfy the epidemiological target outcomes outlined by James *et al.* [57] - namely, a 50% reduction in clinical malaria incidence for a duration of at least three years, and a time to impact of less than a year. These outcomes represent the most demanding criteria specified by James *et al.* [57] to reflect the fact that models, as a simplified representation of the real world, may potentially overestimate the success of a tool that has not yet been field tested. To seed the population with the gene drive system, we simulate eight consecutive weekly releases of gene drive-modified An. gambiae, and consider this alongside existing interventions - long-lasting insecticide-treated nets (LLINs), indoor residual spraying with insecticides (IRS), and artemisinin combination therapy drugs (ACTs). We

consider two African settings where gene drive mosquitoes are being actively researched, representing distinct seasonality and intervention profiles - Burkina Faso and Kenya - and consider three transmission settings at each (high, medium and low). To characterize the gene drive construct, we consider parameters describing homing and resistance allele generation rates, the efficacy of the antimalarial effector gene, and fitness costs of gene drive and resistance alleles. We sample plausible ranges for each parameter and use the MGDrivE 3 model of mosquito genetic biocontrol [117], which incorporates a version of the ICL malaria transmission model [25, 61], to calculate epidemiological outcomes. Through analyzing the main drivers of target outcomes, we provide an assessment of gene drive parameter values expected to satisfy TPP criteria, and discuss implications for future development efforts and field measurements.

3.2 Methods

The impact of a population modification gene drive mosquito on malaria transmission will depend on both its product parameters and release setting. With this in mind, we explored the performance of a gene drive at reducing malaria transmission for a range of parameters (rates of homing and resistance allele generation, transmission-blocking efficacy, and fitness effects, Figure 3.1A) in six distinct settings (sites resembling Burkina Faso and Kenya in terms of seasonal rainfall profile and intervention coverage, with three transmission intensities for each, Figure 3.1B). By randomly sampling a set of gene drive parameters for each setting, a set of simulations were defined and run (Figure 3.1C-D) and outcomes of interest were extracted from the simulation output (Figure 3.1E). An emulator was then trained with data from the simulation bank to predict disease outcomes given input parameters [78]. Finally, the emulator was employed to conduct a sensitivity analysis and determine gene drive parameter ranges that satisfy TPP criteria (Figure 3.1F).

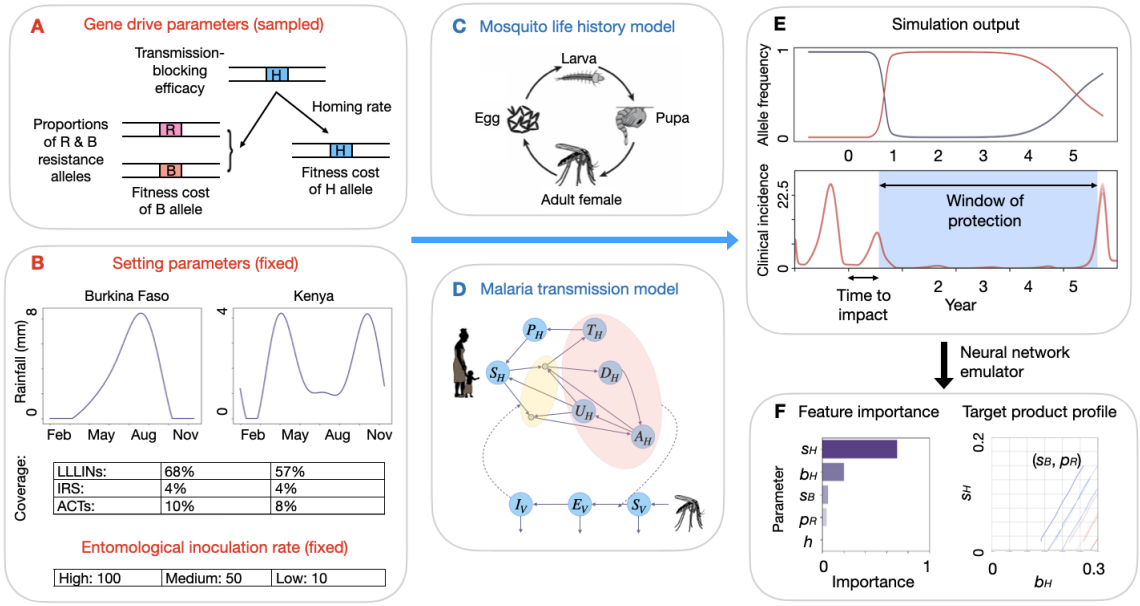

Figure 3.1: **Workflow to assess target product profile of gene drive-modified mosquitoes.** (A) We consider a population modification gene drive system linked to an antimalarial effector gene with a defined transmission-blocking efficacy (b_H). When present in a heterozygote, the gene drive allele (H) cleaves a wild-type allele in the germ line, either converting it into an H allele through homology-directed repair (at a defined homing rate, h), or into a resistance allele that is either in-frame/cost-free (R, with probability p_R), or out-of-frame/otherwise costly (B). Fitness costs are defined for H and B alleles (s_H and s_B, respectively). For each gene drive parameter, a distribution of values are defined and sampled. (B) Simulations are performed for two settings (Burkina Faso and Kenya) and three transmission settings (entomological inoculation rates of 100, 50 and 10 infective bites per person per year). Settings are defined by their seasonal rainfall profile and coverage of currently-available tools - long-lasting insecticide-treated nets (LLINs), indoor residual spraying with insecticides (IRS), and artemisinin combination therapy drugs (ACTs). (C) Simulations are run using the MGDrivE 3 modeling framework [117], which includes modules for gene drive inheritance, mosquito life history and malaria epidemiology. (D) Malaria transmission is modeled according to the Imperial College London malaria model [25, 26]. (E) For each sampled parameter set and setting, gene drive allele frequencies and clinical malaria incidence are recorded for six years. Window of protection (WOP, the duration for which clinical incidence is below 50% its seasonal mean) and time to impact (TTI, the time from initial release to clinical malaria incidence falling to 50% its seasonal mean) are recorded as outcomes of interest. (F) Neural network emulators are trained using gene drive parameter values (b_H, h, p_R, s_H and s_B) and outcomes (WOP and TTI) for each setting. Emulators are then used to calculate the importance of each parameter in predicting WOP and TTI, and to infer regions of gene drive parameter space that satisfy WOP greater than three years and TTI less than one year.

Gene drive and malaria transmission model

We used the MGDrivE 3 framework [117] to simulate releases of *An. gambiae* mosquitoes engineered with a population modification gene drive system and linked antimalarial effector gene. MGDrivE 3 is a stochastic, population-based model that simulates the population dynamics of mosquito genetic control tools and their entomological and epidemiological implications. The framework includes: i) an inheritance module that describes the distribution of offspring genotypes for given maternal and paternal genotypes, ii) a life history module that describes the development of mosquitoes from egg to larva to pupa to adult (Figure 3.1C), and iii) an epidemiology module that describes reciprocal pathogen transmission between mosquitoes and humans (Figure 3.1D). A landscape module that describes the distribution and movement of mosquitoes through a metapopulation is also included, but was not utilized for this analysis. Seasonality in mosquito density is incorporated through time-dependent mosquito bionomic parameters, which are responsive to environmental data. In the present analysis, data on recent rainfall (Figure 3.1B) modulates the carrying capacity of the environment for larvae, which in turn impacts adult mosquito density and malaria transmission.

The MGDrivE 3 framework is linked to an adapted version of the Imperial College London (ICL) malaria transmission model [25, 26] (Figure 3.1D). The ICL malaria model has been fitted to extensive data sets throughout sub-Saharan Africa and captures important details of malaria transmission, including symptomatic and asymptomatic infection, variable parasite density and superinfection in humans, human age structure, mosquito biting heterogeneity, several forms of immunity, and antimalarial drug therapy and prophylaxis. Treatment coverage with ACTs is captured within the ICL malaria model, while coverage with vector control interventions, such as LLINs and IRS, is captured within the mosquito life history module of MGDrivE 3. Here, mosquito life history parameters are modified to reflect the fact that LLINs and IRS increase the mortality rate and decrease the biting rate of adult mosquitoes, and also decrease the egg-laying rate by virtue of extending the gonotrophic cycle [25, 70]. Gene drive interventions are therefore modeled in the context of existing coverage with ACTs, LLINs and IRS (Figure 3.1B). The ICL malaria model permits monitoring a variety of health outcomes - e.g., clinical disease incidence, prevalence and mortality by age group. We focused on all-ages clinical incidence of malaria for this analysis.

Gene drive product parameters and release scheme

MGDrivE 3 allows for flexible specification of genetic constructs and release schemes. To model a generic population modification gene drive, we consider an inheritance cube involving a homing allele (H), wild-type allele (W), and two varieties of homing-resistant alleles - one that is in-frame and cost free (R), and another that is out-of-frame or otherwise costly (B) (Figure 3.1A). Inheritance cubes were introduced in the first version of

MGDrivE [89] and describe the distribution of offspring genotypes given parental genotypes. This inheritance cube has been used to model population modification gene drives in *Anopheles stephensi* [119], *An. gambiae sensu lato* [117, 120], and other species [121, 122]. In this cube, Mendelian inheritance rules apply at the gene drive locus, with the exception that, for adults heterozygous for the H and W alleles, a proportion, c, of W alleles are cleaved, while a proportion, $1-c$, remain as W alleles. Of those that are cleaved, a proportion, h, are subject to accurate homology-directed repair (HDR) and become H alleles, while a proportion, $1-h$, become resistance alleles. Of those that become resistance alleles, a proportion, p_R, become R alleles, while the remainder, $1-p_R$, become B alleles. Each of these parameters may differ depending on the sex of the HW individual; however, to reduce dimensionality, we did not consider sex-specific parameters in this analysis. Fitness effects may be associated with any genotype, however, to reduce dimensionality, we considered just two fitness parameters - s_H, which represents reductions in female fecundity and male mating competitiveness associated with being homozygous for the H allele, and s_B, which represents the same costs associated with being homozygous for the B allele. Fitness costs are assumed to be additive. Finally, the H allele is assumed to be linked to an antimalarial effector gene, and b_H represents the probability of mosquito-to-human infection for a mosquito having at least one copy of the H allele.

For each gene drive parameter, a distribution of values are defined and sampled from to inform the TPP analysis (Figure 3.2). Given perfect or near-perfect cleavage of W alleles in HW heterozygotes for recent *An. gambiae* gene drive constructs [88, 123], we assume a cleavage rate, c, of 1, removing the need to explore this parameter. Probabilities of accurate HDR, h, tend to be high for *Anopheles* gene drives - e.g., ~ 0.98 for AcTP13 in *An. coluzzii* females and males [88], and 0.96 and 0.98 for AgNosCd-1 in *An. gambiae* females and males, respectively [123]. We explore a wider range of homing rates between 0.8 and 1.0 for this TPP analysis, to explore whether smaller rates than those observed may also be acceptable. The proportion of resistance alleles that are in-frame/cost-free (R), p_R, varies depending on the construct, and whether the resistance allele is formed in the gametocyte (e.g., via non-homologous end-joining) or embryo (following maternal deposition of Cas) [124]. For AsMCRkh2 in *An. stephensi*, models fitted to data were consistent with 0.005 of generated resistance alleles being R in gametocytes and 0.22 being R in embryos [125]. For Rec*kh* in *An. stephensi*, fitted models suggested the proportion of R resistance alleles to be 0.17 in both gametocytes and embryos [119]. These estimates are consistent with about a third of mutations preserving the reading frame, and some fraction of those being cost-free (i.e., R). We define an exponential distribution for p_R with a mean of 0.11 to reflect 86% of values being between 0 and 0.22. To reduce dimensionality, we ignore maternal deposition of Cas in this analysis, as model analyses of the AgTP13 and AcTP13 constructs suggest gene drive outcomes are insensitive to the stage of resistance allele generation [88].

	Parameter	Value(s)	
Gene drive mosquito product	Species	*An. gambiae*	
	DNA cleavage rate	1	
	Probability of accurate homology-directed repair given cleavage	~Unif [0.8-1]	
	Proportion of resistant alleles that are in-frame/cost-free (R)	~Exp (mean = 0.11)	
	Reduction in female fecundity & male mating competitiveness in HH individuals	~Unif [0-0.4]	
	Reduction in female fecundity & male mating competitiveness in BB individuals	~Unif [0-0.4]	
	Heterozygosity of fitness costs	0.5	
	Probability of mosquito-to-human infection	~Exp (mean = 0.16)	
	Probability of maternal deposition of Cas	0	
Setting		Burkina Faso	Kenya
	Rainfall seasonality	Unimodal (Fig 1)	Bimodal (Fig 1)
	Long-lasting insecticide-treated net coverage	68%	57%
	Indoor residual spraying coverage	4%	5%
	Artemisinin-based combination therapy coverage	10%	8%
	Entomological inoculation rate	(10, 50, 100) per person per year	

Figure 3.2: **Gene drive and setting parameters used for implementation experiments.**

Fitness costs corresponding to gene drive alleles are somewhat hypothetical at present as they are yet to be estimated in the field, and laboratory estimates are of limited relevance. For AcTP13 in *An. coluzzii*, for instance, laboratory studies suggest that the H allele has a fitness advantage over the W allele [88], which is unlikely to be realized in the field. In other cases, laboratory studies reveal approaches to minimize fitness costs - for AsM-CRkh2 in *An. stephensi*, fitted models were consistent with a fitness cost on H of 0.08 per allele, and a fitness cost on B of 0.18 per allele [125], but when the target kynurenine hydroxylase gene was recoded in the Rec*kh* construct, fitted models suggested a fitness cost on H was no longer present [119]. Given the uncertainty surrounding fitness costs in the field, we consider additive fitness costs between 0 and 0.2 per allele for both H and B alleles; or equivalently, homozygous fitness costs, s_H and s_B, between 0 and 0.4 for HH and BB individuals, respectively. The transmission-blocking efficacy of potential antimalarial transgenes is also quite hypothetical at present, as measurements have been made of parasite life stages in the vector; but not of onward transmission to human hosts [88, 126]. The probability of mosquito-to-human infection for a wild-type mosquito, b, is estimated at 0.55 [127]. Antimalarial effectors in the AgTP13 and AcTP13 constructs

reduce sporozoite density in mosquito salivary glands and, under various assumptions about sporozoite densities required for infection, produce mosquito-to-human infection probabilities, b_H, between 0 and 0.32 [88]. We define an exponential distribution for b_H with a mean of 0.16 to reflect 86% of values being between 0 and 0.32.

Finally, we consider a release scheme consisting of eight consecutive weekly releases of 20,000 HH male *An. gambiae* released at the beginning of the rainy season in each setting. In Burkina Faso, these releases represent an initial population frequency of 0.16 (low EIR), 0.011 (medium EIR) or 0.0024 (high EIR), and in Kenya of 0.28 (low EIR), 0.017 (medium EIR) or 0.0045 (high EIR) as the seasonal rains begin.

Simulated settings, seasonality and other interventions

Using MGDrivE 3, which incorporates the ICL malaria model, we simulate two African settings where gene drive mosquitoes are being actively researched - Burkina Faso and Kenya - and consider three transmission settings for each. Rainfall is a major driver of An. gambiae population dynamics, and these two countries have distinct seasonal rainfall patterns - Burkina Faso has a single rainy season from May through September, while Kenya has a "long rains" season from March through May and a "short rains" season from October through December. Figure 3.1B depicts smoothed rainfall profiles for each country derived using the "umbrella" `R` package [100]. This package fits a mixture of sinusoids to daily rainfall data from the CHIRPS (Climate Hazards Group Infrared Precipitation with Station) database, here representing the three years between January 1st, 2017 and December 31st, 2019. In MGDrivE 3, recent rainfall modulates the carrying capacity of the environment for larvae via a mathematical relationship from White *et al.* [28]. To maintain a persistent *An. gambiae* population throughout the year, we assume larval carrying capacity in the dry season is 5% that of the peak rainy season, qualitatively consistent with entomological data from Burkina Faso [128] and Kenya [129] suggesting vector breeding sites are substantially less abundant during the dry season.

The simulated settings are also characterized by their coverage of existing interventions - LLINs, IRS and ACTs - which are modeled alongside gene drive releases. Country-specific coverage levels for these interventions were obtained from the Malaria Atlas Project [130] and are included in Figure 3.2. Coverage levels with LLINs and IRS modify the mortality, biting and egg-laying rates of adult mosquitoes based on the model of Le Menach *et al.* [70]. Finally, we consider three transmission intensities for each setting - EIRs (entomological inoculation rates) of 100 (high), 50 (medium), and 10 (low) infectious bites per person per year. Time-varying mosquito density was scaled to produce each EIR prior to the gene drive release, accounting for seasonal rainfall profiles and coverage with existing interventions. Simulations were run for a human population size of 1,000, consistent with a medium-sized Burkinabe or Kenyan village.

Target outcomes and metrics

The primary metric for this TPP analysis is model-predicted all-ages clinical incidence of malaria, i.e., the number of new symptomatic malaria cases per day across all age groups. For each simulation, this is generated as a time-series, and two target outcomes are derived: i) window of protection (WOP), which measures the duration for which clinical incidence is below 50% its seasonal mean, and ii) time to impact (TTI), which measures the time from initial release to clinical malaria incidence falling to 50% its seasonal mean (Figure 3.1E). Calculation of clinical incidence at time t, $Inc(t)$, follows from the ICL malaria model [25, 26],

$$Inc(t) = \sum_{a \in A} \lambda_{H,a}(t)\varphi_a(t)(S_a(t) + A_a(t) + U_a(t))$$

Here, $\lambda_{H,a}(t)$ represents the force of infection on humans (probability of infection per person per unit time) for age group a at time t, $\varphi_a(t)$ represents the probability of acquiring clinical disease upon infection for age group a at time t (this depends on age-specific immunity levels in the population), and $S_a(t)$, $A_a(t)$ and $U_a(t)$ represent the number of people in age group a who are either susceptible, asymptomatic but detectable by rapid diagnostic test (RDT), or asymptomatic and undetectable by RDT, respectively, at time t.

As secondary metrics for the TPP analysis, we also calculated all-ages malaria prevalence and malaria-induced mortality over time, calculating WOP and TTI outcomes for each. Malaria prevalence, also referred to as the Plasmodium falciparum parasite rate ($PfPR$), refers to the proportion of the human population that harbors the malaria pathogen, regardless of symptoms or treatment status. For the ICL malaria model [25, 26], this is given by,

$$PfPR(t) = \sum_{a \in A} (A_a(t) + U_a(t) + T_a(t) + D_a(t))/N_H$$

Here, N_H represents the total human population size, $A_a(t)$ and $U_a(t)$ are as previously defined, and $T_a(t)$ and $D_a(t)$ represent the number of people in age group a who are symptomatically infected and either treated or untreated (diseased), respectively, at time t. Finally, for the ICL model [25, 26], malaria-induced mortality is proportional to the incidence of severe malaria at time t, and is given by,

$$\mu(t) = v \sum_{a \in A} \lambda_{H,a}(t)\theta_a(t)(S_a(t) + A_a(t) + U_a(t))$$

Here, $\theta_a(t)$ represents the probability of acquiring severe disease upon infection for age group a at time t (this depends on age-specific immunity levels in the population), and v represents the probability of death for a case of severe disease. The derivation and parameterization of this formula is provided in Griffin *et al.* [91].

Neural network emulator to predict epidemiological impact

In order to rapidly search gene drive parameter space to infer the impact of product parameters on epidemiological target outcomes, we used a database of MGDrivE 3 simulations to train a neural network emulator for each EIR and country setting. To generate the simulation database, we sampled 3,000 gene drive parameter sets per setting/EIR using a Latin hypercube sampling scheme and the parameter distributions specified in Figure 3.2. This provided a total of 18,000 simulations (3,000 parameter sets x 2 settings x 3 EIRs). Each simulation was run ten times, with the mean outcome being recorded, to avoid outliers given the stochastic nature of the model. Input parameters to the neural network for each setting/EIR are those listed in Figure 3.2, i.e.: i) the homing rate, ii) proportion of resistance alleles that are in-frame/cost-free, iii) fitness cost on HH individuals, iv) fitness cost on BB individuals, and v) probability of mosquito-to-human transmission for mosquitoes having the effector gene. Output parameters were the WOP and TTI for the three outcome metrics described in the previous section - clinical incidence of malaria, malaria prevalence, and malaria-induced mortality. The emulators were trained on 90% of the simulation data and evaluated on a 10% hold-out test set. Python packages "tensorflow" and "keras" were used to build each emulator. The emulation utilized a simple feed-forward architecture with {32, 32} nodes in each fully-connected, hidden layer and rectified linear unit activation functions between each hidden layer.

Feature importance and target product profile

To assess the relative importance of each gene drive product parameter on the WOP and TTI target outcomes, we calculated their "feature importance" using the permutation feature importance method (Figure 3.1F). Permutation feature importance measures the decrease in a model score when a single feature value is shuffled, decoupling it from its outcome. The decrease in model score conveys the relative importance of the shuffled feature on the model's outcome on a 0-1 scale. We used the Python package "scikit-learn" to calculate feature importance scores. Having identified the most important gene drive product parameters, we next used the emulator to identify regions of parameter space that satisfy TPP criteria - i.e., a WOP greater than three years, and a TTI less than one year. TPP criteria were identified for each setting/EIR combination, and for each of the three outcome metrics - clinical malaria incidence, malaria prevalence and malaria-induced mortality.

3.3 Results

Target outcomes are most influenced by gene drive allele fitness cost and probability of mosquito-to-human infection

We found a consistent ordering of gene drive product parameters when assessing feature importance for both WOP and TTI outcomes for the clinical malaria incidence metric, regardless of country setting, EIR or target outcome (Figure 3.3). The most influential parameter in all cases was the fitness cost associated with the intact gene drive allele, s_H. Following this was the mosquito-to-human infection probability, b_H, for mosquitoes having the gene drive allele and hence effector gene(s). Notably, the homing rate, h, or rate of accurate HDR given cleavage, was consistently the least influential of all product parameters explored. This is likely due to the high inheritance bias associated with the gene drive allele for the full range of homing rates explored - i.e., from 0.8 to 1 - despite the lower bound of this range being substantially lower than values published for recently engineered population modification gene drives in Anopheles species [56, 88, 119, 123, 125]. Of moderate influence were resistance allele parameters - the fitness cost associated with out-of-frame or otherwise costly resistance B alleles, s_B, followed by the proportion of generated resistance alleles that are in-frame and cost-free, p_R.

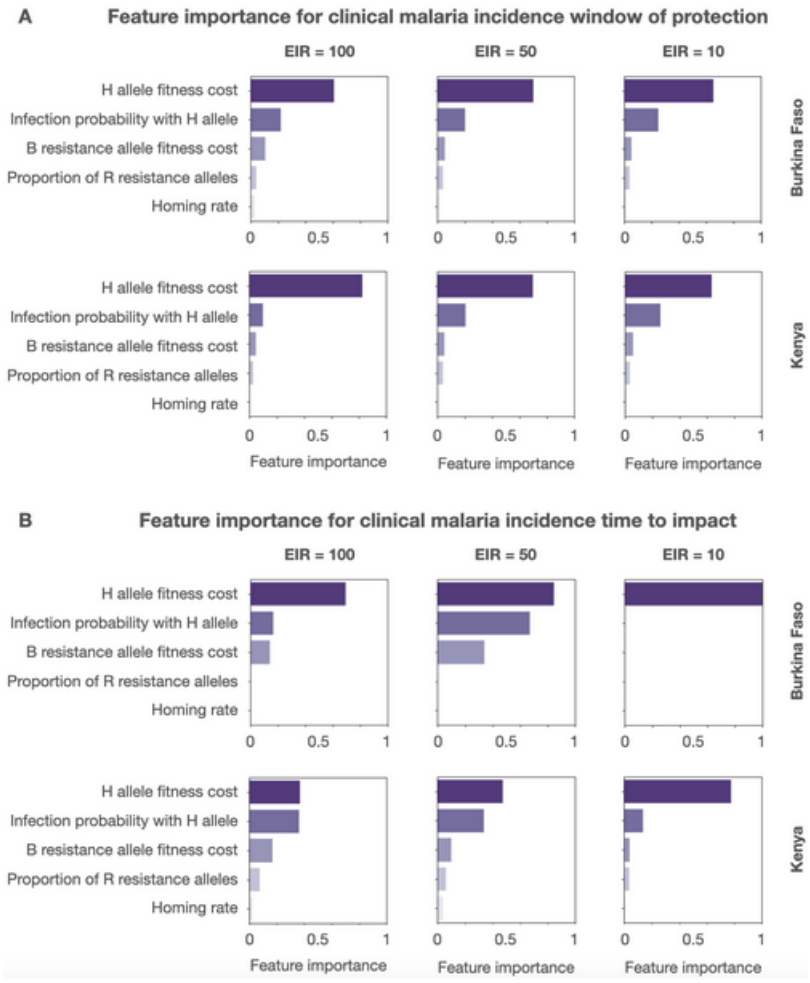

Figure 3.3: **Feature importance of gene drive product parameters.** Permutation feature importance values are depicted for gene drive product parameters for two country settings (Burkina Faso and Kenya), three transmission intensities (entomological inoculation rates of 100, 50 and 10 per person per year), and two target outcomes - (A) window of production (i.e., the duration for which clinical incidence is below 50% its seasonal mean), and (B) time to impact (i.e., the time from initial release to clinical malaria incidence falling to 50% its seasonal mean). Parameters explored include: i) the fitness cost associated with being homozygous for the gene drive (H) allele, ii) the probability of mosquito-to-human transmission for mosquitoes having the H allele with linked antimalarial effector gene(s), iii) the fitness cost associated with being homozygous for the out-of-frame or otherwise costly B resistance allele, iv) the proportion of generated resistance alleles that are in-frame and cost-free (R), and v) the homing rate, or rate of accurate homology-directed repair given cleavage. Permutation feature importance is calculated on a 0-1 scale.

While the ordering of gene drive product parameters with respect to feature importance is consistent, their relative magnitudes vary depending on country setting, EIR and target outcome (Figure 3.3). H allele fitness cost, for instance, has more than double the feature importance magnitude than the next most influential parameter when considering the WOP outcome for clinical malaria incidence, regardless of country setting or EIR; however for the TTI outcome, mosquito-to-human infection probability is a close second in feature importance for high EIRs in both countries and medium EIRs in Kenya. For the TTI outcome, there is also a consistent increase in magnitude of feature importance for resistance allele parameters (B allele fitness cost and proportion of R resistance alleles) with declining EIR; however for the WOP outcome, the feature importance of these parameters remains small across all country settings and EIRs. WOP and TTI feature importance plots for all-ages malaria prevalence and malaria-induced mortality outcomes are shown in Figure 3.4 and Figure 3.5, respectively.

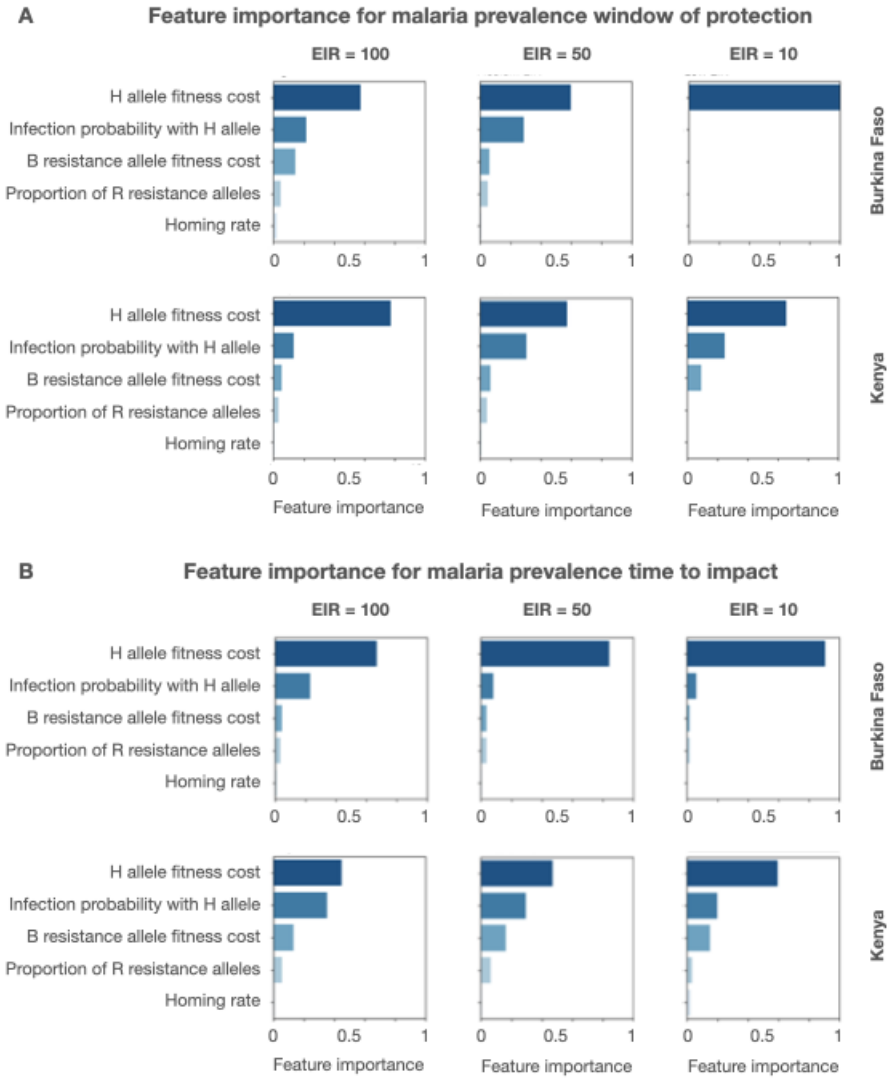

Figure 3.4: **Feature importance of gene drive product parameters.** Permutation feature importance values are depicted for gene drive product parameters for two country settings (Burkina Faso and Kenya), three transmission intensities (entomological inoculation rates of 100, 50 and 10 per person per year), and two target outcomes - (A) window of production (i.e., the duration for which malaria prevalence is below 50% its seasonal mean), and (B) time to impact (i.e., the time from initial release to malaria prevalence falling to 50% its seasonal mean).

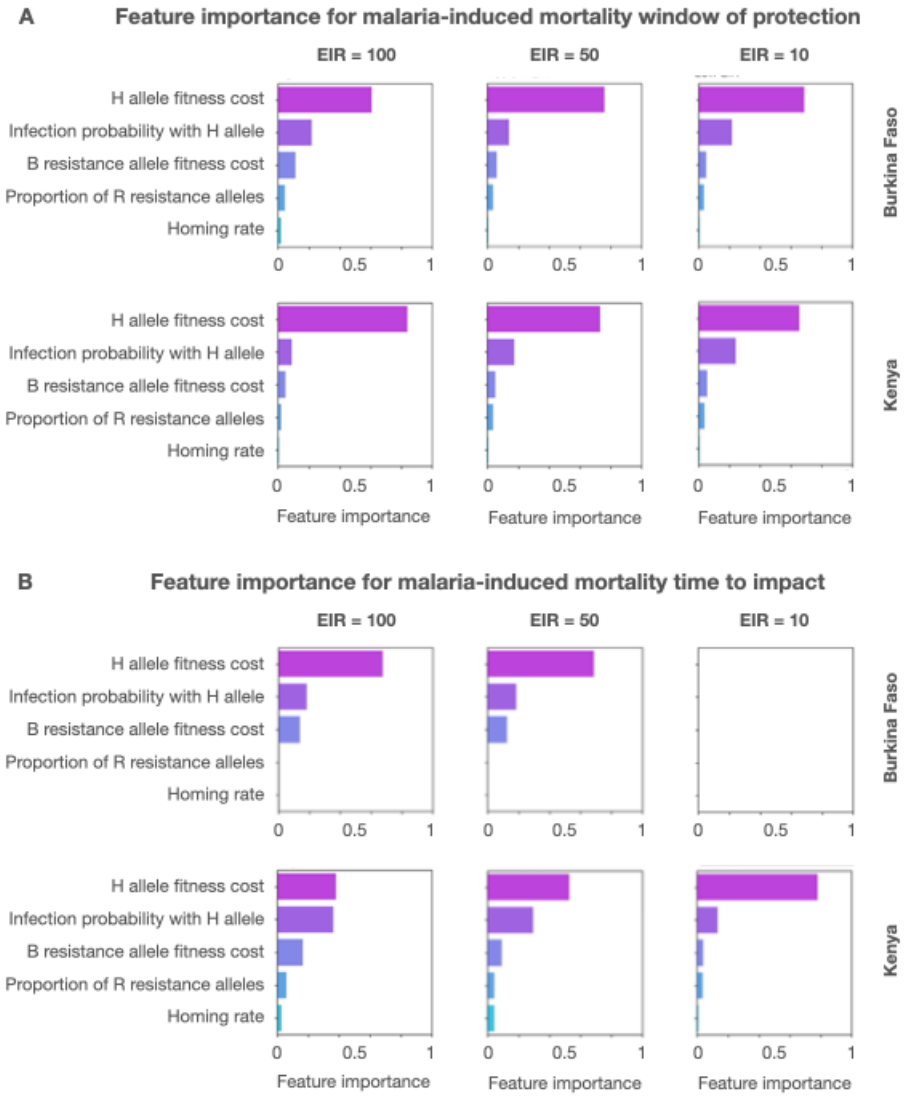

Figure 3.5: **Feature importance of gene drive product parameters.** Permutation feature importance values are depicted for gene drive product parameters for two country settings (Burkina Faso and Kenya), three transmission intensities (entomological inoculation rates of 100, 50 and 10 per person per year), and two target outcomes - (A) window of production (i.e., the duration for which malaria-induced mortality is below 50% its seasonal mean), and (B) time to impact (i.e., the time from initial release to malaria-induced mortality falling to 50% its seasonal mean).

Trade-offs between gene drive allele fitness cost and probability of mosquito-to-human infection

To characterize regions of gene drive parameter space that satisfy TPP outcome criteria, we visualize WOP for a > 50% reduction in clinical malaria incidence as it varies with the four most influential product parameters - s_H, b_H, s_B and p_R - for both country settings and three EIRs for each (Figure 3.6). We dropped the homing rate parameter, h, from this analysis since all proposed outcome criteria were found to be insensitive to its value within the range 0.8 to 1. We set the default value for h to be 0.95, as this is a relatively high homing rate that is exceeded for all constructs, in both female and male lines, that are currently being considered for malaria vector control [56, 88, 119].

Results in Figure 3.6 suggest a trade-off between gene drive allele fitness cost, s_H, and effector gene efficacy, b_H, for satisfying clinical malaria incidence WOP criteria. For most settings (country and EIR), there are scenarios in which the WOP exceeds three years for an infection probability of $b_H \leq 0.3$ in the absence of a gene drive fitness cost, and for an infection probability $b_H \leq 0.1$ in the presence of a fitness cost of $s_H \leq 0.1$. If the target outcome is relaxed to a WOP exceeding two years, for most settings (country and EIR), there are scenarios in which this outcome is satisfied for an infection probability of $b_H \leq 0.3$ in the absence of a gene drive fitness cost, for an infection probability $b_H \leq 0.2$ in the presence of a fitness cost of $s_H \leq 0.1$, and for perfect transmission-blocking in the presence of a fitness cost of $s_H \leq 0.2$. That is, higher gene drive allele fitness costs can be tolerated for lower infection probabilities (i.e., higher effector gene efficacies). Results for moderate-to-high EIRs (50-100 infective bites per person per year) are relatively consistent; however, for low-to-moderate EIRs (10-50 infective bites per person per year), slightly higher infection probabilities can be tolerated for the same gene drive allele fitness cost.

Gene drive parameter values that satisfy WOP criteria for malaria-induced mortality reflect those for clinical malaria incidence, partly due to the fact that malaria-induced mortality is calculated as a proportion of the incidence of severe malaria, which differs from the incidence of clinical malaria by only one term. That said; WOP criteria for malaria-induced mortality are satisfied for a slightly wider range of gene drive allele fitness and infection probability parameters, possibly due to the fact that reductions in severe disease occur more quickly than reductions in clinical disease following an intervention-induced reduction in transmission. WOP criteria based on the malaria prevalence metric are more restrictive on gene drive parameter space, likely due to the fact that untreated malaria infections can last for months to years [108], meaning that the greatest reduction in prevalence may not be seen until intervention impact begins to wane due to resistance allele spread in some cases.

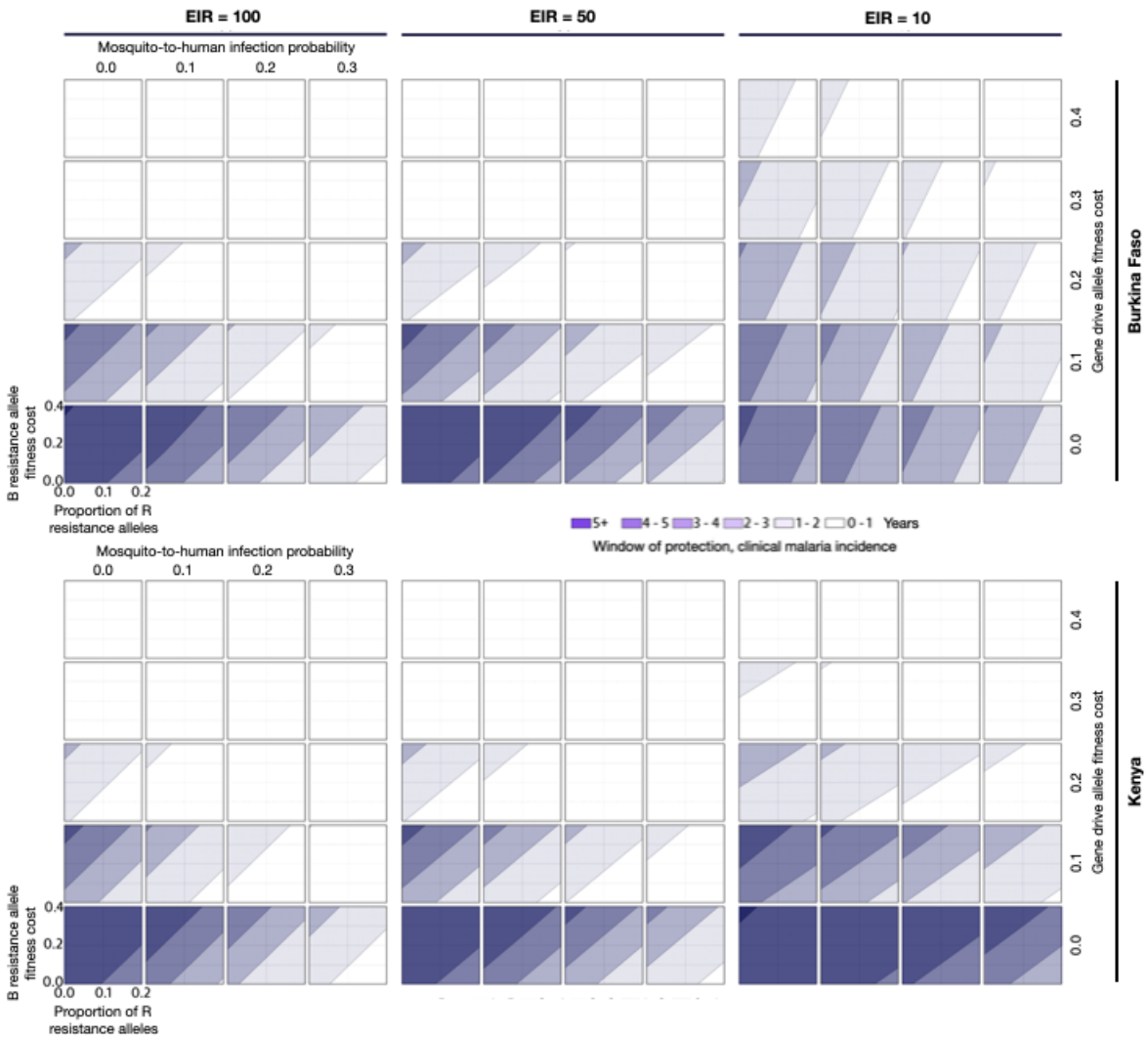

Figure 3.6: **Gene drive parameter space satisfying a** > 50% **reduction in clinical malaria incidence for defined durations (i.e., window of protection, or WOP).** WOPs are depicted for two country settings (Burkina Faso and Kenya, defined by their seasonal profile in Figure 3.1B and intervention coverage profile) and three transmission settings (entomological inoculation rates, or EIRs, of 100, 50 and 10 infective bites per person per year). Gene drive parameters explored include: i) the fitness cost associated with being homozygous for the gene drive (H) allele, ii) the probability of mosquito-to-human transmission for mosquitoes having the H allele, iii) the fitness cost associated with being homozygous for the out-of-frame or otherwise costly B resistance allele, and iv) the proportion of generated resistance alleles that are in-frame and cost-free (R). The homing rate parameter is fixed at 0.95, since proposed outcome criteria were found to be insensitive to its value within a feasible range.

Gene drive products are favored that generate fewer cost-free R resistance alleles and B resistance alleles that are more costly

The potential of a gene drive system to persist in a population for a sustained period of time, once most available wild-type alleles have been cleaved, is dependent on its ability to compete with drive-resistant alleles. In this sense, resistance allele parameters have a large impact on WOP criteria. To illustrate this, Figure 3.7 depicts threshold values of s_H and b_H below which the clinical malaria incidence WOP exceeds three years, and above which it does not, for distinct sets of resistance allele parameters - s_B and p_R. Diagonal straight lines on this plot represent the trade-off between gene drive allele fitness cost and probability of mosquito-to-human infection in satisfying the WOP criterion. The movement of these lines upwards with decreasing values of the proportion of R alleles and/or increasing values B allele fitness costs implies that, as cost-free resistance alleles are generated less frequently and as costly resistance alleles are associated with greater costs, greater drive allele fitness costs can be tolerated and/or lower effector gene efficacies.

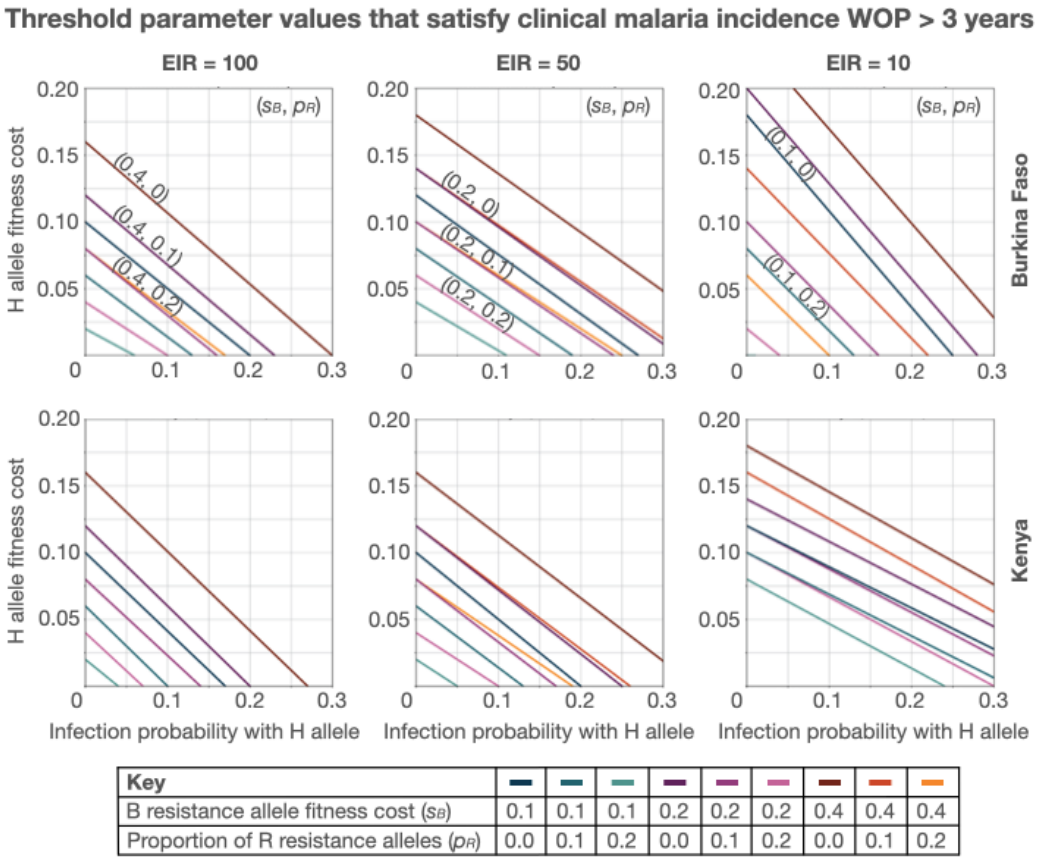

Figure 3.7: **Threshold gene drive parameter values satisfying clinical malaria incidence window of protection greater than three years.** Lines depict values of s_H (H allele fitness cost) and b_H (mosquito-to-human infection probability for mosquitoes having the H allele) below which the clinical malaria incidence window of protection exceeds three years, and above which it does not. Each line depicts a distinct set of resistance allele parameters - i.e., s_B (B resistance allele fitness cost) and p_R (proportion of R resistance alleles). The homing rate parameter, h, is fixed at 0.95. Threshold parameter values are depicted for two country settings (Burkina Faso and Kenya, defined by their seasonal profile in Figure 3.1B and intervention coverage profile) and three transmission settings (entomological inoculation rates, or EIRs, of 100, 50 and 10 infective bites per person per year).

The same trends in higher tolerable s_H and b_H values for smaller p_R values and higher s_B values are seen for the alternative outcome metrics - malaria-induced mortality and malaria prevalence. Threshold parameter values satisfying the malaria-induced mortality WOP criterion closely reflect thresholds for the clinical malaria incidence metric, likely due to the similarity in how mortality (a fraction of severe malaria incidence)

and clinical malaria incidence are calculated. Threshold parameter values satisfying the malaria prevalence WOP criterion are more restrictive, especially for EIRs of 50-100 infective bites per person per year. This is again due to the delay in prevalence reductions being observed as a result of long-lasting untreated malaria infections.

Target gene drive parameter values are interdependent

Our results demonstrate that target gene drive parameter values are interdependent - i.e., the value of one parameter required to achieve a target outcome depends on the values of others. We therefore consider a range of assumptions and design options for potential gene drive constructs, and consider target parameters for each (Figure 3.8). Given the insensitivity of target outcome criteria to the homing rate, h, we set this parameter to 0.95, reflecting constructs currently being considered for malaria vector control [56, 88, 119]. Second, given uncertainty surrounding fitness costs in the field, and especially regarding resistance alleles, we consider three scenarios for B allele fitness costs, s_B: 0.1, 0.2 and 0.4. Third, for the proportion of resistance alleles that are in-frame/cost-free, p_R, we consider a default value of $\frac{1}{6}$. This is consistent with the estimated value for the Rec*kh* construct in *An. stephensi* [119], and also with the ballpark estimate that about a third of mutations preserve the reading frame, and about half of those are cost-free. We also consider potential reductions in the value of p_R achieved through guide RNA multiplexing - i.e., if multiple guide RNAs (gRNAs) within a drive construct target multiple nearby sequences within the target site, then the chance of generating in-frame/cost-free resistance alleles could be reduced multiplicatively [124, 131]. We consider additional values of p_R of $\frac{1}{6}^2$ and $\frac{1}{6}^3$ representing constructs having two and three gRNAs, respectively. Fourth, given the promise of current malaria-refractory effector genes available for *An. gambiae* [88, 126], we consider mosquito-to-human infection probabilities, b_H, of 0.01, 0.05 and 0.10. The probability of mosquito-to-human infection for a wild-type mosquito is estimated at 0.55 [127], so these represent infection-blocking efficacies of 99%, 91% and 82%, respectively. Finally, we determine threshold parameter values for the H allele fitness cost, s_H, that satisfy the target outcome of a clinical malaria incidence WOP exceeding three years. Similar thresholds for malaria-induced mortality and all-ages malaria prevalence are shown in Figure 3.9.

B allele fitness cost (s_B)	Proportion of R resistance alleles (p_R)	Probability of mosquito-to-human infection with H allele (b_H)		
		0.01	0.05	0.10
0.1	1/6	0.03	0.00	-
	$(1/6)^2$	0.08	0.06	0.03
	$(1/6)^3$	0.09	0.07	0.04
0.2	1/6	0.05	0.03	-
	$(1/6)^2$	0.11	0.08	0.05
	$(1/6)^3$	0.11	0.09	0.06
0.4	1/6	0.09	0.07	0.04
	$(1/6)^2$	0.15	0.12	0.09
	$(1/6)^3$	0.16	0.13	0.10

Figure 3.8: **Threshold gene drive allele fitness cost (s_H) satisfying clinical malaria incidence window of protection greater than three years.** Results are depicted for the most conservative setting (Kenya) and EIR (100 infective bites per person per year), and a homing rate, h, of 0.95.

		Malaria-induced mortality			Malaria prevalence		
B allele fitness cost (s_B)	**Proportion of R resistance alleles (p_R)**	**Probability of mosquito-to-human infection with H allele (b_H)**					
		0.01	0.05	0.10	0.01	0.05	0.10
0.1	1/6	0.04	0.02	0.01	-	-	-
	$(1/6)^2$	0.09	0.07	0.04	0.03	-	-
	$(1/6)^3$	0.10	0.08	0.05	0.04	0	-
0.2	1/6	0.06	0.04	0.01	0	-	-
	$(1/6)^2$	0.11	0.09	0.06	0.06	0	-
	$(1/6)^3$	0.12	0.10	0.07	0.07	0.01	-
0.4	1/6	0.10	0.07	0.05	0.05	0	-
	$(1/6)^2$	0.15	0.13	0.10	0.12	0.05	-
	$(1/6)^3$	0.16	0.14	0.11	0.13	0.07	0.01

Figure 3.9: **Threshold gene drive allele fitness cost (s_H) satisfying malaria-induced mortality and all-ages malaria prevalence window of protection greater than three years.** Results are depicted for the most conservative setting (Kenya) and EIR (100 infective bites per person per year), and a homing rate, h, of 0.95.

3.4 Discussion

Model-informed TPPs for gene drive mosquito products are especially important given that the epidemiological target outcomes of interest can only be observed following a release [58], and such a release may be difficult to remediate [103]. Through modeling, we simulated a broad range of gene drive product parameters for releases in two country settings and at three malaria transmission levels. This allowed us to characterize regions of gene drive parameter space expected to satisfy target outcome criteria: a 50% reduction in clinical malaria incidence, a rate of spread that would produce this impact in less than a year, and a duration of impact of at least three years. We found that the TTI criterion was automatically satisfied in all cases where the WOP criterion was satisfied, allowing us to focus on the latter - i.e., a 50% reduction in clinical malaria incidence for a period of at least three years. We also explored alternative outcome metrics - reductions in malaria-induced mortality and prevalence. Reductions in malaria-induced mortality mirrored those for clinical incidence, while the prevalence metric led to overly restrictive outcome criteria due to delays in reductions in prevalence resulting from enduring untreated infections.

Regarding gene drive product parameters, we explored rates of homing and resistance allele generation, fitness costs associated with the gene drive and out-of-frame/costly resistance alleles, and the efficacy of the effector gene at reducing the probability of mosquito-to-human infection. Simulations suggest that, for feasible parameter ranges, target outcomes are notably least influenced by the homing rate, and are most influenced by fitness costs associated with the gene drive allele, and the efficacy of the effector gene at reducing transmission. A trade-off between homing allele fitness cost and effector gene efficacy is apparent in which, for high effector gene efficacies, larger homing allele fitness costs can be accommodated, and vice versa. Resistance allele parameters are also highly influential on target outcomes, as they determine how long the gene drive allele persists in the population after most available wild-type alleles have been cleaved. If fewer in-frame/cost-free resistance alleles are generated, and if out-of-frame/otherwise costly resistance alleles have larger fitness costs, then a wider range of effector gene efficacies and home allele fitness costs can be accommodated. Since target parameter values are interdependent, it is not possible to specify a single TPP threshold for each. We therefore discuss criteria for each in the following paragraphs.

Fitness of gene drive and resistance alleles are highly influential on outcome criteria, but difficult to measure prior to a release

In the interests of parsimony, we considered just two fitness parameters in our analysis - s_H and s_B, which represent fitness costs associated with being homozygous for the H and B alleles, respectively. Fitness costs were assumed to be additive. Outcomes of interest, including both TTI and WOP for all three outcome metrics, were found to be most sensitive to s_H, while s_B was found to be the third most important parameter. This presents a conundrum for assessing product readiness according to a TPP because, while the performance of a gene drive product is highly dependent on these parameters, fitness is difficult, if not impossible, to measure prior to a field release. Nevertheless, this provides an incentive for gene drive developers to focus engineering efforts on minimizing likely gene drive fitness costs, while maximizing likely costs on non-functional resistance alleles. One approach that seeks to address both criteria is to have the gRNA target site be an essential gene, while including a copy of this gene within the drive construct. This approach was employed for the Rec*kh* construct in *An. stephensi*, for which BB females were rendered unviable, while lab measurements indicated no fitness cost on the H allele [119]. It has also been employed in *Drosophila*, described as the home-and-rescue (HomeR) design, with a similar lab fitness profile [121]. Other approaches to minimizing H allele fitness cost include using promoters that restrict Cas9 expression to the germline, hence having little effect on somatic tissue, and choosing gRNA target sites having minimal fitness consequences, although this latter approach would also reduce the fitness costs associated with B alleles.

As a ballpark, we recommend an H allele fitness cost, $s_H, \leq 0.10$ for and a B allele fitness cost, $s_B, \geq 0.20$ for homozygotes which, given our assumptions, implies ≤ 0.05 for H allele heterozygotes and ≥ 0.10 for B allele heterozygotes. Higher H allele costs and lower B allele costs are tolerable under permissive values of b_H and p_R in our model; however, these thresholds allow other parameters to also vary within a reasonable range while still satisfying the TPP criteria. Importantly, these should be interpreted as fitness costs several generations after a release, by which time these alleles will have introgressed into the wild genetic background and shed fitness effects associated with the genetic background of the release strain. This post-introgression fitness should reflect the competition dynamics between drive and drive-resistant alleles once the majority of wild-type alleles in the population have been cleaved, while higher release strain fitness costs prior to introgression may be offset through supplemental releases.

Efficacy of malaria-refractory effector gene is highly influential and can be measured by proxy

Our results indicate that the efficacy of the malaria-refractory effector gene, b_H, is highly influential on the TTI and WOP outcomes of interest. While this value can be difficult to measure directly in the field due to lack of resources and adequate field trial control arms, biological proxies can shed some light onto this parameter. For example, Carballar-Lejarazú *et al.* measured sporozoite loads in the salivary glands of TP13 mosquitoes, and models used these data to infer the reduction in infection potential as compared to wildtype mosquitoes [88]. Other studies have measured delays in sporozoite development, which correlates with reduced proportions of sporozoites that develop within the mosquito lifetime, and hence the proportion of mosquitoes that become infectious. Hoermann *et al.* [126] for example developed an effector mechanism which hampers parasite sporogonic development and delays the emergence of infectious sporozoites via a mitochondria-interrupting gene. This paradigm also conferred a reduction in the lifespan of modified female mosquitoes, thereby reducing infection potential from two angles [126]. Our results broadly suggest that a focus on robust effector genes is a means by which replacement gene drive products can achieve TPP criteria in a range of settings.

Rates of homing and resistance allele generation are measurable but less influential

With respect to the rate of homing, h, and the rate of resistance allele generation, p_R, our models suggest that these values are less influential in achieving WOP and TTI criteria. These values are, however, more easily measured in a lab setting as compared to fitness and infection blocking properties. *Anopheles* gene drive constructs have demonstrated very high rates of successful homing [88, 123], and therefore may not require additional

focus by product developers. Similarly, the proportion of resistance alleles varies depending on the construct. For AsMCRkh2 in *An. stephensi* and Rec*kh* in *An. stephensi*, model estimates are consistent with about a third of mutations preserving the reading frame, and some fraction of those being cost-free (i.e., R). WOP threshold calculations do suggest that lower rates of resistance allele generation allow for higher fitness cost values on the H allele, but broadly these gains are minor as compared to reductions in fitness cost and infection probability.

Modeling framework and limitations

The modeling presented here has provided a quantitative evaluation of gene drive parameters against conservative TPP criteria, in order to better understand the relationship between genetic parameters, environment, and expected performance. Our study should be interpreted within the context of its limitations. In order to maintain parsimony, we opted to model country-level, single node dynamics. Unlike other work incorporating fine-scale spatial resolution [34, 79], we only broadly estimate the expected impact of gene drive releases for a given seasonality and intervention profile. While these models serve as a useful starting point to understand the epidemiological dynamics associated with a gene drive's parameter set, they do not take into account spatial spread, human mobility, and additional climate drivers of transmission. Understanding spatial dynamics are important in understanding the extent of a gene drive's spread and should be considered for purposes of monitoring and potential remediation in advance of a field trial [47]. Additionally, we are considering the primary malaria vector *An. gambiae* in these analyses, but there are several malaria vectors such as *An. coluzzii* and *An. stephensi*, for which gene drives have been developed [88, 97, 119]. An understanding of the local vector population in potential field sites can help to further improve model-based estimates of a gene drive program.

As interest in gene drive products grows, we hope that models can inform the next generation of these critically important vector control interventions. We continue to refine our models to suit different constructs, such as suppression-based sterile insect technique (SIT) [41–43]. TPPs, when deployed carefully, can serve as useful policy planning tools. As the efficacy of other vector control interventions stagnates [132], we hope that this work can bolster the dialogue between lab scientists, field trial designers, and community stakeholders as gene drive products mature toward the field.

Chapter 4

Multitask deep learning for the emulation and calibration of an agent-based malaria transmission model

4.1 Introduction

Despite progress in recent decades, the burden of malaria remains unacceptably high, especially in sub-Saharan Africa [133]. Due to numerous factors including seasonal heterogeneity, complex immune landscapes, and the spatial distribution of vectors and interventions, designing effective malaria control strategies is difficult. Mathematical models of disease transmission can aid in the design of these programs by parameterizing the scientific processes that underlie transmission in a given setting. For novel interventions such as genetic vector control tools and updated vaccines [58, 65], for which field data do not yet exist, mathematical models can bridge the gap between expected outcomes and intervention parameters. Epidemiological models have been widely employed for uses of policy planning, prediction, and etiology [25, 27, 33, 91, 117]. These models generally provide a mechanistic framework by which to understand the progression of a disease from biological to socio-demographic facets. For vector-borne diseases such as malaria, the progression of disease represents a complex relationship between vector, host, and environment. Though simple models of malaria transmission have been used for over a century [24], in recent years, more complex models have been developed. These models explicitly parameterize the development of the pathogen in the vector and can take into account heterogeneity in transmission such as age structure, immunity, species, and spatial landscape. While these models can accurately describe the processes involved in disease progression, they tend to require large amounts of computational resources to estimate parameters for a wide range of outcomes and settings. Additionally, calibrating (i.e., aligning model parameters) to external field data can be challenging, as exploring multidimensional parameter spaces can quickly become intractable. Traditionally, tech-

niques such as Bayesian Markov chain Monte Carlo, sequential Monte Carlo, and approximate Bayesian computation have been employed to fit mechanistic models to data [134–137]. However, with large parameter and state spaces, these techniques demand large amounts of computational resources.

Recent literature has proposed the development of machine learning (ML) model "surrogates" or "emulators" to complex disease transmission models [78, 138, 139]. These models allow for the computationally efficient evaluation and prediction of disease dynamics as compared to the original model. While there are many techniques to develop an emulator model (e.g., long short-term memory networks [140], bidirectional neural networks [141], and Gaussian processes [142]) we focus here on the application of deep learning as an emulator for a complex model of malaria transmission. Mathematically, we are interested in training a deep neural network (DNN) to infer a function mapping a vector of parameters $\mathbf{x}$ to a set of time series outputs $y_i(t)$, for $i \in [1, n]$ outputs and time t, where the inputs and outputs correspond to realizations of the original mechanistic model:

$$f : \mathbf{x} \mapsto \{y_1(t), ..., y_n(t)\}$$

Each input parameter set will map to multiple time series outputs simultaneously, leveraging methods from multitask learning. In this framework, one neural network predicts multiple outcomes, allowing the network to learn shared patterns in the simulation data and eliminate the need to train several emulators separately [143].

With respect to calibration, the trained emulator can be used to rapidly search parameter space to identify inputs whose outputs align with reference data, as the evaluation of trained DNNs is orders of magnitude faster than the underlying mechanistic model. We develop three separate calibration techniques (drawing on Bayesian and numerical optimization methodologies) to identify site-agnostic sets of immune parameters whose simulated outputs align with field data. Finally, as we are interested in the universality of these biological parameters across study sites, we test the emulator-calibrated parameter sets against outputs from study sites not seen during training. Thus, in this work, we show that i) deep learning techniques can act as emulators to complex epidemiological models, ii) these deep learning emulators can be used to calibrate the underlying mechanistic model to field data, and iii) biological parameters identified by the emulator can capture immune dynamics in study sites not previously seen during training.

4.2 Methods

Malaria transmission model and parameter space

Simulations were conducted using the EMOD framework [31, 32]. EMOD is an agent-based, stochastic mechanistic model of malaria transmission and incorporates within-

host parasite and immune dynamics alongside vector life cycle and human demography. Here, we are interested in calibrating parameters associated with adaptive immunity within the host that are stimulated by blood-stage malaria infection. Our ultimate goal in this study is to identify a universal set of immune factors across eight sub-Saharan African study sites which closely align with collected parasite density and epidemiological outcome data. As such, in order to build a suite of simulations on which the DNN is trained, we generate 2000 Latin hypercube-sampled parameter sets per site, with 10 stochastic repetitions per set, resulting in 160000 (8 sites x 2000 parameter sets x 10 stochastic repetitions) total simulations. Descriptions of the immune parameters and their biologically relevant ranges are given in Table 4.1. Following the methodology in Selvaraj *et al.* [144], each study site has its own set of vector lifecycle, transmission, antimalarial intervention, and case management parameters, which remain unchanged across simulations for a given site. As outputs, we track four channels corresponding to available reference data: annual clinical incidence by age group, annual *P. falciparum* prevalence by age group, asexual parasite density by age group by month, and gametocyte density by age group by month. Each site's reference data corresponds to a unique set of age and density bins, and each simulation set outputs the associated outcomes, binned in alignment with the reference data.

Parameter	Description	Range
Antigen switch rate	The antigenic switching rate per infected red blood cell per asexual cycle.	$[10^{-9}, 1]$
Falciparum MSP variants	The number of distinct merozoite surface protein variants for *P. falciparum* malaria in the overall parasite population in the simulation, not necessarily in an individual.	$[1, 500]$
Falciparum nonspecific types	The number of distinct non-specific types of *P. falciparum* malaria.	$[1, 500]$
Falciparum PfEMP1 variants	The number of distinct *Plasmodium falciparum* erythrocyte membrane protein 1 (PfEMP1) variants for *P. falciparum* malaria in the overall parasite population in the simulation.	$[1, 10000]$
Max individual infections	The limit on the number of infections that an individual can have simultaneously.	$[6, 12]$
MSP merozoite kill fraction	The fraction of merozoites inhibited from invading new erythrocytes when MSP1-specific antibody level is 1.	$[0.01, 1]$
Nonspecific antigenicity factor	The nonspecific antigenicity factor that adjusts antibody iRBC kill rate to account for iRBCs caused by antibody responses to antigenically weak surface proteins.	$[10^{-9}, 1]$

Table 4.1: **Overview of immune parameters used to generate Latin hypercube samples with which to simulate.**

Data sources

In order to validate the ability of the model emulator to produce epidemiologically relevant outputs, we calibrate the emulator against field data from eight African sites. The Garki project [145] was a multi-year study in the 1970s. Its goal was to understand the feasibility of malaria elimination in a sub-Saharan African setting (Nigeria), collecting parasitology data to supplement epidemiological measurements. Additional field data from Senegal, Tanzania, and Burkina Faso were used to evaluate the emulator [146–148]. Each reference site recorded data in a structure unique to the site's resources. The Garki sites (Matsari, Rafin Marke, and Sugungum) recorded month and age-binned asexual parasite density, the Senegal (Ndiop and Dielmo) sites recorded age-binned annual clinical malaria incidence, the Burkina Faso sites (Dapelogo and Laye) recorded month and

age-binned asexual parasite and gametocyte density, and the Tanazania site (Namawala) recorded age-binned malaria prevalence. With respect to data collection, parasite density data from the Garki and Burkina Faso sites were collected via microscopy and real-time quantitative nucleic acid sequence-based amplification (QT-NASBA) respectively [145], Giemsa stains were used to ascertain malaria prevalence in the Tanzania site [146], and active surveillance was used to ascertain clinical malaria incidence in the Senegal sites [147]. Our simulations however record all of these outcomes for each site-specific simulation. In a simulation, we are able to export fine-grained data for a range of outcomes and aggregate them to match the study site reference data. Then, despite a small reference dataset, we can train our emulator on multiple outcomes such that it can infer patterns between the input parameters and each outcome. In the calibration step, when comparing the emulator's outputs to the reference data for a site, only the relevant outputs are selected and compared. Table 4.2 shows an overview of the associated data for each study site.

Site name	**Country**	**Data type**
Matsari	Nigeria	Asexual parasite density by age by month
Rafin Marke	Nigeria	Asexual parasite density by age by month
Sugungum	Nigeria	Asexual parasite density by age by month
Ndiop	Senegal	Clinical incidence by age
Dielmo	Senegal	Clinical incidence by age
Dapelogo	Burkina Faso	Asexual parasite, gametocyte density by age by month
Laye	Burkina Faso	Asexual parasite, gametocyte density by age by month
Namawala	Tanzania	Malaria prevalence by age

Table 4.2: **Overview of study sites and reference data to which the model emulator is calibrated.**

Deep learning architecture

Once the simulation suite had been run, a DNN was trained on top of simulation outputs. As stated, our goal is to learn a function f that maps the input space (the immune parameters and the study site) to the time series for each of the n outcomes:

$$f : \mathbf{x} \mapsto \{y_1(t), ..., y_n(t)\}$$

We model f as a feed-forward, multitask neural network with six fully-connected shared, hidden layers and five fully-connected task-specific layers. Rectified linear units (ReLU)

were used to introduce nonlinearity into the network, and dropout and batch normalization were used to prevent overfitting. Figure 4.1 shows the architecture of the neural network. Input features were standardized using min-max scaling and outputs were normalized between 0-1. This allowed us to use a sigmoid activation function to bound the outputs of the neural network to biologically plausible values:

$$\sigma(x) = \frac{1}{1 + e^{-x}}$$

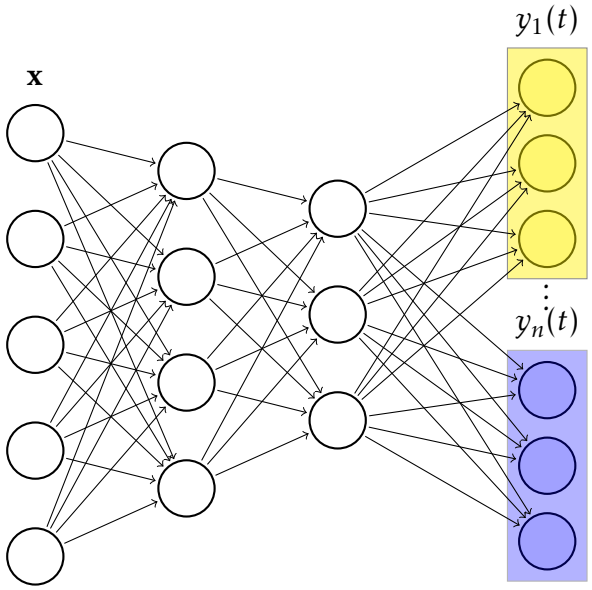

Figure 4.1: **Sample architecture for a multitask neural network emulator.** Input parameters **x** (i.e., immune parameters described in Table 4.1 are mapped via hidden shared and task-specific layers simultaneously to time series for epidemiological simulation outputs $\{y_1(t), ..., y_n(t)\}$ described in Table 4.2.

Model training and hyperparameter tuning

Training a neural network involves iteratively optimizing the model's "weights" (i.e., the strengths of connection between different layers in the neural network) in order to minimize the discrepancy between model output and training data. Then, the model is evaluated on a previously-unseen data subset to evaluate its performance on new values. We define the *loss function* as the numerical discrepancy between the neural network's output and the training data. While there are many loss functions for different modeling goals, a widely-used loss function is the ℓ_2 loss, corresponding to the mean squared error between model outputs $f(\vec{\theta})$ and training data $y(\vec{\theta})$ for a given set of input parameters $\vec{\theta}$ and N

data samples:

$$\mathcal{L}(y(\vec{\theta}), f(\vec{\theta})) = \frac{1}{N}\sum_{i=0}^{N}(f(\vec{\theta})_i - y(\vec{\theta})_i)^2$$

In a multitask learning framework, we further segment this loss function per task, such that the overall goal of training is to minimize the joint loss across n tasks:

$$\mathcal{L}(y(\vec{\theta}), f(\vec{\theta})) = \sum_{i \in n} \mathcal{L}_i(y_i(\vec{\theta}), f_i(\vec{\theta}))$$

Because our emulator is relatively simple, we employ uniform loss weighting, but for more complex networks, the relative importance of each task's loss becomes important [149]. Many methods have been proposed to address balancing the losses between tasks to ensure the model jointly learns each output type. We use the Adam stochastic gradient descent algorithm [150] to optimize the emulator's weights and minimize the multitask loss function.

A final component of model specification involves the selection of *hyperparameters*. In contrast to model weights, which are learned during the optimization process, hyperparameters are fixed attributes of the model that are selected prior to training. These include parameters associated with network architecture (number of hidden layers, number of neurons per layer), training (learning rate, batch size), and regularization (dropout probability, weight decay). In order to select hyperparameters for our model, we randomly sampled 100 hyperparameter sets and used the ASHA [151] algorithm to efficiently select the sets that minimized the joint loss on a hold-out data subset after training. Once the neural network was trained, we were able to evaluate its ability to calibrate the underlying model to reference data.

Calibration workflow

To assess the emulator's ability to calibrate the underlying mechanistic model, three calibration methodologies were tested. These methods involve using the emulator to search parameter space and compare the output to the field data. Stochastic gradient descent, Bayesian likelihood maximization, and nearest neighbors approaches were used. Figure 4.2 shows a schematic workflow of the emulation and calibration process.

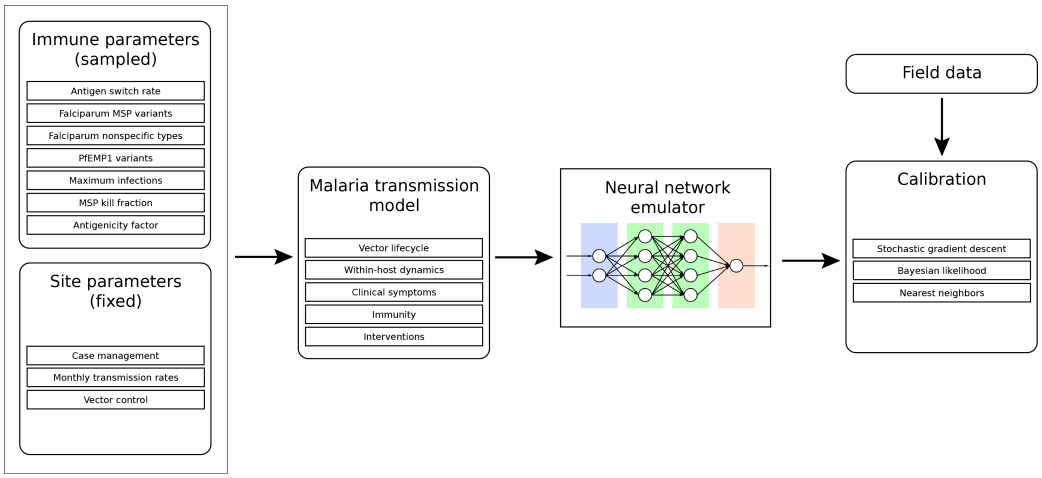

Figure 4.2: **Emulation and calibration workflow.** First, immune parameters are sampled, and site-specific parameters are specified. Then, the malaria transmission model (EMOD) is run for all sampled parameter sets. A neural network emulator is trained on the simulation data. Finally, calibration proceeds by comparing emulated output to field data.

Stochastic gradient descent

The first calibration approach used numerical optimization techniques to allow the emulator to explore regions of parameter space efficiently and outside the bounds on which the emulator was trained. At a high level, the algorithm proceeds as follows: 1) first, we randomly sampled 1000 initial parameter sets, 2) for each parameter set, we evaluated a loss function comparing the emulated outcomes for the parameter set against the reference, 3) we updated the parameter sets based on gradient descent (i.e., in the direction of the gradient of the loss function with respect to the parameters), 4) we iteratively continued steps 1-3 until a convergence criterion was met. Additionally, parameter values during optimization were constrained to their biologically plausible values (i.e., integer parameters were rounded, and all parameters were constrained to be positive). Finally, we selected the optimized parameter set which leads to the smallest loss value. The key component of gradient descent is its iterative updating. For a parameter set $\vec{\theta}$ at iteration t, its update rule is given by:

$$\vec{\theta}_{t+1} = \vec{\theta}_t - \gamma \nabla \mathcal{L}(\vec{\theta}_t)$$

for a learning rate γ and loss function $\mathcal{L}$. This allowed us to explore regions of parameter space that the emulator was not explicitly trained on. As before, we use the joint ℓ_2 loss function:

$$\sum_{s \in \mathcal{S}} MSE_{\vec{\theta}}(s, f(\vec{\theta}), d_s)),$$

where

$$MSE_{\vec{\theta}}(s, f(\vec{\theta}), d_s)) = \frac{1}{N_s} \sum_{i=0}^{N} (f(\vec{\theta})_i - d_{s,i})^2$$

for sites $s \in \mathcal{S}$, emulated outcomes $f(\vec{\theta})$, and reference data for site d_s. We used the Adam [150] variant of the stochastic gradient descent algorithm to efficiently search parameter space. We additionally tested different learning rates to ensure the optimization did not terminate in local extrema.

Bayesian likelihood maximization

Next, we used a Bayesian likelihood-based approach to find the parameter set which maximized the joint likelihood across sites as compared to the reference data. This approach, previously detailed [144, 152, 153], is described briefly here. For each data type, an initial uniform prior is updated by the simulated (or emulated) outcomes. Then, a likelihood is calculated against the reference data by marginalizing over the true parameter of the prior distribution. Incidence is modeled as a gamma-Poisson conjugate distribution, prevalence is modeled as a beta-binomial distribution, and parasite/gametocyte density is modeled as a Dirichlet-multinomial distribution. For the latter, we show the derivation of the likelihood, adapted from Gerardin *et al.* [152]. The likelihood of the parameter set $\vec{\theta}$ given the reference data d (which consists of n_d total measurements, and $\vec{k}_d$ counts in each density and age bin) is initially modeled as a symmetric Dirichlet distribution with multinomial probability $\vec{p}$. Then the simulated (or emulated) distribution of counts $\vec{k}_s$ is used to inform the posterior distribution:

$$Dir(\vec{p} \mid \vec{1}) \rightarrow Dir(\vec{p} \mid \vec{1} + \vec{k}_s)$$

Then, the likelihood of the parameter set is approximated by marginalizing over the probability vector $\vec{p}$:

$$\begin{aligned}
\mathcal{L}(\vec{\theta} \mid d) &= P(d \mid \vec{\theta}) \\
&= \int P(d \mid \vec{p}) P(\vec{p} \mid \vec{\theta}) d\vec{p} \\
&= \int Mult(\vec{k_d} \mid n_d, \vec{p}) Dir(\vec{p} \mid \vec{1} + \vec{k}_s) d\vec{p} \\
&= DirMult(\vec{k_d} \mid n_d, 1 + \vec{k}_s)
\end{aligned}$$

The joint likelihood is the product of likelihoods for each age group, month, study site, and parasite bin, which is also multiplied with the likelihoods from prevalence and incidence outcomes to obtain the total likelihood of the parameter set. That is, for all sites $s \in \mathcal{S}$, and associated likelihood function $\mathcal{L}_s(\vec{\theta}|d_s)$ (with site-specific reference data d_s), we

aim to find:

$$\max_{\vec{\theta}} \prod_{s \in \mathcal{S}} \mathcal{L}_s(\vec{\theta}|d_s)$$

Nearest neighbors

Finally, we tested finding the parameter set which minimized the ℓ_2 distance between emulated outcomes and the reference data across sites, in order to find the parameter set whose emulated outcomes are nearest to the reference data. As stated previously, the ℓ_2 distance is the represents the mean squared numerical discrepancy between two vectors. Here, the goal is to minimize the total ℓ_2 distance given by:

$$\min_{\vec{\theta}} \sum_{s \in \mathcal{S}} MSE_{\vec{\theta}}(s, f(\vec{\theta}), d_s)),$$

where

$$MSE_{\vec{\theta}}(s, f(\vec{\theta}), d_s)) = \frac{1}{N_s} \sum_{i=0}^{N} (f(\vec{\theta})_i - d_{s,i})^2$$

for sites $s \in \mathcal{S}$, emulated outcomes $f(\vec{\theta})$, and reference data for site d_s.

New site inference

In addition to evaluating the emulator's ability to capture epidemiological dynamics across study sites, we are interested in assessing i) the relationship between site-specific data and emulator performance, and ii) how applicable chosen parameter sets are to new study sites. Assessing emulator performance in the context of new field data will be important in understanding whether an emulator can capture patterns in simulation data without the need to retrain the entire system. In order to evaluate the inference ability of the emulator to unseen sites, we train eight emulators on all simulation data *except* from an excluded site. We additionally augment the training data with site-specific epidemiological parameters such as monthly transmission rates and intervention coverages. Then, for each study site, we use the emulator not trained on that site to calibrate the remaining sites. Finally, we compare the simulation outputs corresponding to the calibrated parameter set on the site excluded during training. As models are reevaluated as new field data are obtained, this workflow will allow for an assessment of the emulator's ability to capture dynamics in new sites, given sufficient site-specific data are included in the emulator's training.

Sensitivity analysis

An area of concern for the developers of emulator models will be the size of the training dataset. As running complex epidemiological simulations can take long periods of

time and demand large amounts of computational resources, it will be important to understand the relationship between the size of the underlying simulation suite and the performance of the emulator and calibration. To test this, we run the emulation and calibration workflow for various subsets of the full training data and assess the performance for each subset. 50 replicates were run to understand the variance in performance. Our goal is to learn the smallest data subset before the emulator performance degrades. For this initial exploration, we purposefully ran a very large simulation suite, but we hope that this sensitivity analysis can shed light onto the size of simulation sets required to minimize computational resources require for future analyses.

4.3 Results

Emulator performance

First, we show the ability of the emulator to capture simulated model dynamics. After hyperparameter tuning, the final model parameters (shown in Table 4.3) were used to construct the neural network. Similarly, Table 4.4 shows the final task-specific ℓ_2 losses on a holdout, previously-unseen data subset.

Parameter	Description	Value
n_1	Number of neurons in first shared layer	256
n_2	Number of neurons in second shared layer	128
n_3	Number of neurons in third shared layer	64
n_4	Number of neurons in fourth shared layer	128
n_5	Number of neurons in fifth shared layer	256
n_6	Number of neurons in sixth shared layer	16
n_7	Number of neurons in first task-specific layer	32
n_8	Number of neurons in second task-specific layer	32
n_9	Number of neurons in third task-specific layer	16
n_{10}	Number of neurons in fourth task-specific layer	256
n_{11}	Number of neurons in fifth task-specific layer	128
γ	Learning rate	0.0014
b	Batch size	32
p	Dropout probability	0.007
λ	Weight decay	$1.42e-5$

Table 4.3: **Overview of final neural network hyperparameters.**

Task	Test set loss
Annual clinical incidence by age bin	0.036
Annual *P. falciparum* prevalence by age bin	0.010
Gametocytemia by age bin by month	0.013
Parasitemia by age bin by month (Matsari, Rafin Marke, Sugungum)	0.013
Parasitemia by age bin by month (Dapelogo, Laye)	0.014

Table 4.4: **Overview of task-specific losses of trained emulator.**

Calibration

Here, we show the ability of the emulator to calibrate the underlying transmission model to field (reference) data. Three calibration methodologies were compared: stochastic gradient descent, likelihood, and nearest neighbors. We also show the biological parameters for each calibration methodology that led to the best-fit to the reference data. We reiterate here that the goal is to find a single set of parameters that results in the best fit to the reference data across all study sites, comparing the emulator output to the reference.

Stochastic gradient descent

First, we show the calibrated parameter set for the stochastic gradient descent (SGD) method. As mentioned, this calibration methodology allows us to explore parameter sets on which the emulator was not explicitly trained. We used the SGD method to find the parameter set leading to the lowest discrepancy (loss), comparing emulated outputs to reference data. Then, we ran the original simulation model with the selected parameters to see the relationship between the selected parameter set, the underlying simulation, the emulated outcomes, and the reference data. Figure 4.3 shows the calibrated simulation, emulator, and reference data for the Dielmo, Ndiop, and Namawala study sites, corresponding to the annual incidence and prevalence outcomes, respectively. Figure 4.4 shows the calibrated simulation, emulator, and reference data for the Dapelogo and Laye study sites, corresponding to density and age-binned, monthly parasitemia and gametocytemia outcomes. Figure 4.5 shows the calibrated simulation, emulator, and reference data for the Matsari, Rafin Marke, and Sugungum study sites, corresponding to density and age-binned, monthly parasitemia outcomes. Table 4.5 shows the calibrated parameter set giving rise to the best-fit outcomes.

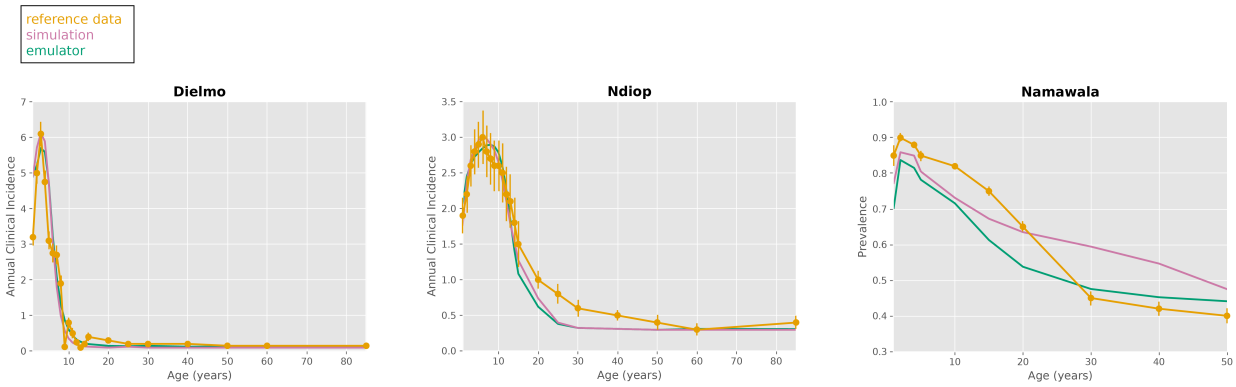

Figure 4.3: **SGD calibration plots for Dielmo, Ndiop, and Namawala sites.** These plots show the simulation, emulator, and reference data for the study sites corresponding to the annual clinical incidence and malaria prevalence outcomes, calibrated via the stochastic gradient descent method.

Parameter	**Value**
Antigen switch rate	$6.9e-04$
Falciparum MSP variants	5
Falciparum nonspecific types	160
Falciparum PfEMP1 variants	2663
Max individual infections	11
MSP merozoite kill fraction	0.11
Nonspecific antigenicity factor	0.54

Table 4.5: **Best fit immune parameters from SGD calibration.**

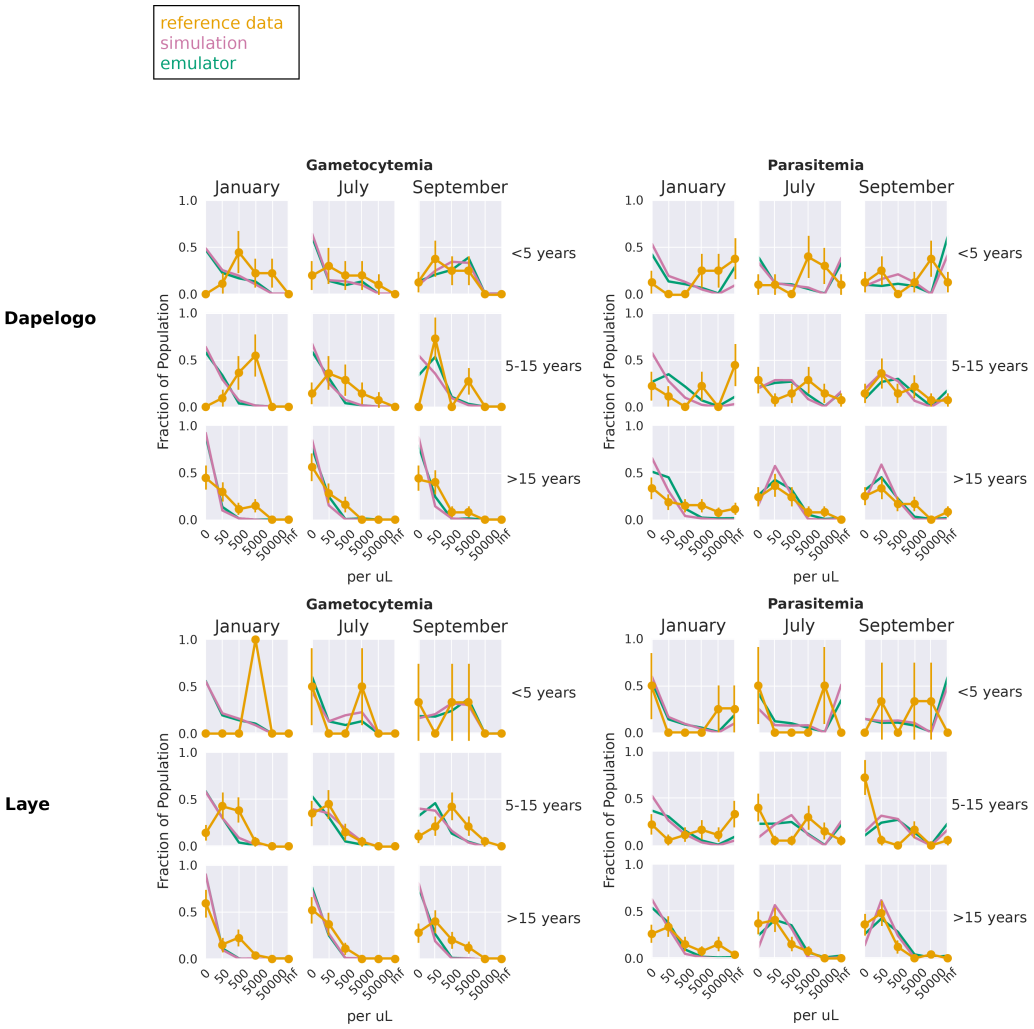

Figure 4.4: **SGD calibration plots for Dapelogo and Laye sites.** These plots show the simulation, emulator, and reference data for the study sites corresponding to the parasitemia and gametocytemia outcomes, calibrated via the stochastic gradient descent method.

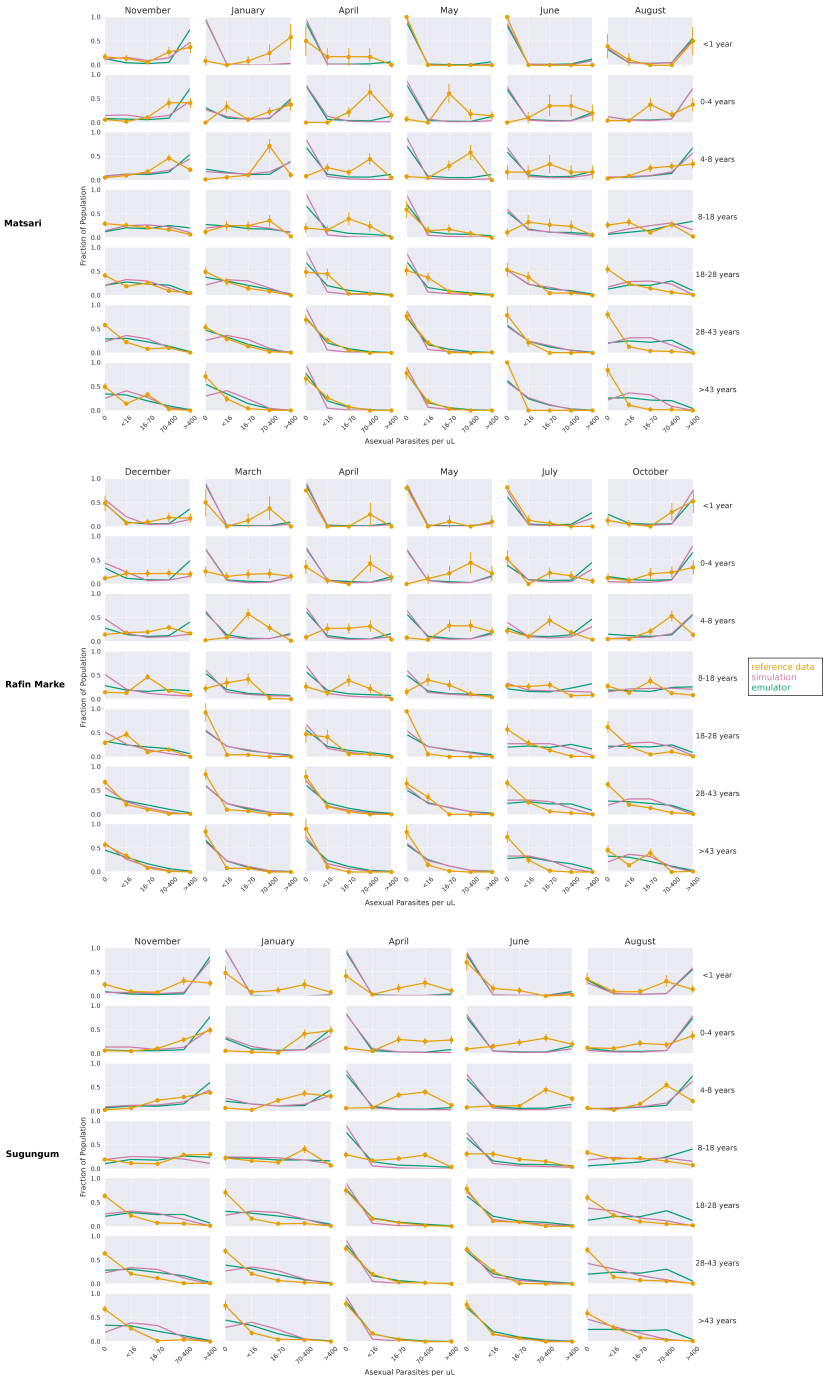

Figure 4.5: **SGD calibration plots for Matsari, Rafin Marke and Sugungum sites.** These plots show the simulation, emulator, and reference data for the study sites corresponding to the parasitemia outcomes, calibrated via the stochastic gradient descent method.

Likelihood

Next, we show the calibrated parameter set for the likelihood-based approach to aligning simulation data with reference data. Figure 4.6 shows the calibrated simulation, emulator, and reference data for the Dielmo, Ndiop, and Namawala study sites, corresponding to the annual incidence and prevalence outcomes, respectively. Figure 4.7 shows the calibrated simulation, emulator, and reference data for the Dapelogo and Laye study sites, corresponding to density and age-binned, monthly parasitemia and gametocytemia outcomes. Figure 4.8 shows the calibrated simulation, emulator, and reference data for the Matsari, Rafin Marke, and Sugungum study sites, corresponding to density and age-binned, monthly parasitemia outcomes. Table 4.6 shows the calibrated parameter set giving rise to the best-fit outcomes.

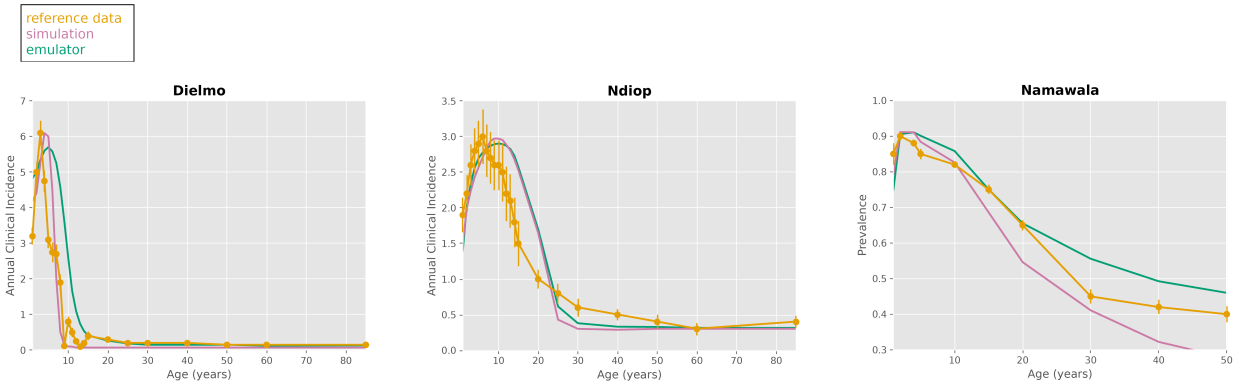

Figure 4.6: **Likelihood calibration plots for Dielmo, Ndiop, and Namawala sites.** These plots show the simulation, emulator, and reference data for the study sites corresponding to the annual clinical incidence and malaria prevalence outcomes, calibrated via the likelihood method.

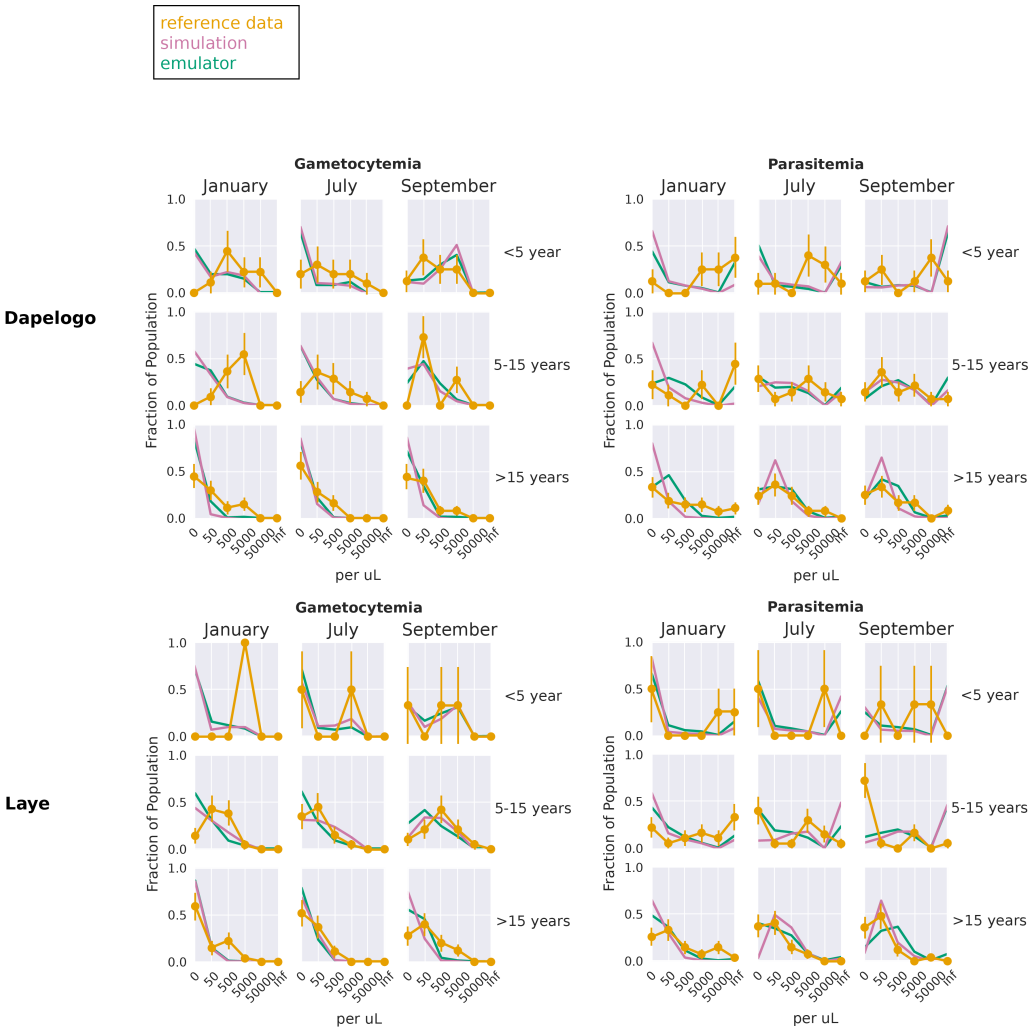

Figure 4.7: **Likelihood calibration plots for Dapelogo and Laye sites.** These plots show the simulation, emulator, and reference data for the study sites corresponding to the parasitemia and gametocytemia outcomes, calibrated via the likelihood method.

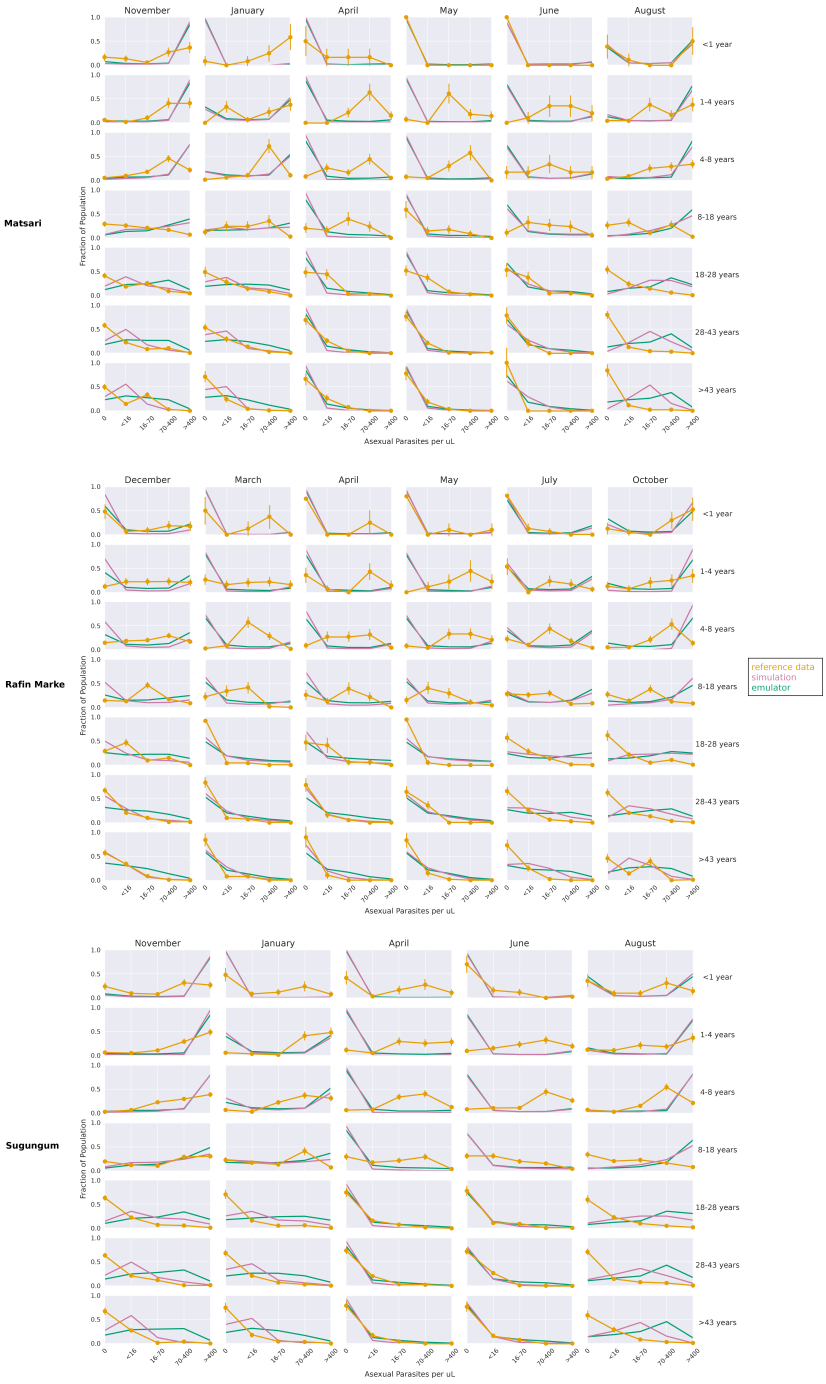

Figure 4.8: **Likelihood calibration plots for Matsari, Rafin Marke and Sugungum sites.** These plots show the simulation, emulator, and reference data for the study sites corresponding to the parasitemia outcomes, calibrated via the likelihood method.

Parameter	Value
Antigen switch rate	0.18
Falciparum MSP variants	154
Falciparum nonspecific types	305
Falciparum PfEMP1 variants	3651
Max individual infections	9
MSP merozoite kill fraction	0.83
Nonspecific antigenicity factor	0.46

Table 4.6: **Best fit immune parameters from likelihood calibration.**

Nearest neighbors

Finally, we tested was a nearest neighbors approach to calibration. Here we show the parameter set whose emulated outputs were nearest to the reference data with respect to the ℓ_2 loss criterion. Figure 4.9 shows the calibrated simulation, emulator, and reference data for the Dielmo, Ndiop, and Namawala study sites, corresponding to the annual incidence and prevalence outcomes, respectively. Figure 4.10 shows the calibrated simulation, emulator, and reference data for the Dapelogo and Laye study sites, corresponding to density and age-binned, monthly parasitemia and gametocytemia outcomes. Figure 4.11 shows the calibrated simulation, emulator, and reference data for the Matsari, Rafin Marke, and Sugungum study sites, corresponding to density and age-binned, monthly parasitemia outcomes. Table 4.7 shows the calibrated parameter set giving rise to the best-fit outcomes.

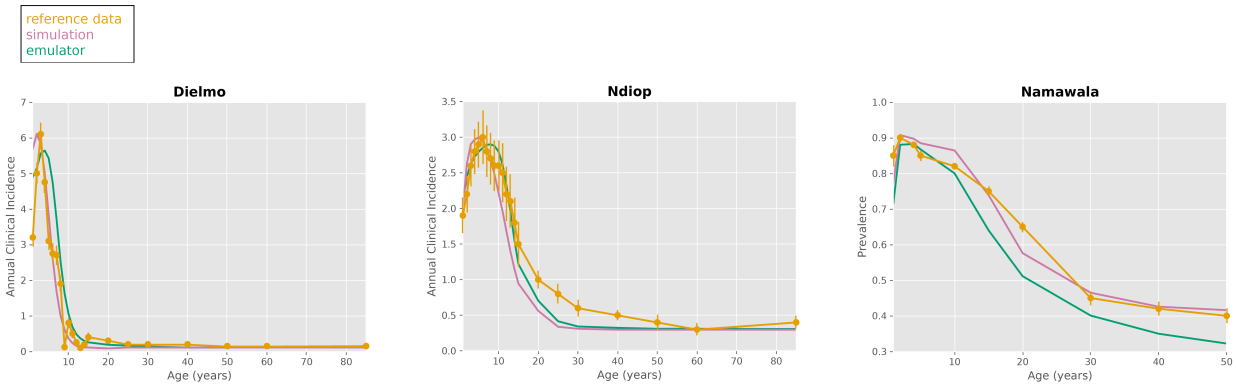

Figure 4.9: **Nearest neighbor calibration plots for Dielmo, Ndiop, and Namawala sites.** These plots show the simulation, emulator, and reference data for the study sites corresponding to the annual clinical incidence and malaria prevalence outcomes, calibrated via the nearest neighbors method.

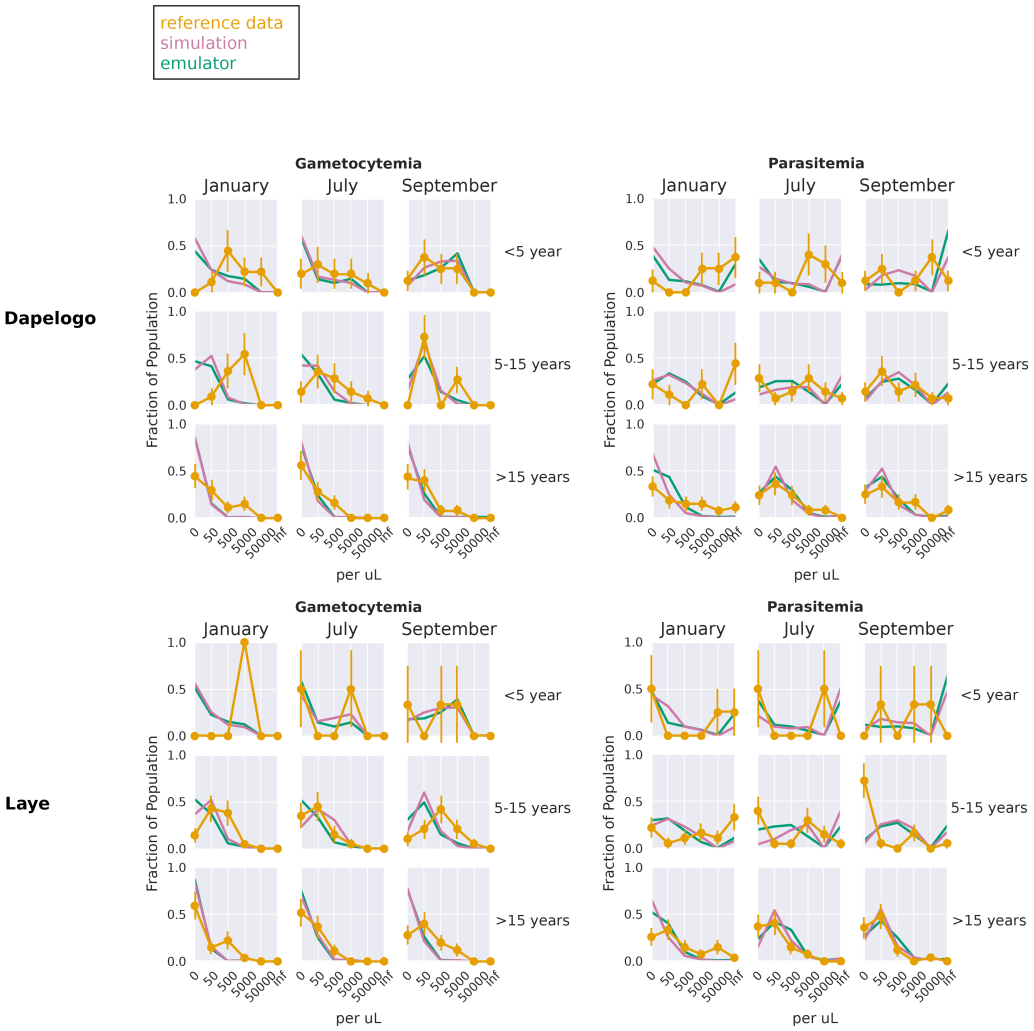

Figure 4.10: **Nearest neighbor calibration plots for Dapelogo and Laye sites.** These plots show the simulation, emulator, and reference data for the study sites corresponding to the parasitemia and gametocytemia outcomes, calibrated via the nearest neighbors method.

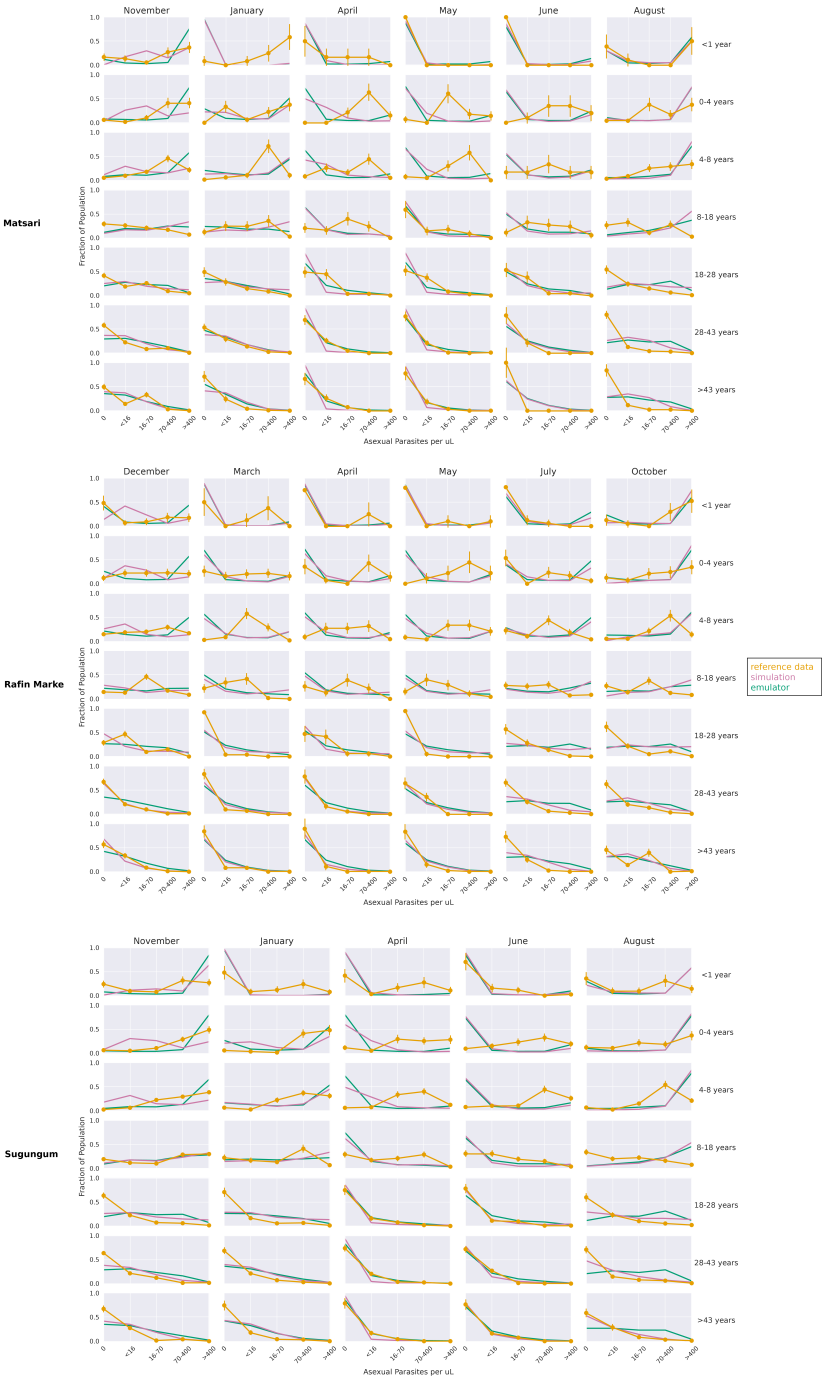

Figure 4.11: **Nearest neighbor calibration plots for Matsari, Rafin Marke and Sugungum sites.** These plots show the simulation, emulator, and reference data for the study sites corresponding to the parasitemia outcomes, calibrated via the nearest neighbors method.

Parameter	Value
Antigen switch rate	$4.6e-06$
Falciparum MSP variants	6
Falciparum nonspecific types	300
Falciparum PfEMP1 variants	1739
Max individual infections	9
MSP merozoite kill fraction	0.67
Nonspecific antigenicity factor	$9.4e-06$

Table 4.7: **Best fit immune parameters from nearest neighbors calibration.**

Sensitivity analysis

Figure 4.12 shows the relationship between the size of the dataset on which the emulator was trained versus its ability to predict outcomes in a previously-unseen simulation data subset. Training of ML models is generally the most computationally expensive step in the inference pipeline, and therefore there is a tradeoff between training models on more data and resource usage. For more simple models, such as the feed-forward network used to emulate EMOD, we see that the emulator can learn patterns in the simulation data even when trained on smaller data subsets. However, for more complex models such as vision or large language models [154, 155], the size of the training data is more relevant. Additionally, we see that providing the model with too much training data leads to an increase in the variance of loss for the unseen data subset, indicating that the model has overfit (i.e., the model learns noise in the training data and is unable to extrapolate on unseen data).

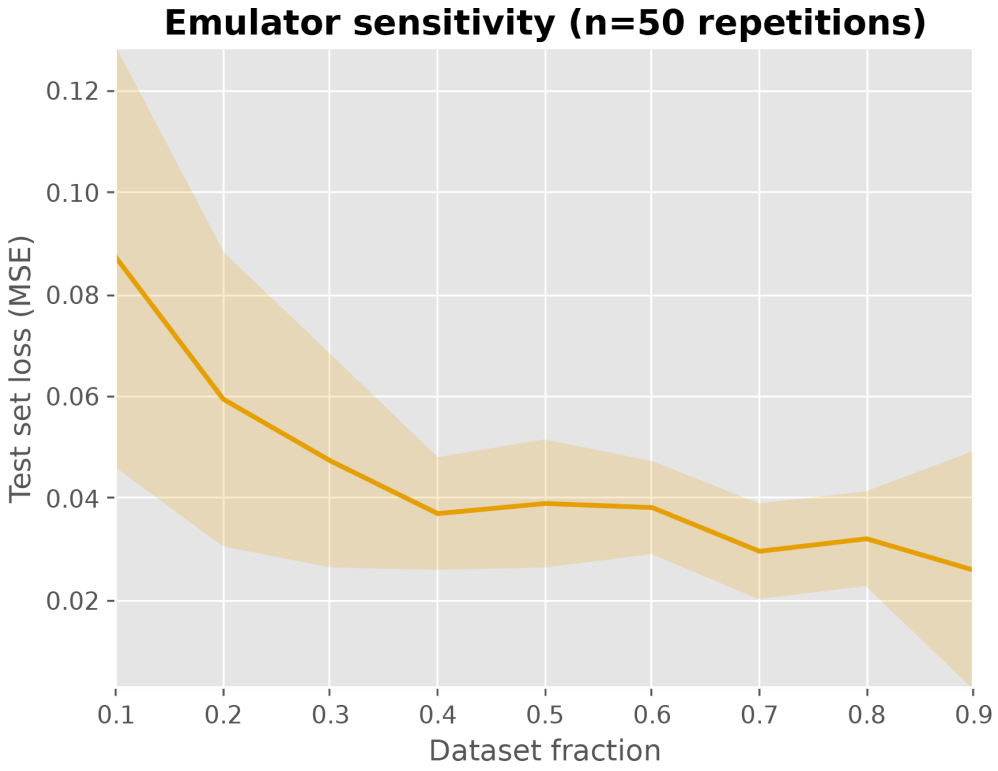

Figure 4.12: **Sensitivity analysis for emulator training dataset size.**

New site inference

For each study site, an emulator was trained on all simulation data, excluding the data for the site. Inputs were augmented with site-specific data such as monthly transmission rates and interventions. Calibration were conducted across all sites (excluding the new site), and the underlying simulation was run with the calibrated parameters for all sites. The subsequent figures show results for stochastic gradient descent calibrations. Figure 4.13 shows the calibrated simulation, emulator, and reference data for the Dielmo, Ndiop, and Namawala study sites, corresponding to the annual incidence and prevalence outcomes, respectively. Figure 4.14 shows the calibrated simulation, emulator, and reference data for the Dapelogo and Laye study sites, corresponding to density and age-binned, monthly parasitemia and gametocytemia outcomes. Figure 4.15 shows the calibrated simulation, emulator, and reference data for the Matsari, Rafin Marke, and Sugungum study sites, corresponding to density and age-binned, monthly parasitemia outcomes.

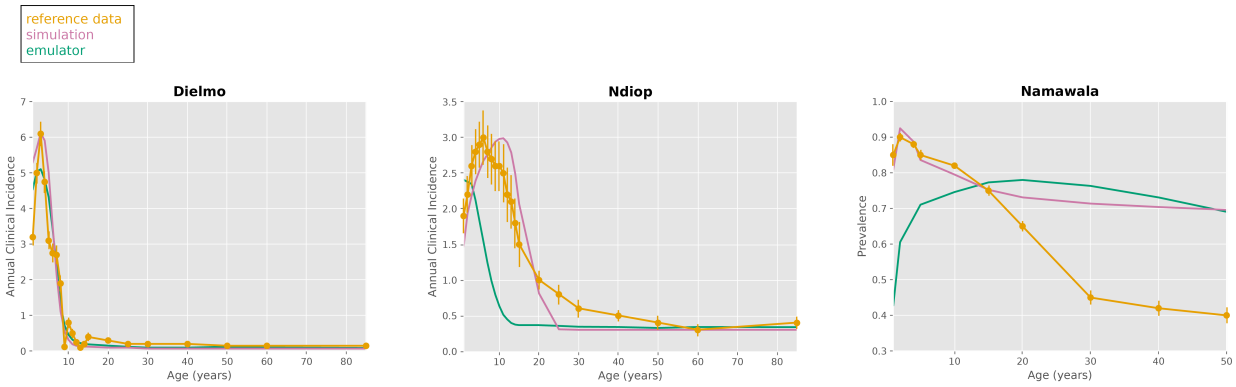

Figure 4.13: **Site-excluded SGD calibration plots for Dielmo, Ndiop, and Namawala sites.** These plots show the simulation, emulator, and reference data for the study sites corresponding to the annual clinical incidence and malaria prevalence outcomes, calibrated via the stochastic gradient descent method, using emulators not explicitly trained on data from these sites.

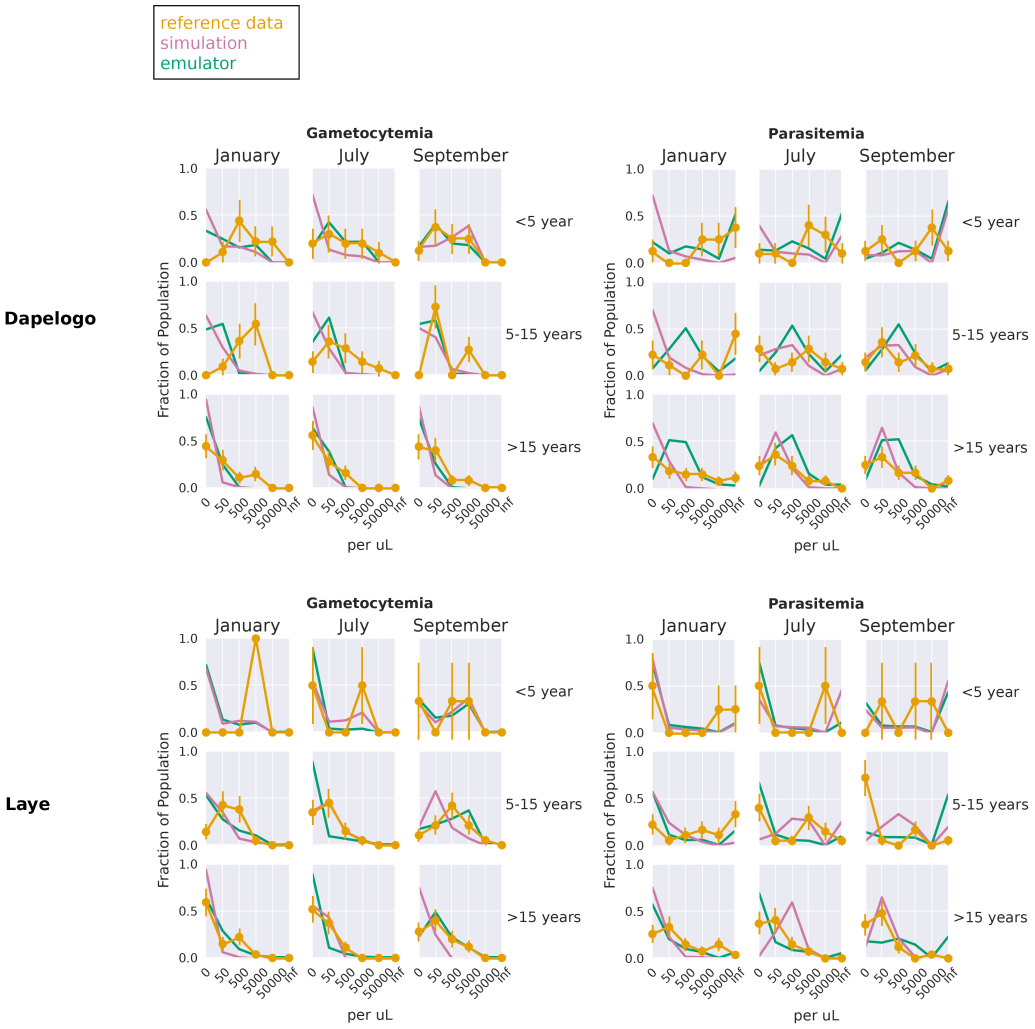

Figure 4.14: **Site-excluded SGD calibration plots for Dapelogo and Laye sites.** These plots show the simulation, emulator, and reference data for the study sites corresponding to the parasitemia and gametocytemia outcomes, calibrated via the stochastic gradient descent method, using emulators not explicitly trained on data from these sites.

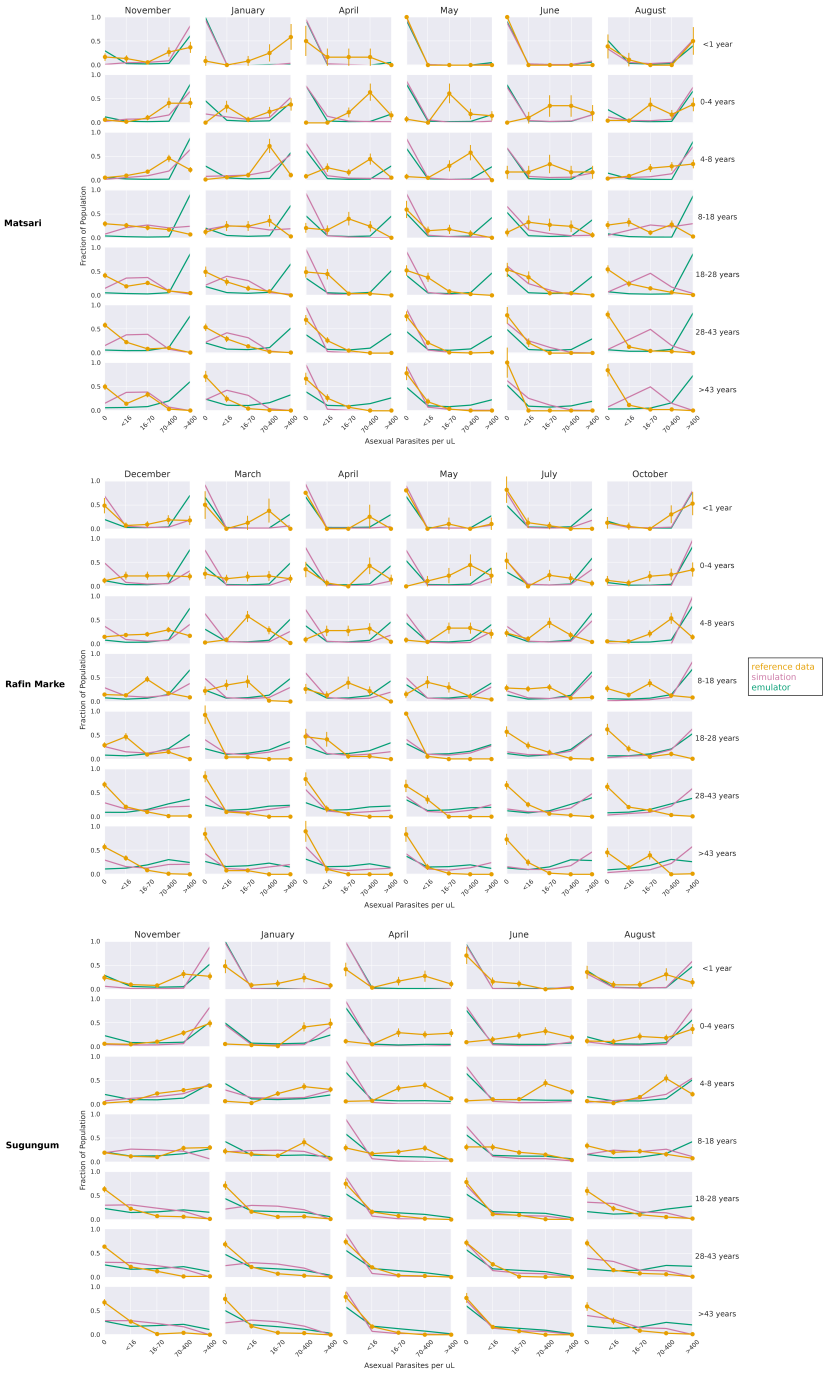

Figure 4.15: **Site-excluded SGD calibration plots for Matsari, Rafin Marke and Sugungum sites.** These plots show the simulation, emulator, and reference data for the study sites corresponding to the parasitemia outcomes, calibrated via the stochastic gradient descent method, using emulators not explicitly trained on data from these sites.

4.4 Discussion and future directions

Here, we have described a workflow to 1) emulate a complex malaria transmission model using deep neural networks, 2) calibrate the underlying model to reference data using the emulator, and 3) assess the emulator's ability to predict outputs for study sites not seen during training. Through careful sampling of the underlying parameter space, calibration methodology, and neural network architecture, we have shown that machine learning alternatives to traditional model calibration techniques (e.g., Markov chain Monte Carlo, particle filters) can be used to rapidly search parameter space and align mechanistic models to field data. In terms of model architecture, we employed a multitask, feed-forward neural network mapping the input parameters (in this case, parameters associated with immunological dynamics of malaria transmission) to age and density-binned epidemiological outcomes. While more complex architectures exist (e.g., recurrent or transformer-based models) for time series inference, these models require more resources to train properly. The multitask architecture allowed for simultaneous inference of different outcomes across study sites, to easily align with site-specific reference data. Three calibration methodologies were tested: loss minimization (nearest neighbors), likelihood maximization, and constrained optimization (stochastic gradient descent), allowing exploration of parameter space both within and outside the region on which the emulator was trained.

We have additionally shown that neural network emulator models can predict outcomes for previously-unseen sites, allowing for more flexibility as more field data are obtained. Though the emulator performance is slightly degraded due to less training data and extrapolation to new study sites, the fits suggest that the emulator can still narrow down parameter space to reasonable values, given that the emulator training is augmented with suitable site-specific data such as transmission rates and intervention coverages. In our analysis, the structure of the field data matches the simulation data on which the emulator was trained, but future directions could consider updating the final layers of the neural network to output new data structures, as is done in other domains [156, 157]. This would allow even more flexibility when calibrating new field sites. With respect to the emulator's performance and the size of the training data, our study found that smaller parameter sets can still capture the underlying simulation's dynamics, albeit with more variance. This can inform the design of emulators in the context of limited computational resources.

Interpretability of ML models

A major challenge with the acceptance of ML models is their interpretability [158]. That is, most traditional ML models are trained by minimizing the loss between the training data and the predicted outputs; the mechanisms on *how* they learn these patterns can be hard to discern, especially as model complexity increases. For some applications, under-

standing the underlying mechanisms of an ML model may be less of a concern. But for epidemiological models, the mechanisms of disease transmission are important to understanding how interventions are expected to behave on outcomes of interest. Additionally, in the calibration phase, it is important to ensure that model inputs and outputs correspond to biologically plausible parameter values (for example, by constraining values to realistic ranges, even if other values improve numerical performance).

An active area of ML research is improving the interpretability of models. Methods include reinforcement learning with human feedback and mixture of experts, among others [159, 160]. In the disease modeling realm, trusting inferences from ML models will require an understanding of the mechanisms by which an inference is made. Fine-tuning may also be required to ensure the model outputs are aligned with biologically plausible values. In our work, we have shown that ML emulators can rapidly search parameter space in order to align model outputs with reference data. Our three calibration methods however found different parameter sets which minimize this discrepancy. Calibration outputs should be assessed against domain knowledge to identify which parameter sets are the most feasible given transmission setting and model dynamics [139]. Recent methods have been introduced to even incorporate domain knowledge into the training of ML models [161].

Transfer learning

An active area of ML research is *transfer learning* or *zero-shot learning* [156, 157, 162–166]. In this paradigm, models predict outputs on samples not observed during training. Through data augmentation or other techniques, transfer learning can allow for inference on a wide range of outcomes without the need to re-train the model. In the context of emulation and calibration, an interesting application of transfer learning is re-calibrating after new field data are obtained. For example, if we augment the training data with more study-site specific variables (e.g., monthly EIR, anti-malaria intervention coverages, rainfall, etc.), the surrogate can learn the relationship between these variables and the epidemiological outcomes. Then, if field data are obtained for a new study, the calibration process can proceed for the new study site without the need to retrain the underlying model (the most computationally demanding process in the workflow). The neural network may need to be modified to accommodate new data formats.

Limitations

This study has several limitations. Mechanistic models of malaria transmission must be sufficiently complex to capture the seasonal and heterogeneous (by age, species, and location) nature of the disease. Even with complex models, capturing age-based heterogeneity is difficult [133] due to the nature of immune dynamics in children (i.e., children often experience more severe cases of malaria after maternal immunity has waned, but

exposure immunity has not yet developed). Our calibration methodology aimed to find one set of immune parameters that best fit the reference data across age groups, but we see that the fits for parasite density are markedly worse in juvenile age groups, particularly for the Garki sites. This finding suggests that 1) one set of immune parameters may not be fully appropriate across the age spectrum and that juvenile dynamics should be calibrated separately, and/or 2) the underlying model does not capture the complexity of juvenile transmission dynamics well. Both of these aspects limit the ability of the calibration workflow to extend to younger age groups. From an intervention planning perspective, these dynamics should be better understood, as interventions often target children to reduce the significant morbidity and mortality they face from malaria.

A main challenge with of ML models is the principled development of the emulator. Many architectures, hyperparameters, and training data sampling schemes must be considered. While some tools exist to help design these models, many choices must be made beforehand to ensure the emulator is capturing the dynamics of the transmission model. We have shown a use case where interpretability is not a primary concern (as we are using the emulator to search parameter space instead of explaining a phenomenon). For other use cases where the mechanisms of the ML model are important to understand, careful attention must be paid to the development of the emulator to ensure it accurately represents the underlying scientific process [139]. Additionally, the tradeoff between simulation dataset size and model accuracy must be considered in the context of limited computational resources. We deliberately sampled a large range of parameter space as a proof-of-concept, but future studies should explore more deeply the ability of the emulator to learn simulation dynamics with more limited training datasets.

A final concern relates to the validation of the calibration workflow. We have shown that three different calibration methodologies produce different parameter sets whose outputs align with the reference data. Biological parameters can be difficult to validate, as most studies cannot infer these immune parameters directly. Nonetheless, selected parameter sets should be compared against previous literature and domain knowledge to ensure that they are biologically feasible, as the emulator itself is agnostic to the underlying mechanisms. While our constrained optimization limited these values to be within broad biological ranges, more fine-tuning *post hoc* can help to explore the parameter space more realistically. A central challenge in the development of emulator models is the desire to minimize numerical discrepancy between emulated outcomes and reference data while maintaining biological feasibility.

Chapter 5

Conclusion and future directions

5.1 Overview of this work

In this work, we have shown three related, but distinct components of designing computational methods with respect to vector-borne disease transmission and genetic vector control. In Chapter 2, we outlined a novel mechanistic model to link the entomology and epidemiology of gene drive interventions. Using a computationally efficient representation of a Markov chain entomology model linked to a partial differential equation model of human disease dynamics, we showed that flexible adaptations of different modeling frameworks can be coalesced to estimate clinical outcomes associated with gene drive interventions. Additionally, we included a spatial module which is able to simulate the placement of traps across a geospatial landscape, in order to inform the post-release monitoring of a gene drive program. In Chapter 3, we used the framework described in Chapter 2 in order to interrogate the genetic parameters of a population replacement gene drive system and their expected impacts on epidemiological outcomes (clinical incidence of malaria, prevalence, and mortality) in two hypothetical African settings. We then 1) identified regions of parameter space that would lead to conservative reductions in these outcomes, and 2) established the relative importance of each parameter on each outcome of interest. Due to the absence of reliable field data, modeling analyses can help to elucidate the relationship between genetic parameters (e.g., fitness, infection blocking) and effects on human health in a given population. Due to the flexibility of the framework, we parametrized the simulations to two settings (Kenya and Burkina Faso) using environmental and intervention data from these locations. Finally, in an application of machine learning, we showed that a deep neural network can be used to emulate a complex model of malaria transmission and calibrate it to reference (field) data. Compared to more traditional calibration methodologies, using a neural network emulator can dramatically reduce the time required to fit complex models to external data. Additionally, by leveraging methods from multitask learning, we simultaneously emulated numerous epidemiological outcomes across different EIRs, case management strategies,

and physical locations. Taken together, this work provides new perspectives on how to integrate computational models into the design and evaluation of critically-needed gene drive products for genetic vector control.

5.2 Future directions

Biosafety and remediation

An important consideration of gene drive technology is risk and biosafety. While gene drive technology holds promise in reducing the burden of vector borne disease, ecological and societal risks must be well-understood prior to release. According to Devos *et al.* [47], potential risks include eradication (instead of control) of the target species, uncontrolled spread, interactions with non-target species, and negative impacts to biodiversity and health. Among their recommendations, they say that modeling can help "ensure a dynamic interplay between risk assessment and risk management." Just as we have shown that models can shed light on the influence of genetic parameters on epidemiological outcomes, models of spread and remediation can help to inform the design of field trials and surveillance programs. Chennuri *et al.* [167] reviewed various strategies for remediating gene drive releases. They include strategies to target specific populations of a species (synthetic alleles), halt or delete gene drives (reversal drives, anti-drives), regulate gene drive propagation (programmable drives), excise gene drive without restoration of wild-type (chemical controllable gene drives), regulate spatio-temporal gene drive activity (inducible gene drives, switchable gene drives), and drive extinction through introgressed resistance (synthetic resistance). Models have been used to estimate the impacts of reversal drives [85] and "biodegradable" gene drives [168], and can serve as useful tools in the risk assessment of various gene drive products. Future modeling work could guide the development of remediation strategies and be tailored to specific constructs, locations, and demographics.

Field trial design

The design of field trials for gene drive products will be critical to ensuring their safety and success. Because they can encompass large spatial areas and affect everyone living in the radius of effect, gene drive trials will look fundamentally different to those for traditional health interventions such as medication or bednets. Rašić *et al.* [87] have identified monitoring priorities for *Anopheles* gene drive trials such as vector abundance, environmental drivers of mosquito population, mosquito movement patterns, resistance to insecticides, biting rates, and prevalence of transgenic mosquitoes (among others). Of these, models can help to bolster the planning of a field trial by parameterizing environmental conditions, simulating trap placement, and estimating the dispersal of released mosquitoes. Monitoring and risk/benefit assessments form a part of the core commit-

ments for field trials of gene drive organisms [169], and thus models should be used to inform these aspects of gene drive field trials in the absence of field data.

Spatial dynamics

Understanding the spatial dynamics of gene drive releases will be relevant to the design of small and large-scale trials and interventions. Alongside the need to monitor the physical distribution of genes [87], an understanding of dispersal and gene flow from a spatial perspective will help to inform the expected efficacy of a gene drive intervention. From an epidemiological perspective, models can also help to illustrate the expected impact on health outcomes as a result of a gene drive intervention from a spatial scale. For example, an important question will be the "spillover effect" of a gene drive intervention on neighboring locations. Some models have been developed to understand the spatial dynamics of gene drive spread from both entomological [89, 101, 117], genetic [170–174], and epidemiological [34, 92] perspectives. Of note, as climate change is expected to fundamentally alter the dynamics of mosquito habitation [15, 175], models incorporating explicit climactic drivers will be useful in understanding the expected dynamics of a gene drive program.

Eco-evolutionary considerations

Though the expected timeframe for epidemiological impact of gene drive interventions is expected to be under ten years [41, 88], nonetheless there are questions around the long-term ecological and evolutionary behavior of these genetically modified organisms. Combs *et al.* [176] proposed using dynamical models from ecology literature to guide risk assessment for gene drive products. Further, Kim *et al.* [177] argue that the release of gene drive organisms may result in strong eco-evolutionary feedbacks. They state that factors such as population structure, life history, environmental variation, and mode of selection should be incorporated into gene drive models. Building on prior theoretical understanding of pathogen virulence and evolution, models could help to understand the long-term dynamics of genetic resistance, competition between wild-type and transgenic species, immunity, and virulence [178–180].

Advances in ML/AI modeling

Finally, we briefly touch on the role of machine learning and artificial intelligence (ML/AI) in epidemiology. The last decade has seen immense progress in the development and deployment of these technologies, ranging from state-of-the-art text generation [181, 182], computer vision [183], and time series forecasting [184–186]. In the domain of biology and health, there has been an increased interest in utilizing ML/AI to design proteins and bio-therapeutics [187–190], as well as tools for diagnostics and clinical decision support [191–194]. With respect to epidemiological models, we have shown in Chapter 4

that neural networks can be used as surrogates to emulate complex mechanistic models and rapidly search the parameter space to calibrate them to external data. Additional use cases under development include vision models for the classification of mosquito species [195], causal identification of treatment effects in observational data [196, 197], and "nowcasting" disease trajectories [198, 199]. As interest in ML/AI technologies (as well as access to computational resources) continues to grow, epidemiological modelers will benefit from their ability to understand patterns in large datasets and apply them to specific use cases.

Bibliography

[1] C. Pak, *The Poet Who Conquered Malaria: Medical Humanities and the Public Understanding of Science*, Jan. 2023.

[2] R. K. Borchering *et al.*, "Impacts of Zika emergence in Latin America on endemic dengue transmission," en, *Nat Commun*, vol. 10, no. 1, p. 5730, Dec. 2019, ISSN: 2041-1723. DOI: 10.1038/s41467-019-13628-x.

[3] V. Wiwanitkit, "Concurrent malaria and dengue infection: A brief summary and comment," en, *Asian Pacific Journal of Tropical Biomedicine*, vol. 1, no. 4, pp. 326–327, Aug. 2011, ISSN: 22211691. DOI: 10.1016/S2221-1691(11)60053-1.

[4] F. Okumu, "The fabric of life: What if mosquito nets were durable and widely available but insecticide-free?" en, *Malar J*, vol. 19, no. 1, p. 260, Dec. 2020, ISSN: 1475-2875. DOI: 10.1186/s12936-020-03321-6.

[5] World Health Organization, *Indoor residual spraying: an operational manual for indoor residual spraying (IRS) for malaria transmission control and elimination*, en, 2nd ed. Geneva: World Health Organization, 2015, ISBN: 978-92-4-150894-0.

[6] F. Kané *et al.*, "Performance of IRS on malaria prevalence and incidence using pirimiphos-methyl in the context of pyrethroid resistance in Koulikoro region, Mali," en, *Malar J*, vol. 19, no. 1, p. 286, Dec. 2020, ISSN: 1475-2875. DOI: 10.1186/s12936-020-03357-8.

[7] J. Pryce, N. Medley, and L. Choi, "Indoor residual spraying for preventing malaria in communities using insecticide-treated nets," en, *Cochrane Database of Systematic Reviews*, vol. 2022, no. 1, Cochrane Infectious Diseases Group, Ed., Jan. 2022, ISSN: 14651858. DOI: 10.1002/14651858.CD012688.pub3.

[8] H. Guyatt, "A comparative cost analysis of insecticide-treated nets and indoor residual spraying in highland Kenya," *Health Policy and Planning*, vol. 17, no. 2, pp. 144–153, Jun. 2002, ISSN: 14602237. DOI: 10.1093/heapol/17.2.144.

[9] N. J. White, "Antimalarial drug resistance," en, *J. Clin. Invest.*, vol. 113, no. 8, pp. 1084–1092, Apr. 2004, ISSN: 0021-9738. DOI: 10.1172/JCI21682.

[10] A. Mayor and Q. Bassat, ""Resistance" to diagnostics: A serious biological challenge for malaria control and elimination," en, *EBioMedicine*, vol. 50, pp. 9–10, Dec. 2019, ISSN: 23523964. DOI: 10.1016/j.ebiom.2019.11.041.

[11] C. for Disease Control and Prevention, *Malaria's Impact Worldwide*.

[12] A. Haakenstad *et al.*, "Tracking spending on malaria by source in 106 countries, 2000–16: An economic modelling study," en, *The Lancet Infectious Diseases*, vol. 19, no. 7, pp. 703–716, Jul. 2019, ISSN: 14733099. DOI: 10.1016/S1473-3099(19)30165-3.

[13] N. Tian *et al.*, "Dengue Incidence Trends and Its Burden in Major Endemic Regions from 1990 to 2019," en, *TropicalMed*, vol. 7, no. 8, p. 180, Aug. 2022, ISSN: 2414-6366. DOI: 10.3390/tropicalmed7080180.

[14] M. C. Thomson and L. R. Stanberry, "Climate Change and Vectorborne Diseases," en, *N Engl J Med*, vol. 387, no. 21, C. G. Solomon and R. N. Salas, Eds., pp. 1969–1978, Nov. 2022, ISSN: 0028-4793, 1533-4406. DOI: 10.1056/NEJMra2200092.

[15] E. A. Mordecai *et al.*, "Optimal temperature for malaria transmission is dramatically lower than previously predicted," en, *Ecol Lett*, vol. 16, no. 1, P. Thrall, Ed., pp. 22–30, Jan. 2013, ISSN: 1461023X. DOI: 10.1111/ele.12015.

[16] S. J. Ryan, C. J. Carlson, E. A. Mordecai, and L. R. Johnson, "Global expansion and redistribution of Aedes-borne virus transmission risk with climate change," en, *PLoS Negl Trop Dis*, vol. 13, no. 3, B. A. Han, Ed., e0007213, Mar. 2019, ISSN: 1935-2735. DOI: 10.1371/journal.pntd.0007213.

[17] I.-A. Yeo, S.-H. Yoon, and J.-J. Yee, "Development of an urban energy demand forecasting system to support environmentally friendly urban planning," en, *Applied Energy*, vol. 110, pp. 304–317, Oct. 2013, ISSN: 03062619. DOI: 10.1016/j.apenergy.2013.04.065.

[18] T. Novosel *et al.*, "Agent based modelling and energy planning – Utilization of MATSim for transport energy demand modelling," en, *Energy*, vol. 92, pp. 466–475, Dec. 2015, ISSN: 03605442. DOI: 10.1016/j.energy.2015.05.091.

[19] D. B. Nelson and K. Ramaswamy, "Simple Binomial Processes as Diffusion Approximations in Financial Models," en, *Rev. Financ. Stud.*, vol. 3, no. 3, pp. 393–430, Jul. 1990, ISSN: 0893-9454, 1465-7368. DOI: 10.1093/rfs/3.3.393.

[20] A. Ay and D. N. Arnosti, "Mathematical modeling of gene expression: A guide for the perplexed biologist," en, *Critical Reviews in Biochemistry and Molecular Biology*, vol. 46, no. 2, pp. 137–151, Apr. 2011, ISSN: 1040-9238, 1549-7798. DOI: 10.3109/10409238.2011.556597.

[21] M. C. Reed *et al.*, "A Mathematical Model Gives Insights into Nutritional and Genetic Aspects of Folate-Mediated One-Carbon Metabolism," en, *The Journal of Nutrition*, vol. 136, no. 10, pp. 2653–2661, Oct. 2006, ISSN: 00223166. DOI: 10.1093/jn/136.10.2653.

[22] L. V. Stepanov, A. S. Koltsov, A. V. Parinov, and A. S. Dubrovin, "Mathematical modeling method based on genetic algorithm and its applications," *J. Phys.: Conf. Ser.*, vol. 1203, p. 012 082, Apr. 2019, ISSN: 1742-6588, 1742-6596. DOI: 10.1088/1742-6596/1203/1/012082.

[23] M. W. Libbrecht and W. S. Noble, "Machine learning applications in genetics and genomics," en, *Nat Rev Genet*, vol. 16, no. 6, pp. 321–332, Jun. 2015, ISSN: 1471-0056, 1471-0064. DOI: 10.1038/nrg3920.

[24] D. L. Smith, K. E. Battle, S. I. Hay, C. M. Barker, T. W. Scott, and F. E. McKenzie, "Ross, macdonald, and a theory for the dynamics and control of mosquito-transmitted pathogens," eng, *PLoS Pathog*, vol. 8, no. 4, e1002588, 2012, ISSN: 1553-7374. DOI: 10.1371/journal.ppat.1002588.

[25] J. T. Griffin *et al.*, "Reducing Plasmodium falciparum Malaria Transmission in Africa: A Model-Based Evaluation of Intervention Strategies," en, *PLoS Med*, vol. 7, no. 8, S. Krishna, Ed., e1000324, Aug. 2010, ISSN: 1549-1676. DOI: 10.1371/journal.pmed.1000324.

[26] K. J. Fraser *et al.*, "Estimating the potential impact of Attractive Targeted Sugar Baits (ATSBs) as a new vector control tool for Plasmodium falciparum malaria," en, *Malar J*, vol. 20, no. 1, p. 151, Dec. 2021, ISSN: 1475-2875. DOI: 10.1186/s12936-021-03684-4.

[27] M. A. Penny *et al.*, "Public health impact and cost-effectiveness of the RTS,S/AS01 malaria vaccine: A systematic comparison of predictions from four mathematical models," en, *The Lancet*, vol. 387, no. 10016, pp. 367–375, Jan. 2016, ISSN: 01406736. DOI: 10.1016/S0140-6736(15)00725-4.

[28] M. T. White, J. T. Griffin, T. S. Churcher, N. M. Ferguson, M.-G. Basáñez, and A. C. Ghani, "Modelling the impact of vector control interventions on Anopheles gambiae population dynamics," en, *Parasites Vectors*, vol. 4, no. 1, p. 153, Dec. 2011, ISSN: 1756-3305. DOI: 10.1186/1756-3305-4-153.

[29] T. Smith *et al.*, "Towards a comprehensive simulation model of malaria epidemiology and control," en, *Parasitology*, vol. 135, no. 13, pp. 1507–1516, Nov. 2008, ISSN: 0031-1820, 1469-8161. DOI: 10.1017/S0031182008000371.

[30] T. Reiker *et al.*, "Emulator-based Bayesian optimization for efficient multi-objective calibration of an individual-based model of malaria," en, *Nat Commun*, vol. 12, no. 1, p. 7212, Dec. 2021, ISSN: 2041-1723. DOI: 10.1038/s41467-021-27486-z.

[31] P. A. Eckhoff, "A malaria transmission-directed model of mosquito life cycle and ecology," en, *Malar J*, vol. 10, no. 1, p. 303, Dec. 2011, ISSN: 1475-2875. DOI: 10.1186/1475-2875-10-303.

[32] P. A. Eckhoff, "Malaria parasite diversity and transmission intensity affect development of parasitological immunity in a mathematical model," en, *Malar J*, vol. 11, no. 1, p. 419, Dec. 2012, ISSN: 1475-2875. DOI: 10.1186/1475-2875-11-419.

[33] P. Eckhoff, "Mathematical Models of Within-Host and Transmission Dynamics to Determine Effects of Malaria Interventions in a Variety of Transmission Settings," en, *The American Journal of Tropical Medicine and Hygiene*, vol. 88, no. 5, pp. 817–827, May 2013, ISSN: 0002-9637, 1476-1645. DOI: 10.4269/ajtmh.12-0007.

[34] S. Leung, N. Windbichler, E. A. Wenger, C. A. Bever, and P. Selvaraj, "Population replacement gene drive characteristics for malaria elimination in a range of seasonal transmission settings: A modelling study," en, *Malar J*, vol. 21, no. 1, p. 226, Dec. 2022, ISSN: 1475-2875. DOI: 10.1186/s12936-022-04242-2.

[35] T. Bousema *et al.*, "Hitting Hotspots: Spatial Targeting of Malaria for Control and Elimination," en, *PLoS Med*, vol. 9, no. 1, e1001165, Jan. 2012, ISSN: 1549-1676. DOI: 10.1371/journal.pmed.1001165.

[36] T. S. Churcher, N. Lissenden, J. T. Griffin, E. Worrall, and H. Ranson, "The impact of pyrethroid resistance on the efficacy and effectiveness of bednets for malaria control in Africa," en, *eLife*, vol. 5, e16090, Aug. 2016, ISSN: 2050-084X. DOI: 10.7554/eLife.16090.

[37] G.-H. Wang *et al.*, "Combating mosquito-borne diseases using genetic control technologies," en, *Nat Commun*, vol. 12, no. 1, p. 4388, Dec. 2021, ISSN: 2041-1723. DOI: 10.1038/s41467-021-24654-z.

[38] A. Nuss, A. Sharma, and M. Gulia-Nuss, "Genetic Manipulation of Ticks: A Paradigm Shift in Tick and Tick-Borne Diseases Research," *Front. Cell. Infect. Microbiol.*, vol. 11, p. 678 037, May 2021, ISSN: 2235-2988. DOI: 10.3389/fcimb.2021.678037.

[39] S. G. Breeland *et al.*, "Release of Chemosterilized Males for the Control of Anopheles Albimanus in El Salvador: III. Field Methods and Population Control*,†," en, *The American Journal of Tropical Medicine and Hygiene*, vol. 23, no. 2, pp. 288–297, Mar. 1974, ISSN: 0002-9637, 1476-1645. DOI: 10.4269/ajtmh.1974.23.288.

[40] L. Alphey *et al.*, "Sterile-Insect Methods for Control of Mosquito-Borne Diseases: An Analysis," en, *Vector-Borne and Zoonotic Diseases*, vol. 10, no. 3, pp. 295–311, Apr. 2010, ISSN: 1530-3667, 1557-7759. DOI: 10.1089/vbz.2009.0014.

[41] R. A. Apte *et al.*, "Eliminating malaria vectors with precision-guided sterile males," en, *Proc. Natl. Acad. Sci. U.S.A.*, vol. 121, no. 27, e2312456121, Jul. 2024, ISSN: 0027-8424, 1091-6490. DOI: 10.1073/pnas.2312456121.

[42] N. P. Kandul, J. Liu, H. M. Sanchez C., S. L. Wu, J. M. Marshall, and O. S. Akbari, "Transforming insect population control with precision guided sterile males with demonstration in flies," en, *Nat Commun*, vol. 10, no. 1, p. 84, Jan. 2019, ISSN: 2041-1723. DOI: 10.1038/s41467-018-07964-7.

[43] M. Li *et al.*, "Suppressing mosquito populations with precision guided sterile males," en, *Nat Commun*, vol. 12, no. 1, p. 5374, Sep. 2021, ISSN: 2041-1723. DOI: 10.1038/s41467-021-25421-w.

[44] J. B. Connolly *et al.*, "Recommendations for environmental risk assessment of gene drive applications for malaria vector control," en, *Malar J*, vol. 21, no. 1, p. 152, Dec. 2022, ISSN: 1475-2875. DOI: 10.1186/s12936-022-04183-w.

[45] N. M. Guruprasad, S. K. Jalali, and H. P. Puttaraju, "Wolbachia-a foe for mosquitoes," en, *Asian Pacific Journal of Tropical Disease*, vol. 4, no. 1, pp. 78–81, Feb. 2014, ISSN: 22221808. DOI: 10.1016/S2222-1808(14)60319-4.

[46] J. T. Lim *et al.*, "Efficacy of Wolbachia-mediated sterility to reduce the incidence of dengue: A synthetic control study in Singapore," en, *The Lancet Microbe*, S266652472300397X, Feb. 2024, ISSN: 26665247. DOI: 10.1016/S2666-5247(23)00397-X.

[47] Y. Devos, J. D. Mumford, M. B. Bonsall, D. C. Glandorf, and H. D. Quemada, "Risk management recommendations for environmental releases of gene drive modified insects," en, *Biotechnology Advances*, vol. 54, p. 107 807, Jan. 2022, ISSN: 07349750. DOI: 10.1016/j.biotechadv.2021.107807.

[48] M. E. Sinka *et al.*, "The dominant Anopheles vectors of human malaria in Africa, Europe and the Middle East: Occurrence data, distribution maps and bionomic précis," en, *Parasites Vectors*, vol. 3, no. 1, p. 117, Dec. 2010, ISSN: 1756-3305. DOI: 10.1186/1756-3305-3-117.

[49] E. Bier, "Gene drives gaining speed," en, *Nat Rev Genet*, vol. 23, no. 1, pp. 5–22, Jan. 2022, ISSN: 1471-0056, 1471-0064. DOI: 10.1038/s41576-021-00386-0.

[50] H. Bastide, M. Cazemajor, D. Ogereau, N. Derome, F. Hospital, and C. Montchamp-Moreau, "Rapid Rise and Fall of Selfish Sex-Ratio X Chromosomes in Drosophila simulans: Spatiotemporal Analysis of Phenotypic and Molecular Data," en, *Molecular Biology and Evolution*, vol. 28, no. 9, pp. 2461–2470, Sep. 2011, ISSN: 1537-1719, 0737-4038. DOI: 10.1093/molbev/msr074.

[51] R. Corbett-Detig, P. Medina, H. Frérot, C. Blassiau, and V. Castric, "Bulk pollen sequencing reveals rapid evolution of segregation distortion in the male germline of Arabidopsis hybrids," en, *Evolution Letters*, vol. 3, no. 1, pp. 93–103, Feb. 2019, ISSN: 2056-3744. DOI: 10.1002/ev13.96.

[52] S. B. Kingan, D. Garrigan, and D. L. Hartl, "Recurrent Selection on the Winters *sex-ratio* Genes in *Drosophila simulans*," en, *Genetics*, vol. 184, no. 1, pp. 253–265, Jan. 2010, ISSN: 1943-2631. DOI: 10.1534/genetics.109.109587.

[53] H. P. Döring, E. Tillmann, and P. Starlinger, "DNA sequence of the maize transposable element Dissociation," en, *Nature*, vol. 307, no. 5947, pp. 127–130, Jan. 1984, ISSN: 0028-0836, 1476-4687. DOI: 10.1038/307127a0.

[54] G. Wallau, P. Capy, E. Loreto, and A. Hua-Van, "Genomic landscape and evolutionary dynamics of mariner transposable elements within the Drosophila genus," en, *BMC Genomics*, vol. 15, no. 1, p. 727, 2014, ISSN: 1471-2164. DOI: 10.1186/1471-2164-15-727.

[55] A. Hammond *et al.*, "A CRISPR-Cas9 gene drive system targeting female reproduction in the malaria mosquito vector Anopheles gambiae," en, *Nat Biotechnol*, vol. 34, no. 1, pp. 78–83, Jan. 2016, ISSN: 1087-0156, 1546-1696. DOI: 10.1038/nbt.3439.

[56] K. Kyrou *et al.*, "A CRISPR–Cas9 gene drive targeting doublesex causes complete population suppression in caged Anopheles gambiae mosquitoes," en, *Nat Biotechnol*, vol. 36, no. 11, pp. 1062–1066, Nov. 2018, ISSN: 1087-0156, 1546-1696. DOI: 10.1038/nbt.4245.

[57] S. L. James, J. M. Marshall, G. K. Christophides, F. O. Okumu, and T. Nolan, "Toward the Definition of Efficacy and Safety Criteria for Advancing Gene Drive-Modified Mosquitoes to Field Testing," en, *Vector-Borne and Zoonotic Diseases*, vol. 20, no. 4, pp. 237–251, Apr. 2020, ISSN: 1530-3667, 1557-7759. DOI: 10.1089/vbz.2019.2606.

[58] A. Mondal, V. N. Vásquez, and J. M. Marshall, "Target Product Profiles for Mosquito Gene Drives: Incorporating Insights From Mathematical Models," *Front. Trop. Dis*, vol. 3, p. 828 876, Mar. 2022, ISSN: 2673-7515. DOI: 10.3389/fitd.2022.828876.

[59] R. Carballar-Lejarazú and A. A. James, "Population modification of Anopheline species to control malaria transmission," *Pathogens and Global Health*, vol. 111, no. 8, pp. 424–435, 2017. DOI: 10.1080/20477724.2018.1427192.

[60] N. Chitnis, T. Smith, and R. Steketee, "A mathematical model for the dynamics of malaria in mosquitoes feeding on a heterogeneous host population," en, *Journal of Biological Dynamics*, vol. 2, no. 3, pp. 259–285, Jul. 2008, ISSN: 1751-3758, 1751-3766. DOI: 10.1080/17513750701769857.

[61] P. G. T. Walker, J. T. Griffin, N. M. Ferguson, and A. C. Ghani, "Estimating the most efficient allocation of interventions to achieve reductions in Plasmodium falciparum malaria burden and transmission in Africa: A modelling study," en, *The Lancet Global Health*, vol. 4, no. 7, e474–e484, Jul. 2016, ISSN: 2214109X. DOI: 10.1016/S2214-109X(16)30073-0.

[62] M. M. Traore *et al.*, "Large-scale field trial of attractive toxic sugar baits (ATSB) for the control of malaria vector mosquitoes in Mali, West Africa," en, *Malar J*, vol. 19, no. 1, p. 72, Dec. 2020, ISSN: 1475-2875. DOI: 10.1186/s12936-020-3132-0.

[63] A. B. Hogan, P. Winskill, and A. C. Ghani, "Estimated impact of RTS,S/AS01 malaria vaccine allocation strategies in sub-Saharan Africa: A modelling study," en, *PLoS Med*, vol. 17, no. 11, E. A. Ashley, Ed., e1003377, Nov. 2020, ISSN: 1549-1676. DOI: 10.1371/journal.pmed.1003377.

[64] F. O. Okumu, E. P. Madumla, A. N. John, D. W. Lwetoijera, and R. D. Sumaye, "Attracting, trapping and killing disease-transmitting mosquitoes using odor-baited stations -The Ifakara Odor-Baited Stations," en, *Parasites Vectors*, vol. 3, no. 1, p. 12, 2010, ISSN: 1756-3305. DOI: 10.1186/1756-3305-3-12.

[65] L. Burgert, T. Reiker, M. Golumbeanu, J. J. Möhrle, and M. A. Penny, "Model-informed target product profiles of long-acting-injectables for use as seasonal malaria prevention," en, *PLOS Glob Public Health*, vol. 2, no. 3, C. Boëte, Ed., e0000211, Mar. 2022, ISSN: 2767-3375. DOI: 10.1371/journal.pgph.0000211.

[66] G. F. Killeen, N. Chitnis, S. J. Moore, and F. O. Okumu, "Target product profile choices for intra-domiciliary malaria vector control pesticide products: Repel or kill?" en, *Malar J*, vol. 10, no. 1, p. 207, Dec. 2011, ISSN: 1475-2875. DOI: 10.1186/1475-2875-10-207.

[67] G. F. Killeen and S. J. Moore, "Target product profiles for protecting against outdoor malaria transmission," en, *Malar J*, vol. 11, no. 1, p. 17, Dec. 2012, ISSN: 1475-2875. DOI: 10.1186/1475-2875-11-17.

[68] G. Müller and Y. Schlein, "Sugar questing mosquitoes in arid areas gather on scarce blossoms that can be used for control," en, *International Journal for Parasitology*, vol. 36, no. 10-11, pp. 1077–1080, Sep. 2006, ISSN: 00207519. DOI: 10.1016/j.ijpara.2006.06.008.

[69] G. C. Müller *et al.*, "Successful field trial of attractive toxic sugar bait (ATSB) plant-spraying methods against malaria vectors in the Anopheles gambiae complex in Mali, West Africa," en, *Malar J*, vol. 9, no. 1, p. 210, Dec. 2010, ISSN: 1475-2875. DOI: 10.1186/1475-2875-9-210.

[70] A. Le Menach *et al.*, "An elaborated feeding cycle model for reductions in vectorial capacity of night-biting mosquitoes by insecticide-treated nets," en, *Malar J*, vol. 6, no. 1, p. 10, Dec. 2007, ISSN: 1475-2875. DOI: 10.1186/1475-2875-6-10.

[71] R. D. Sjogren and J. F. Day, "Vector Control by Removal Trapping," en, *The American Journal of Tropical Medicine and Hygiene*, vol. 50, no. 6_Suppl, pp. 126–133, Jan. 1994, ISSN: 0002-9637, 1476-1645. DOI: 10.4269/ajtmh.1994.50.126.

[72] C. Costantini, G. Gibson, J. Brady, L. Merzagora, and M. Coluzzi, "A new odour-baited trap to collect host-seeking mosquitoes," eng, *Parassitologia*, vol. 35, no. 1-3, pp. 5–9, Dec. 1993, ISSN: 0048-2951.

[73] F. O. Okumu *et al.*, "Development and Field Evaluation of a Synthetic Mosquito Lure That Is More Attractive than Humans," en, *PLoS ONE*, vol. 5, no. 1, L. Rénia, Ed., e8951, Jan. 2010, ISSN: 1932-6203. DOI: 10.1371/journal.pone.0008951.

[74] G. F. Killeen *et al.*, "Preventing Childhood Malaria in Africa by Protecting Adults from Mosquitoes with Insecticide-Treated Nets," en, *PLoS Med*, vol. 4, no. 7, J. Dushoff, Ed., e229, Jul. 2007, ISSN: 1549-1676. DOI: 10.1371/journal.pmed.0040229.

[75] F. O. Okumu, N. J. Govella, S. J. Moore, N. Chitnis, and G. F. Killeen, "Potential Benefits, Limitations and Target Product-Profiles of Odor-Baited Mosquito Traps for Malaria Control in Africa," en, *PLoS ONE*, vol. 5, no. 7, L. Rénia, Ed., e11573, Jul. 2010, ISSN: 1932-6203. DOI: 10.1371/journal.pone.0011573.

[76] F. Macintyre *et al.*, "Injectable anti-malarials revisited: Discovery and development of new agents to protect against malaria," en, *Malar J*, vol. 17, no. 1, p. 402, Dec. 2018, ISSN: 1475-2875. DOI: 10.1186/s12936-018-2549-1.

[77] N. Chitnis, D. Hardy, and T. Smith, "A Periodically-Forced Mathematical Model for the Seasonal Dynamics of Malaria in Mosquitoes," en, *Bull Math Biol*, vol. 74, no. 5, pp. 1098–1124, May 2012, ISSN: 0092-8240, 1522-9602. DOI: 10.1007/s11538-011-9710-0.

[78] M. Golumbeanu *et al.*, "Leveraging mathematical models of disease dynamics and machine learning to improve development of novel malaria interventions," en, *Infect Dis Poverty*, vol. 11, no. 1, p. 61, Dec. 2022, ISSN: 2049-9957. DOI: 10.1186/s40249-022-00981-1.

[79] A. R. North, A. Burt, and H. C. J. Godfray, "Modelling the potential of genetic control of malaria mosquitoes at national scale," en, *BMC Biol*, vol. 17, no. 1, p. 26, Dec. 2019, ISSN: 1741-7007. DOI: 10.1186/s12915-019-0645-5.

[80] P. A. Eckhoff, E. A. Wenger, H. C. J. Godfray, and A. Burt, "Impact of mosquito gene drive on malaria elimination in a computational model with explicit spatial and temporal dynamics," en, *Proc. Natl. Acad. Sci. U.S.A.*, vol. 114, no. 2, Jan. 2017, ISSN: 0027-8424, 1091-6490. DOI: 10.1073/pnas.1611064114.

[81] D. L. Smith, F. E. McKenzie, R. W. Snow, and S. I. Hay, "Revisiting the Basic Reproductive Number for Malaria and Its Implications for Malaria Control," en, *PLoS Biol*, vol. 5, no. 3, B. T. Grenfell, Ed., e42, Feb. 2007, ISSN: 1545-7885. DOI: 10.1371/journal.pbio.0050042.

[82] Committee on Gene Drive Research in Non-Human Organisms: Recommendations for Responsible Conduct, Board on Life Sciences, Division on Earth and Life Studies, and National Academies of Sciences, Engineering, and Medicine, *Gene Drives on the Horizon: Advancing Science, Navigating Uncertainty, and Aligning Research with Public Values*. Washington, D.C.: National Academies Press, Jul. 2016, Pages: 23405, ISBN: 978-0-309-43787-5. DOI: 10.17226/23405.

[83] J. M. Marshall and O. S. Akbari, "Can CRISPR-Based Gene Drive Be Confined in the Wild? A Question for Molecular and Population Biology," en, *ACS Chem. Biol.*, vol. 13, no. 2, pp. 424–430, Feb. 2018, ISSN: 1554-8929, 1554-8937. DOI: 10.1021/acschembio.7b00923.

[84] M. R. Vella, C. E. Gunning, A. L. Lloyd, and F. Gould, "Evaluating strategies for reversing CRISPR-Cas9 gene drives," en, *Sci Rep*, vol. 7, no. 1, p. 11 038, Dec. 2017, ISSN: 2045-2322. DOI: 10.1038/s41598-017-10633-2.

[85] X.-R. S. Xu *et al.*, "Active Genetic Neutralizing Elements for Halting or Deleting Gene Drives," en, *Molecular Cell*, vol. 80, no. 2, 246–262.e4, Oct. 2020, ISSN: 10972765. DOI: 10.1016/j.molcel.2020.09.003.

[86] N. Metchanun *et al.*, "Modeling impact and cost-effectiveness of driving-Y gene drives for malaria elimination in the Democratic Republic of the Congo," en, *Evolutionary Applications*, vol. 15, no. 1, pp. 132–148, Jan. 2022, ISSN: 1752-4571, 1752-4571. DOI: 10.1111/eva.13331.

[87] G. Rašić, N. F. Lobo, E. H. Jeffrey Gutiérrez, H. M. Sánchez C., and J. M. Marshall, "Monitoring Needs for Gene Drive Mosquito Projects: Lessons From Vector Control Field Trials and Invasive Species," *Front. Genet.*, vol. 12, p. 780 327, Jan. 2022, ISSN: 1664-8021. DOI: 10.3389/fgene.2021.780327.

[88] R. Carballar-Lejarazú *et al.*, "Dual effector population modification gene-drive strains of the African malaria mosquitoes, *Anopheles gambiae* and *Anopheles coluzzii*," en, *Proc. Natl. Acad. Sci. U.S.A.*, vol. 120, no. 29, e2221118120, Jul. 2023, ISSN: 0027-8424, 1091-6490. DOI: 10.1073/pnas.2221118120.

[89] H. M. Sánchez C., S. L. Wu, J. B. Bennett, and J. M. Marshall, "MGDrivE: A modular simulation framework for the spread of gene drives through spatially explicit mosquito populations," en, *Methods Ecol Evol*, vol. 11, no. 2, N. Golding, Ed., pp. 229–239, Feb. 2020, ISSN: 2041-210X, 2041-210X. DOI: 10.1111/2041-210X.13318.

[90] K. Magori *et al.*, "Skeeter Buster: A Stochastic, Spatially Explicit Modeling Tool for Studying Aedes aegypti Population Replacement and Population Suppression Strategies," en, *PLoS Negl Trop Dis*, vol. 3, no. 9, P. Kittayapong, Ed., e508, Sep. 2009, ISSN: 1935-2735. DOI: 10.1371/journal.pntd.0000508.

[91] J. T. Griffin *et al.*, "Potential for reduction of burden and local elimination of malaria by reducing Plasmodium falciparum malaria transmission: A mathematical modelling study," en, *The Lancet Infectious Diseases*, vol. 16, no. 4, pp. 465–472, Apr. 2016, ISSN: 14733099. DOI: 10.1016/S1473-3099(15)00423-5.

[92] S. L. Wu, J. B. Bennett, H. M. Sánchez C., A. J. Dolgert, T. M. León, and J. M. Marshall, "MGDrivE 2: A simulation framework for gene drive systems incorporating seasonality and epidemiological dynamics," en, *PLoS Comput Biol*, vol. 17, no. 5, M. Marz, Ed., e1009030, May 2021, ISSN: 1553-7358. DOI: 10.1371/journal.pcbi.1009030.

[93] N. R. Smith *et al.*, "Agent-based models of malaria transmission: A systematic review," en, *Malar J*, vol. 17, no. 1, p. 299, Dec. 2018, ISSN: 1475-2875. DOI: 10.1186/s12936-018-2442-y.

[94] S. L. Wu *et al.*, "Vector bionomics and vectorial capacity as emergent properties of mosquito behaviors and ecology," en, *PLoS Comput Biol*, vol. 16, no. 4, J. Lloyd-Smith, Ed., e1007446, Apr. 2020, ISSN: 1553-7358. DOI: 10.1371/journal.pcbi.1007446.

[95] H. J. Wearing and P. Rohani, "Ecological and immunological determinants of dengue epidemics," en, *Proc. Natl. Acad. Sci. U.S.A.*, vol. 103, no. 31, pp. 11 802–11 807, Aug. 2006, ISSN: 0027-8424, 1091-6490. DOI: 10.1073/pnas.0602960103.

[96] N. Wang, "The Citrus Huanglongbing Crisis and Potential Solutions," en, *Molecular Plant*, vol. 12, no. 5, pp. 607–609, May 2019, ISSN: 16742052. DOI: 10.1016/j.molp.2019.03.008.

[97] V. M. Gantz *et al.*, "Highly efficient Cas9-mediated gene drive for population modification of the malaria vector mosquito *Anopheles stephensi*," en, *Proc. Natl. Acad. Sci. U.S.A.*, vol. 112, no. 49, Dec. 2015, ISSN: 0027-8424, 1091-6490. DOI: 10.1073/pnas.1521077112.

[98] A. M. Dondorp *et al.*, "The Relationship between Age and the Manifestations of and Mortality Associated with Severe Malaria," en, *CLIN INFECT DIS*, vol. 47, no. 2, pp. 151–157, Jul. 2008, ISSN: 1058-4838, 1537-6591. DOI: 10.1086/589287.

[99] S. S. Kiware *et al.*, "Attacking the mosquito on multiple fronts: Insights from the Vector Control Optimization Model (VCOM) for malaria elimination," en, *PLoS ONE*, vol. 12, no. 12, P. L. Oliveira, Ed., e0187680, Dec. 2017, ISSN: 1932-6203. DOI: 10.1371/journal.pone.0187680.

[100] P. Winskill, *Umbrella: Rainfall & seasonality*, 2022.

[101] H. M. Sánchez C., D. L. Smith, and J. M. Marshall, "MGSurvE: A framework to optimize trap placement for genetic surveillance of mosquito population," en, Bioinformatics, preprint, Jun. 2023. DOI: 10.1101/2023.06.26.546301.

[102] G. C. Lanzaro *et al.*, "Selection of sites for field trials of genetically engineered mosquitoes with gene drive," en, *Evolutionary Applications*, vol. 14, no. 9, pp. 2147–2161, Sep. 2021, ISSN: 1752-4571, 1752-4571. DOI: 10.1111/eva.13283.

[103] S. James *et al.*, "Pathway to Deployment of Gene Drive Mosquitoes as a Potential Biocontrol Tool for Elimination of Malaria in Sub-Saharan Africa: Recommendations of a Scientific Working Group †," en, *The American Journal of Tropical Medicine and Hygiene*, vol. 98, no. 6_Suppl, pp. 1–49, Jun. 2018, ISSN: 0002-9637, 1476-1645. DOI: 10.4269/ajtmh.18-0083.

[104] A. S. Yaro *et al.*, "The distribution of hatching time in Anopheles gambiae," en, *Malar J*, vol. 5, no. 1, p. 19, Dec. 2006, ISSN: 1475-2875. DOI: 10.1186/1475-2875-5-19.

[105] M. Bayoh and S. Lindsay, "Effect of temperature on the development of the aquatic stages of *Anopheles gambiae* sensu stricto (Diptera: Culicidae)," en, *Bull. Entomol. Res.*, vol. 93, no. 5, pp. 375–381, Sep. 2003, ISSN: 0007-4853, 1475-2670. DOI: 10.1079/BER2003259.

[106] A. A. Hoffmann *et al.*, "Successful establishment of Wolbachia in Aedes populations to suppress dengue transmission," en, *Nature*, vol. 476, no. 7361, pp. 454–457, Aug. 2011, ISSN: 0028-0836, 1476-4687. DOI: 10.1038/nature10356.

[107] D. O. Carvalho *et al.*, "Suppression of a Field Population of Aedes aegypti in Brazil by Sustained Release of Transgenic Male Mosquitoes," en, *PLoS Negl Trop Dis*, vol. 9, no. 7, K. E. Olson, Ed., e0003864, Jul. 2015, ISSN: 1935-2735. DOI: 10.1371/journal.pntd.0003864.

[108] E. A. Ashley and N. J. White, "The duration of Plasmodium falciparum infections," en, *Malar J*, vol. 13, no. 1, p. 500, Dec. 2014, ISSN: 1475-2875. DOI: 10.1186/1475-2875-13-500.

[109] N. A. H. Van Hest, F. Smit, and J. P. Verhave, "Underreporting of malaria incidence in the Netherlands: Results from a capture–recapture study," en, *Epidemiol. Infect.*, vol. 129, no. 2, pp. 371–377, Oct. 2002, ISSN: 0950-2688, 1469-4409. DOI: 10.1017/S0950268802007306.

[110] T. Leon, H. M. S. Castellanos, Yoosook Lee, and J. M. Marshall, "New methods for modeling Anopheles gambiae s.l. movement with environmental and genetic data," en, 2020, Publisher: [object Object]. DOI: 10.13140/RG.2.2.32130.91845.

[111] C. Taylor *et al.*, "Gene Flow Among Populations of the Malaria Vector, *Anopheles gambiae* , in Mali, West Africa," en, *Genetics*, vol. 157, no. 2, pp. 743–750, Feb. 2001, ISSN: 1943-2631. DOI: 10.1093/genetics/157.2.743.

[112] M. C. Thomson, S. J. Connor, M. L. Quiñones, M. Jawara, J. Todd, and B. M. Greenwood, "Movement of Anopheles gambiae s.l. malaria vectors between villages in The Gambia," en, *Medical Vet Entomology*, vol. 9, no. 4, pp. 413–419, Oct. 1995, ISSN: 0269-283X, 1365-2915. DOI: 10.1111/j.1365-2915.1995.tb00015.x.

[113] W. G. Landis, "The Origin, Development, Application, Lessons Learned, and Future Regarding the Bayesian Network Relative Risk Model for Ecological Risk Assessment," en, *Integr Envir Assess & Manag*, vol. 17, no. 1, pp. 79–94, Jan. 2021, ISSN: 1551-3777, 1551-3793. DOI: 10.1002/ieam.4351.

[114] S. Bhatt *et al.*, "The effect of malaria control on Plasmodium falciparum in Africa between 2000 and 2015," en, *Nature*, vol. 526, no. 7572, pp. 207–211, Oct. 2015, ISSN: 0028-0836, 1476-4687. DOI: 10.1038/nature15535.

[115] J. B. Connolly *et al.*, "Considerations for first field trials of low-threshold gene drive for malaria vector control," en, *Malar J*, vol. 23, no. 1, p. 156, May 2024, ISSN: 1475-2875. DOI: 10.1186/s12936-024-04952-9.

[116] B. C. Haller and P. W. Messer, "SLiM 3: Forward Genetic Simulations Beyond the Wright–Fisher Model," en, *Molecular Biology and Evolution*, vol. 36, no. 3, R. Hernandez, Ed., pp. 632–637, Mar. 2019, ISSN: 0737-4038, 1537-1719. DOI: 10.1093/molbev/msy228.

[117] A. Mondal, H. M. Sánchez C., and J. M. Marshall, "MGDrivE 3: A decoupled vector-human framework for epidemiological simulation of mosquito genetic control tools and their surveillance," en, *PLoS Comput Biol*, vol. 20, no. 5, J. L. Rasgon, Ed., e1012133, May 2024, ISSN: 1553-7358. DOI: 10.1371/journal.pcbi.1012133.

[118] P. A. Hancock *et al.*, *The potential of gene drive releases in malaria vector species to reduce the malaria burden in different African environments*, en, Apr. 2024. DOI: 10.1101/2024.04.08.588513.

[119] A. Adolfi *et al.*, "Efficient population modification gene-drive rescue system in the malaria mosquito Anopheles stephensi," en, *Nat Commun*, vol. 11, no. 1, p. 5553, Nov. 2020, ISSN: 2041-1723. DOI: 10.1038/s41467-020-19426-0.

[120] G. C. Lanzaro, H. M. Sánchez C., T. C. Collier, J. M. Marshall, and A. A. James, "Population modification strategies for malaria vector control are uniquely resilient to observed levels of gene drive resistance alleles," en, *BioEssays*, vol. 43, no. 8, p. 2 000 282, Aug. 2021, ISSN: 0265-9247, 1521-1878. DOI: 10.1002/bies.202000282.

[121] N. P. Kandul, J. Liu, J. B. Bennett, J. M. Marshall, and O. S. Akbari, *A home and rescue gene drive efficiently spreads and persists in populations*, en, Aug. 2020. DOI: 10.1101/2020.08.21.261610.

[122] M. Li *et al.*, "Development of a confinable gene drive system in the human disease vector Aedes aegypti," en, *eLife*, vol. 9, e51701, Jan. 2020, ISSN: 2050-084X. DOI: 10.7554/eLife.51701.

[123] R. Carballar-Lejarazú *et al.*, "Next-generation gene drive for population modification of the malaria vector mosquito, *Anopheles gambiae*," en, *Proc. Natl. Acad. Sci. U.S.A.*, vol. 117, no. 37, pp. 22 805–22 814, Sep. 2020, ISSN: 0027-8424, 1091-6490. DOI: 10.1073/pnas.2010214117.

[124] J. Champer *et al.*, "Reducing resistance allele formation in CRISPR gene drive," en, *Proc. Natl. Acad. Sci. U.S.A.*, vol. 115, no. 21, pp. 5522–5527, May 2018, ISSN: 0027-8424, 1091-6490. DOI: 10.1073/pnas.1720354115.

[125] T. B. Pham *et al.*, "Experimental population modification of the malaria vector mosquito, Anopheles stephensi," en, *PLoS Genet*, vol. 15, no. 12, C. Desplan, Ed., e1008440, Dec. 2019, ISSN: 1553-7404. DOI: 10.1371/journal.pgen.1008440.

[126] A. Hoermann *et al.*, "Gene drive mosquitoes can aid malaria elimination by retarding *Plasmodium* sporogonic development," en, *Sci. Adv.*, vol. 8, no. 38, eabo1733, Sep. 2022, ISSN: 2375-2548. DOI: 10.1126/sciadv.abo1733.

[127] D. L. Smith and F. Ellis McKenzie, "Statics and dynamics of malaria infection in Anopheles mosquitoes," *Malar J*, vol. 3, no. 1, p. 13, 2004, ISSN: 14752875. DOI: 10.1186/1475-2875-3-13.

[128] W. Mamai *et al.*, "Monitoring Dry Season Persistence of *Anopheles gambiae* s.l. Populations in a Contained Semi-Field System in Southwestern Burkina Faso, West Africa," en, *J Med Entomol*, vol. 53, no. 1, pp. 130–138, Jan. 2016, ISSN: 0022-2585, 1938-2928. DOI: 10.1093/jme/tjv174.

[129] A. O. Mala *et al.*, "Dry season ecology of Anopheles gambiae complex mosquitoes at larval habitats in two traditionally semi-arid villages in Baringo, Kenya," en, *Parasites Vectors*, vol. 4, no. 1, p. 25, Dec. 2011, ISSN: 1756-3305. DOI: 10.1186/1756-3305-4-25.

[130] D. A. Pfeffer *et al.*, "malariaAtlas: An R interface to global malariometric data hosted by the Malaria Atlas Project," en, *Malar J*, vol. 17, no. 1, p. 352, Dec. 2018, ISSN: 1475-2875. DOI: 10.1186/s12936-018-2500-5.

[131] J. M. Marshall, A. Buchman, H. M. Sánchez C., and O. S. Akbari, "Overcoming evolved resistance to population-suppressing homing-based gene drives," en, *Sci Rep*, vol. 7, no. 1, p. 3776, Jun. 2017, ISSN: 2045-2322. DOI: 10.1038/s41598-017-02744-7.

[132] N. F. Lobo, N. L. Achee, J. Greico, and F. H. Collins, "Modern Vector Control," en, *Cold Spring Harb Perspect Med*, vol. 8, no. 1, a025643, Jan. 2018, ISSN: 2157-1422. DOI: 10.1101/cshperspect.a025643.

[133] D. Shi, L. Wei, H. Liang, D. Yan, J. Zhang, and Z. Wang, "Trends of the Global, Regional and National Incidence, Mortality, and Disability-Adjusted Life Years of Malaria, 1990–2019: An Analysis of the Global Burden of Disease Study 2019," en, *RMHP*, vol. Volume 16, pp. 1187–1201, Jun. 2023, ISSN: 1179-1594. DOI: 10.2147/RMHP.S419616.

[134] R. Verity *et al.*, "Estimates of the severity of coronavirus disease 2019: A model-based analysis," en, *The Lancet Infectious Diseases*, vol. 20, no. 6, pp. 669–677, Jun. 2020, ISSN: 14733099. DOI: 10.1016/S1473-3099(20)30243-7.

[135] M. Li, J. Dushoff, and B. M. Bolker, "Fitting mechanistic epidemic models to data: A comparison of simple Markov chain Monte Carlo approaches," en, *Stat Methods Med Res*, vol. 27, no. 7, pp. 1956–1967, Jul. 2018, ISSN: 0962-2802, 1477-0334. DOI: 10.1177/0962280217747054.

[136] A. B. Hogan *et al.*, "Estimating long-term vaccine effectiveness against SARS-CoV-2 variants: A model-based approach," en, *Nat Commun*, vol. 14, no. 1, p. 4325, Jul. 2023, ISSN: 2041-1723. DOI: 10.1038/s41467-023-39736-3.

[137] K. M. Fornace *et al.*, "No evidence of sustained nonzoonotic Plasmodium knowlesi transmission in Malaysia from modelling malaria case data," en, *Nat Commun*, vol. 14, no. 1, p. 2945, Jun. 2023, ISSN: 2041-1723. DOI: 10.1038/s41467-023-38476-8.

[138] I. M. Gherman, Z. S. Abdallah, W. Pang, T. E. Gorochowski, C. S. Grierson, and L. Marucci, "Bridging the gap between mechanistic biological models and machine learning surrogates," en, *PLoS Comput Biol*, vol. 19, no. 4, M. H. Schulz, Ed., e1010988, Apr. 2023, ISSN: 1553-7358. DOI: 10.1371/journal.pcbi.1010988.

[139] J. J. Thiagarajan *et al.*, "Designing accurate emulators for scientific processes using calibration-driven deep models," en, *Nat Commun*, vol. 11, no. 1, p. 5622, Nov. 2020, ISSN: 2041-1723. DOI: 10.1038/s41467-020-19448-8.

[140] S. Wang *et al.*, "Massive computational acceleration by using neural networks to emulate mechanism-based biological models," en, *Nat Commun*, vol. 10, no. 1, p. 4354, Sep. 2019, ISSN: 2041-1723. DOI: 10.1038/s41467-019-12342-y.

[141] L. Liang, M. Liu, C. Martin, and W. Sun, "A machine learning approach as a surrogate of finite element analysis–based inverse method to estimate the zero-pressure geometry of human thoracic aorta," en, *Numer Methods Biomed Eng*, vol. 34, no. 8, e3103, Aug. 2018, ISSN: 2040-7939, 2040-7947. DOI: 10.1002/cnm.3103.

[142] V. Davies *et al.*, "Fast Parameter Inference in a Biomechanical Model of the Left Ventricle by Using Statistical Emulation," en, *Journal of the Royal Statistical Society Series C: Applied Statistics*, vol. 68, no. 5, pp. 1555–1576, Nov. 2019, ISSN: 0035-9254, 1467-9876. DOI: 10.1111/rssc.12374.

[143] M. Crawshaw, *Multi-Task Learning with Deep Neural Networks: A Survey*, Version Number: 1, 2020. DOI: 10.48550/ARXIV.2009.09796.

[144] P. Selvaraj, E. A. Wenger, and J. Gerardin, "Seasonality and heterogeneity of malaria transmission determine success of interventions in high-endemic settings: A modeling study," en, *BMC Infect Dis*, vol. 18, no. 1, p. 413, Dec. 2018, ISSN: 1471-2334. DOI: 10.1186/s12879-018-3319-y.

[145] L. Molineaux and G. Gramiccia, *The Garki project: Research on the epidemiology and control of malaria in the Sudan savanna of West Africa*, 1980.

[146] T. Smith *et al.*, "Absence of seasonal variation in malaria parasitaemia in an area of intense seasonal transmission," en, *Acta Tropica*, vol. 54, no. 1, pp. 55–72, Jun. 1993, ISSN: 0001706X. DOI: 10.1016/0001-706X(93)90068-M.

[147] C. Rogier, A. Tall, N. Diagne, D. Fontenille, A. Spiegel, and J. F. Trape, "Plasmodium falciparum clinical malaria: Lessons from longitudinal studies in Senegal," eng, *Parassitologia*, vol. 41, no. 1-3, pp. 255–259, Sep. 1999, ISSN: 0048-2951.

[148] A. L. Ouédraogo *et al.*, "Dynamics of the Human Infectious Reservoir for Malaria Determined by Mosquito Feeding Assays and Ultrasensitive Malaria Diagnosis in Burkina Faso," en, *J Infect Dis.*, vol. 213, no. 1, pp. 90–99, Jan. 2016, ISSN: 0022-1899, 1537-6613. DOI: 10.1093/infdis/jiv370.

[149] B. Lin, F. Ye, Y. Zhang, and I. W. Tsang, "Reasonable Effectiveness of Random Weighting: A Litmus Test for Multi-Task Learning," 2021, Publisher: [object Object] Version Number: 2. DOI: 10.48550/ARXIV.2111.10603.

[150] D. P. Kingma and J. Ba, "Adam: A Method for Stochastic Optimization," 2014, Publisher: [object Object] Version Number: 9. DOI: 10.48550/ARXIV.1412.6980.

[151] L. Li *et al.*, "A System for Massively Parallel Hyperparameter Tuning," 2018, Publisher: [object Object] Version Number: 5. DOI: 10.48550/ARXIV.1810.05934.

[152] J. Gerardin, A. L. Ouédraogo, K. A. McCarthy, P. A. Eckhoff, and E. A. Wenger, "Characterization of the infectious reservoir of malaria with an agent-based model calibrated to age-stratified parasite densities and infectiousness," en, *Malar J*, vol. 14, no. 1, p. 231, Dec. 2015, ISSN: 1475-2875. DOI: 10.1186/s12936-015-0751-y.

[153] K. A. McCarthy, E. A. Wenger, G. H. Huynh, and P. A. Eckhoff, "Calibration of an intrahost malaria model and parameter ensemble evaluation of a pre-erythrocytic vaccine," en, *Malar J*, vol. 14, no. 1, p. 6, Dec. 2015, ISSN: 1475-2875. DOI: 10.1186/1475-2875-14-6.

[154] V. U. Prabhu and A. Birhane, *Large image datasets: A pyrrhic win for computer vision?* Version Number: 2, 2020. DOI: 10.48550/ARXIV.2006.16923.

[155] Y. Liu, J. Cao, C. Liu, K. Ding, and L. Jin, *Datasets for Large Language Models: A Comprehensive Survey*, Version Number: 1, 2024. DOI: 10.48550/ARXIV.2402.18041.

[156] C. Zhou *et al.*, "A Comprehensive Survey on Pretrained Foundation Models: A History from BERT to ChatGPT," 2023, Publisher: [object Object] Version Number: 3. DOI: 10.48550/ARXIV.2302.09419.

[157] L. Yuan *et al.*, "Florence: A New Foundation Model for Computer Vision," 2021, Publisher: [object Object] Version Number: 1. DOI: 10.48550/ARXIV.2111.11432.

[158] M. Du, N. Liu, and X. Hu, *Techniques for Interpretable Machine Learning*, Version Number: 3, 2018. DOI: 10.48550/ARXIV.1808.00033.

[159] X. Wu, S. Huang, W. Wang, and F. Wei, *Multi-Head Mixture-of-Experts*, Version Number: 1, 2024. DOI: 10.48550/ARXIV.2404.15045.

[160] T. Kaufmann, P. Weng, V. Bengs, and E. Hüllermeier, *A Survey of Reinforcement Learning from Human Feedback*, Version Number: 2, 2023. DOI: 10.48550/ARXIV.2312.14925.

[161] T. Dash, S. Chitlangia, A. Ahuja, and A. Srinivasan, *Incorporating Domain Knowledge into Deep Neural Networks*, Version Number: 2, 2021. DOI: 10.48550/ARXIV.2103.00180.

[162] F. Pourpanah *et al.*, "A Review of Generalized Zero-Shot Learning Methods," *IEEE Trans. Pattern Anal. Mach. Intell.*, pp. 1–20, 2022, ISSN: 0162-8828, 2160-9292, 1939-3539. DOI: 10.1109/TPAMI.2022.3191696.

[163] K. Weiss, T. M. Khoshgoftaar, and D. Wang, "A survey of transfer learning," en, *J Big Data*, vol. 3, no. 1, p. 9, Dec. 2016, ISSN: 2196-1115. DOI: 10.1186/s40537-016-0043-6.

[164] M. Moor *et al.*, "Foundation models for generalist medical artificial intelligence," en, *Nature*, vol. 616, no. 7956, pp. 259–265, Apr. 2023, ISSN: 0028-0836, 1476-4687. DOI: 10.1038/s41586-023-05881-4.

[165] R. Bommasani *et al.*, "On the Opportunities and Risks of Foundation Models," 2021, Publisher: [object Object] Version Number: 3. DOI: 10.48550/ARXIV.2108.07258.

[166] Y. Qin *et al.*, "Tool Learning with Foundation Models," 2023, Publisher: [object Object] Version Number: 2. DOI: 10.48550/ARXIV.2304.08354.

[167] P. R. Chennuri, Z. N. Adelman, and K. M. Myles, "Genetic Approaches for Controlling CRISPR-based Autonomous Homing Gene Drives," *Front. Bioeng. Biotechnol.*, vol. 10, p. 897 231, Jun. 2022, ISSN: 2296-4185. DOI: 10.3389/fbioe.2022.897231.

[168] J. Zapletal, N. Najmitabrizi, M. Erraguntla, M. A. Lawley, K. M. Myles, and Z. N. Adelman, "Making gene drive biodegradable," en, *Phil. Trans. R. Soc. B*, vol. 376, no. 1818, p. 20 190 804, Feb. 2021, ISSN: 0962-8436, 1471-2970. DOI: 10.1098/rstb.2019.0804.

[169] K. C. Long, "Core commitments for field trials of gene drive organisms," *Science*, vol. 370, no. 6523, pp. 1417–1419, Dec. 2020. DOI: DOI:10.1126/science.abd1908.

[170] A. R. North and H. C. J. Godfray, "The dynamics of disease in a metapopulation: The role of dispersal range," en, *Journal of Theoretical Biology*, vol. 418, pp. 57–65, Apr. 2017, ISSN: 00225193. DOI: 10.1016/j.jtbi.2017.01.037.

[171] A. North, A. Burt, and H. C. J. Godfray, "Modelling the spatial spread of a homing endonuclease gene in a mosquito population," en, *Journal of Applied Ecology*, vol. 50, no. 5, Y. Buckley, Ed., pp. 1216–1225, Oct. 2013, ISSN: 0021-8901, 1365-2664. DOI: 10.1111/1365-2664.12133.

[172] H. Tanaka, H. A. Stone, and D. R. Nelson, "Spatial gene drives and pushed genetic waves," en, *Proc. Natl. Acad. Sci. U.S.A.*, vol. 114, no. 32, pp. 8452–8457, Aug. 2017, ISSN: 0027-8424, 1091-6490. DOI: 10.1073/pnas.1705868114.

[173] S. Dhole, A. L. Lloyd, and F. Gould, "Gene Drive Dynamics in Natural Populations: The Importance of Density Dependence, Space, and Sex," en, *Annu. Rev. Ecol. Evol. Syst.*, vol. 51, no. 1, pp. 505–531, Nov. 2020, ISSN: 1543-592X, 1545-2069. DOI: 10.1146/annurev-ecolsys-031120-101013.

[174] J. J. Bull, C. H. Remien, R. Gomulkiewicz, and S. M. Krone, "Spatial structure undermines parasite suppression by gene drive cargo," en, *PeerJ*, vol. 7, e7921, Oct. 2019, ISSN: 2167-8359. DOI: 10.7717/peerj.7921.

[175] W. Bao, Y. Du, Z. Lin, and H. Zhu, "Free boundary models for mosquito range movement driven by climate warming," en, *J. Math. Biol.*, vol. 76, no. 4, pp. 841–875, Mar. 2018, ISSN: 0303-6812, 1432-1416. DOI: 10.1007/s00285-017-1159-9.

[176] M. A. Combs *et al.*, "Leveraging eco-evolutionary models for gene drive risk assessment," en, *Trends in Genetics*, vol. 39, no. 8, pp. 609–623, Aug. 2023, ISSN: 01689525. DOI: 10.1016/j.tig.2023.04.004.

[177] J. Kim, K. D. Harris, I. K. Kim, S. Shemesh, P. W. Messer, and G. Greenbaum, "Incorporating ecology into gene drive modelling," en, *Ecology Letters*, vol. 26, no. S1, Sep. 2023, ISSN: 1461-023X, 1461-0248. DOI: 10.1111/ele.14194.

[178] M. Boots and Y. Haraguchi, "The Evolution of Costly Resistance in Host-Parasite Systems," en, *The American Naturalist*, vol. 153, no. 4, pp. 359–370, Apr. 1999, ISSN: 0003-0147, 1537-5323. DOI: 10.1086/303181.

[179] W. T. Garrood, P. Cuber, K. Willis, F. Bernardini, N. M. Page, and R. E. Haghighat-Khah, "Driving down malaria transmission with engineered gene drives," *Front. Genet.*, vol. 13, p. 891 218, Oct. 2022, ISSN: 1664-8021. DOI: 10.3389/fgene.2022.891218.

[180] S. Alizon, J. C. De Roode, and Y. Michalakis, "Multiple infections and the evolution of virulence," en, *Ecology Letters*, vol. 16, no. 4, J. Drake, Ed., pp. 556–567, Apr. 2013, ISSN: 1461-023X, 1461-0248. DOI: 10.1111/ele.12076.

[181] A. Vaswani *et al.*, "Attention Is All You Need," 2017, Publisher: [object Object] Version Number: 7. DOI: 10.48550/ARXIV.1706.03762.

[182] Y. Chang *et al.*, "A Survey on Evaluation of Large Language Models," en, *ACM Trans. Intell. Syst. Technol.*, vol. 15, no. 3, pp. 1–45, Jun. 2024, ISSN: 2157-6904, 2157-6912. DOI: 10.1145/3641289.

[183] K. He, X. Zhang, S. Ren, and J. Sun, "Deep Residual Learning for Image Recognition," 2015, Publisher: [object Object] Version Number: 1. DOI: 10.48550/ARXIV.1512.03385.

[184] N. Gruver, M. Finzi, S. Qiu, and A. G. Wilson, *Large Language Models Are Zero-Shot Time Series Forecasters*, arXiv:2310.07820 [cs], Oct. 2023.

[185] M. Jin *et al.*, *Time-LLM: Time Series Forecasting by Reprogramming Large Language Models*, arXiv:2310.01728 [cs], Jan. 2024.

[186] A. F. Ansari *et al.*, "Chronos: Learning the Language of Time Series," 2024, Publisher: [object Object] Version Number: 1. DOI: 10.48550/ARXIV.2403.07815.

[187] J. Jumper *et al.*, "Highly accurate protein structure prediction with AlphaFold," en, *Nature*, vol. 596, no. 7873, pp. 583–589, Aug. 2021, ISSN: 0028-0836, 1476-4687. DOI: 10.1038/s41586-021-03819-2.

[188] A. W. Senior *et al.*, "Improved protein structure prediction using potentials from deep learning," en, *Nature*, vol. 577, no. 7792, pp. 706–710, Jan. 2020, ISSN: 0028-0836, 1476-4687. DOI: 10.1038/s41586-019-1923-7.

[189] L. Li *et al.*, "Machine learning optimization of candidate antibody yields highly diverse sub-nanomolar affinity antibody libraries," en, *Nat Commun*, vol. 14, no. 1, p. 3454, Jun. 2023, ISSN: 2041-1723. DOI: 10.1038/s41467-023-39022-2.

[190] J. Kim, M. McFee, Q. Fang, O. Abdin, and P. M. Kim, "Computational and artificial intelligence-based methods for antibody development," en, *Trends in Pharmacological Sciences*, vol. 44, no. 3, pp. 175–189, Mar. 2023, ISSN: 01656147. DOI: 10.1016/j.tips.2022.12.005.

[191] V. Baxi, R. Edwards, M. Montalto, and S. Saha, "Digital pathology and artificial intelligence in translational medicine and clinical practice," en, *Modern Pathology*, vol. 35, no. 1, pp. 23–32, Jan. 2022, ISSN: 08933952. DOI: 10.1038/s41379-021-00919-2.

[192] S. Ramgopal, L. N. Sanchez-Pinto, C. M. Horvat, M. S. Carroll, Y. Luo, and T. A. Florin, "Artificial intelligence-based clinical decision support in pediatrics," en, *Pediatr Res*, vol. 93, no. 2, pp. 334–341, Jan. 2023, ISSN: 0031-3998, 1530-0447. DOI: 10.1038/s41390-022-02226-1.

[193] G. T. Berge, O. C. Granmo, T. O. Tveit, B. E. Munkvold, A. L. Ruthjersen, and J. Sharma, "Machine learning-driven clinical decision support system for concept-based searching: A field trial in a Norwegian hospital," en, *BMC Med Inform Decis Mak*, vol. 23, no. 1, p. 5, Jan. 2023, ISSN: 1472-6947. DOI: 10.1186/s12911-023-02101-x.

[194] S. Cabral *et al.*, "Clinical Reasoning of a Generative Artificial Intelligence Model Compared With Physicians," en, *JAMA Intern Med*, Apr. 2024, ISSN: 2168-6106. DOI: 10.1001/jamainternmed.2024.0295.

[195] A. Cannet *et al.*, "Deep learning and wing interferential patterns identify Anopheles species and discriminate amongst Gambiae complex species," en, *Sci Rep*, vol. 13, no. 1, p. 13 895, Aug. 2023, ISSN: 2045-2322. DOI: 10.1038/s41598-023-41114-4.

[196] W. Wei, X. Ma, and J. Wang, "Fair Adaptive Experiments," 2023, Publisher: [object Object] Version Number: 1. DOI: 10.48550/ARXIV.2310.16290.

[197] W. Wei, X. Ma, and J. Wang, "Adaptive Experiments Toward Learning Treatment Effect Heterogeneity," 2023, Publisher: [object Object] Version Number: 2. DOI: 10.48550/ARXIV.2312.06883.

[198] F. Bergström, F. Günther, M. Höhle, and T. Britton, "Bayesian nowcasting with leading indicators applied to COVID-19 fatalities in Sweden," en, *PLoS Comput Biol*, vol. 18, no. 12, C. J. Struchiner, Ed., e1010767, Dec. 2022, ISSN: 1553-7358. DOI: 10.1371/journal.pcbi.1010767.

[199] J. T. Wu *et al.*, "Nowcasting epidemics of novel pathogens: Lessons from COVID-19," en, *Nat Med*, vol. 27, no. 3, pp. 388–395, Mar. 2021, ISSN: 1078-8956, 1546-170X. DOI: 10.1038/s41591-021-01278-w.